EUMETSAT Satellite Application Facility on Climate Monitoring

Visiting Scientist Report

The EUMETSAT Network of Satellite Application Facilities

CM SAF Climate Monitoring

Evaluating the diurnal cycle of clouds using CM-SAF SEVIRI VIS/NIR and TMI microwave retrievals

CDOP VS Study No 19

Date **19. June 2011**

Reference **CLM_AS10_p06**

Evaluating the diurnal cycle of clouds using CM-SAF SEVIRI VIS/NIR and TMI microwave retrievals

CM-SAF VS/AS19 final report

Seethala Chellappan
Royal Netherlands Meteorological Institute, De Bilt, Netherlands (1-11-2010 to 31-01-2011)
Max-Planck Institute for Meteorology, Hamburg, Germany (1-02-2011 to 30-04-2011)

June 2011

Abstract

The objective of the project is to use a dataset of cloud microphysical and optical properties from SEVIRI VIS/NIR generated with the CM-SAF algorithm, as well as cloud liquid water path (LWP) from passive microwave observations to study the diurnal cycle of South Atlantic marine boundary layer clouds and its seasonal variability.

EUMETSAT's SEVIRI is a space-borne instrument with the necessary temporal, spatial, and spectral resolution to resolve the diurnal cycle of clouds. LWP from SEVIRI was compared with LWP from the passive microwave imager TMI. A year (June 2008 to May 2009) worth of collocated SEVIRI and TMI data were processed in order to study the annual and seasonal variation in diurnal cycle of cloud properties, *viz* cloud amount, cloud liquid water path, cloud optical thickness, droplet effective radius, cloud droplet number concentration, and cloud thickness over the South Atlantic marine stratocumulus (Sc) and trade wind cumulus (Cu) regime.

In general, SEVIRI and TMI showed very good agreement for instantaneous and domain mean LWPs in the Sc regime, while the agreement in the trade wind Cu regime was worse. Spatial distributions showed a high correlation of 0.92 and negligible bias on annual basis. For individual seasons the correlation went from 0.9-0.92 with a small bias within ±5 gm^{-2}, except for JJA and SON. In JJA and SON the mean TMI-SEVIRI LWP bias increased to 12-15 gm^{-2}, which is due to the presence of a large amount of absorbing aerosols above the clouds.

We investigated the influence of absorbing aerosols over the Sc domain using AI obtained from OMI. Interestingly, both TMI and SEVIRI LWP increased with AI, but the TMI increase was considerably larger. This was because absorbing aerosols above liquid clouds introduced substantial negative retrieval biases in optical thickness and droplet effective radius and, hence, in the deduced SEVIRI LWP. This SEVIRI LWP bias increased with AI and could be as large as 40 gm^{-2} in instantaneous retrievals. Neglecting aerosol affected pixels with AI>1,

the domain mean TMI-SEVIRI LWP bias could be either completely removed (SON) or at least reduced by half (JJA). Overall, a positive correlation between AI and LWP was seen, which could be due to (i) simple spatial correlations, that is, both aerosol load and cloud optical thickness increased toward the coast or (ii) aerosols actually thickening the underlying cloud layer through dynamical processes.

The diurnal cycles of TMI and SEVIRI LWP were in good agreement within ±10 gm^{-2} in all seasons except JJA and SON. In JJA and SON, larger LWP biases of ~15-30 gm^{-2} were observed due to SEVIRI underestimation of LWP in the presence of absorbing aerosols. After neglecting aerosol affected pixels in JJA and SON data the calculated bias in diurnal cycle was reduced to less than ±10 gm^{-2}. Irrespective of season, both TMI and SEVIRI LWP decreased from morning to late afternoon and thereafter a slight increase was observed. Prior to sunrise clouds are thicker and as the day progresses the cloud layer gets thinner due to the absorption of solar radiation and associated decoupling of the sub-cloud layer. The variation in SEVIRI LWP was mainly due to change in cloud optical thickness/cloud physical thickness as both droplet effective radius and droplet number concentration showed only small diurnal variability.

The largest disagreement was observed over the trade wind Cu, due to the deficit in both microwave and VIS/NIR measurement technique in the low cloud fraction scenes. However, SEVIRI and TMI showed similar variations in diurnal cycle of LWP but with a constant large bias of ~20 gm^{-2} (TMI being higher than SEVIRI). The responsible factors for this large bias could be: a known positive clear-sky bias of 12-15 gm^{-2} and cloud-rain partitioning error in Wentz's microwave algorithm together with microwave less sensitive to low LWP at 37 GHz affecting TMI retrievals, and cloud mask uncertainties, plane-parallel bias, and 3D effects in broken scenes affecting SEVIRI retrievals. We also found that in our study region and at the ~3 km scale of SEVIRI, the VIS/NIR retrievals were rather unaffected by 3D radiative effects at large solar zenith angles.

Finally we have evaluated the sub-pixel scale variability in SEVIRI retrievals based on MODIS Terra+Aqua retrievals. Very good agreement between SEVIRI and MODIS was observed with correlation ≥0.92 in the fully overcast cases. However, over all cloudy cases SEVIRI showed a considerably lower LWP than MODIS. Another important finding of our study is that with the use of the 1.6 µm channel effective radius no adiabatic correction to the SEVIRI LWP for Sc clouds appears to be needed. In contrast, for MODIS LWP retrievals based on the 2.2 µm channel retrieved effective radius, an adiabatic correction factor of 5/6 should be applied.

Table of Contents

1. Introduction

2. Data Description

    2.1 The Spinning Enhanced Visible and InfraRed Imager (SEVIRI)

    2.2 The MODerate resolution Imaging Spectroradiometer (MODIS)

    2.3 The TRMM Microwave Imager (TMI)

    2.4 The Ozone Monitoring Instrument (OMI)

3. Methodology

4. Results and Discussion

  (i) SEVIRI *versus* TMI

    4.1 Effect of Absorbing Aerosols on SEVIRI Retrievals

    4.2 Mean Statistics of Cloud Properties

    4.3 Spatial Distribution of Cloud Properties

    4.4 Diurnal Cycle of Cloud Properties

    4.5 Cloud Fraction Dependency on SEVIRI Retrievals

    4.6 Solar Zenith Angle Dependency on SEVIRI Retrievals

  (ii) SEVIRI *versus* MODIS

    4.7 Spatial Distribution of Cloud Properties

      4.7.1 Total-sky Analysis

      4.7.2 Overcast Analysis

    4.8 An example Mean Statistics of Sc Cloud Properties

5. Conclusion and Outlook

Acknowledgements

Acronyms

References

1. Introduction

Clouds strongly affect the earth's climate by altering the radiative fluxes. Clouds enhance the albedo by reflecting incoming solar radiation back to space and traps thermal radiation than the clear-sky conditions. The low-level marine clouds are particularly important because they constitute the main source of uncertainty in simulated cloud feedbacks [*Bony and Dufresne* 2005]. These clouds typically occur persistently in the subtropical subsidence areas and reflect around 30% of the incoming solar radiation back to space. At the same time, longwave cooling rates are not affected very strongly because of the comparably low temperature difference between the ocean surface and the cloud top. The net energetic effect of these clouds is therefore a cooling of the atmosphere (*Manabe and Strickler* 1964; *Manabe and Wetherald* 1967). Recent observational evidence indicates that low clouds reduce the net radiation balance on a global annually averaged basis by about 15 Wm^{-2} (*Hartmann et al.* 1992). Because of the sensitivity of the earth's radiation budget to low clouds, understanding the characteristics of low clouds is a crucial climate question (*Randall et al.* 1984).

Different general circulation models (GCMs) disagree about the magnitude and even the sign of the cloud feedback (*Cess et al.* 1989). Subtropical Sc clouds have been extensively studied, both by field experiments and using a wide variety of models. In AGCMs the amount of subtropical marine Sc clouds is usually under-predicted, even when the observed sea surface temperatures (SSTs) are prescribed (*Jakob* 1999). When *Duynkerke and Teixeira* [2001] compared ERA results with observations from FIRE, the ERA cloud cover and LWP are strongly underestimated, which causes the ERA downwelling SW radiation at the surface to be much larger than observed. *Duynkerke et al.* [2004] compared results from ten SCMs with observations collected in marine Sc in July 1987 during FIRE and LES results. Many of the SCMs predicted too low LWP and less cloud cover, which leads much larger amount of downwelling SW radiation. They suggested improving the entrainment parameterizations for better representation of Sc clouds in SCMs. *Ma et al.* [1996] demonstrate that in a coupled atmosphere–ocean model an underestimation of Sc cloud amount can lead to positive SST biases of about 5 K. This is of a particular concern for simulations and predictions of ENSO, since such errors can strongly affect the sub/tropical circulations (*Philander et al.* 1996; *Nigam* 1997; *Yu and Mechoso* 1999). Furthermore, the presence of subtropical Sc clouds plays an important role in the entire tropical response to climate perturbations (*Miller* 1997). *Li et al.* [2008] assessed the fidelity of GCMs in simulating LWP using retrieved LWP from several satellites with passive sensors and the vertically-resolved LWC from the CloudSat. The LWP from GCMs are much larger than the

observed estimates and the ECMWF and MERRA analyses. The largest values in the CloudSat LWP occur over the boundary layer Sc regions and this feature is not evident in the analyses or models. Better agreement is found between the two analyses and CloudSat LWP when cases with surface precipitation are excluded. *Medeiros and Stevens* [2011] compared the BL clouds from four GCMs with ERA-40 observations and concluded that the Sc clouds are under-predicted by all the GCMs compensating with the greater frequent trade wind Cu. It is therefore vitally important that in GCMs Sc cloud fields are accurately represented.

The diurnal cycle of marine stratiform clouds has an important influence on their radiative effectiveness, as it affects the radiation budget primarily through their albedo. Stratocumulus clouds can exhibit a marked diurnal cycle (*Wood et al.* 2002). During the night, turbulence is driven by a strong long-wave radiative cooling near the top of the Sc clouds and results in vertically well-mixed stable boundary layer. In contrast, during daytime the transport of heat and moisture from the surface into the cloud layer will be effectively reduced or will even be cut off due to the absorption of solar radiation in the cloud layer and hence the stable boundary layer can become decoupled. Because entrainment maintains a steady supply of relatively warm and dry air from above the inversion into the cloud layer, the cloud layer can rapidly thin or even disappear during daytime. In its Fourth Assessment Report the Intergovernmental Panel on Climate Change (IPCC-AR4) [*Forster et al.* 2007] highlights the diurnal cycle of thin, stratiform clouds to be one of the major uncertainties in current estimates of cloud radiative forcing. *Wilson and Mitchell* [1986] shown that, changing the resolution of the diurnal cycle of cloud and radiative fluxes in an AGCM can affect the simulated climate. *Rozendaal et al.* [1995] inferred that, calculated with diurnally averaged cloud fraction overestimate cloud forcing by up to 3 Wm^{-2} (16%) at the surface and 3 Wm^{-2} (7%) at the top of the atmosphere compared to calculations that account for the diurnal cycle. Comparisons of the observed diurnal cycle of clouds with models also find large and potentially systematic errors in the modelled diurnal cycle [*O'Dell et al.* 2008; *Roebeling and van Meijgaard* 2009]. Similarly, a recent study on aerosol climate influences by the U.S. Climate Change Science Program [*Chin, et al.*, 2009] identifies the diurnal cycle of clouds as one important outstanding science issue. These results suggest that accurate measurements of diurnal properties of Sc clouds are crucial for radiation budget calculations in climate model simulations.

EUMETSAT's SEVIRI is the first space-borne instrument with the necessary temporal, spatial, and spectral resolution to resolve the diurnal cycle of clouds. The objective of the project was to use the existing CM-SAF dataset of cloud microphysical and optical properties from

SEVIRI as well as cloud liquid water path from passive microwave observations to study the diurnal cycle of clouds, with a focus on the diurnal cycle of marine boundary layer clouds.

Droplet number concentration (*CDNC*) is a major parameter affecting cloud physical processes and cloud optical characteristics, and hence to alter the estimate of cloud radiative forcing and aerosol indirect effect. In most climate models, *CDNC* is usually assumed to be constant or a function of the aerosol number concentration. Using constant value in the gamma size distribution of *CDNC* is not unique for all clouds, and moreover *CDNC* is a function of temperature and can affect SW cloud forcing. A comparison of relationships between *CDNC* and aerosol concentration indicates that estimates of *CDNC* from aerosol concentration can have an uncertainty of about 30–50 cm^{-3}, resulting in up to a 42% uncertainty in cloud SW radiative forcing. *Gultepe and Isaac* [2004] suggested, use of relationships between *CDNC* and T, to improve climate simulations. In plane-parallel RT model *CDNC* is retrieved based on cloud radiance measurements and assuming adiabatic conditions. *Brenguier et al.* [2000] inferred that the retrieved *CDNC* is usually underestimated the measurements. The underestimation in *CDNC* leads to larger droplets and more absorption, which imply less radiation reflected at top-of-atmosphere, and this will introduce large error in the radiation budget and hence the climate simulations. Hence, *CDNC* should be estimated to certain accuracy level. Here we evaluated *CDNC* from SEVIRI retrievals and Bennartz [2007].

This study uses cloud products retrieved from SEVIRI measurements using the algorithm developed and run operationally in the CM-SAF. A general overview on the CM-SAF is given in [*Schulz, et al.* 2009]. Basic information on the CM-SAF cloud products used in this study can be found in *Roebeling et al.* [2006] and *Meirink et al*. [2010]. A necessary first step in the working with satellite estimates of LWP is the evaluation of the accuracy of the different datasets. This is especially of importance as SEVIRI is a comparably new instrument and little experience with the stability of SEVIRI retrievals over the course of the day exists. Validation of CM-SAF LWP estimates using ground-based radiometers and radiometer networks have been reported in [*Greuell and Roebeling* 2009; *Roebeling et al*. 2008a; *Roebeling et al*. 2008b]. While this approach can take advantage of the greater accuracy of the ground-based instruments, these are not available for the study area.

Recently, a large number of papers have studied the differences in liquid water path retrieval based on passive microwave and visible/near-infrared satellite observations [*Seethala and Horvath* 2010; *Wilcox et al.* 2009; *Greenwald* 2009; *Bennartz* 2007; *Borg and Bennartz* 2007; *Horvath and Davies* 2007]. Differences between the two methods have been shown to be

correlated with various factors, including cloud fraction, observation geometry, retrieval assumptions, aerosol above clouds, and others. No clear picture has yet emerged. This is partly caused by the correlative nature of the satellite studies, which does not necessarily allow establishing causal relations. A few issues are relatively clear. A slight (mostly) positive bias of passive-microwave derived LWP in cloud-free situations in the order of 10-15 g/m^2 exists, which is cross-correlated with other retrieved variables [*Greenwald* 2009; *Greenwald et al.* 2007]. Also, agreement appears better for more stratiform clouds, where a near-adiabatic cloud liquid water profile can be assumed. Recent studies have revealed a significant bias of cloud SW radiative forcing due to the plane parallel assumption, *Rossow et al.* [2002] reported an overestimation of up to 13 Wm^{-2} in ISCCP and *Oreopoulos et al.* [2009] reported an overestimation of up to 6 Wm^{-2} for liquid water clouds in MODIS.

Because microwave and optical techniques represent fully independent approaches the analysis of retrieval discrepancies can reveal major algorithmic shortcomings, although does not necessarily establish absolute accuracies. Here, the approach of comparing SEVIRI visible/near-infrared observations with passive microwave observations is followed as well. Since the diurnal cycle is targeted here, the use of TRMM observations appears particularly useful. The non sun-synchronous orbit of TRMM allows for a comparison of observations at different local times. Over the course of a month the entire (daylight) diurnal cycle can be evaluated. The TRMM data used in this study were obtained from Remote Sensing Systems and were derived using the algorithms described in [*Hilburn and Wentz* 2008]. The error characteristics and uncertainties of these data are similar to SSM/I and AMSR-E estimates. Various sources of error and potential uncertainties are listed for example in [*O'Dell et al.* 2008].

Another aspect of this project is to evaluate the impact of sub-pixel scale cloud variability in SEVIRI retrievals. Geostationary imagers sample at a coarser resolution than polar imagers. The SEVIRI cloud properties are retrieved at 3x3 km^2 resolution but the MODIS retrievals are done at 1x1 km^2 resolution. A coarser resolution gives rise to systematic biases in the derived cloud physical properties, especially when the cloud is heterogeneous. According to *Henrich et al.* [2010] the resolution with the least bias in the retrieval of optical thickness seems to be the 1km×1km pixel area. Thus, to investigate the pixel size effect on SEVIRI retrieved cloud properties, we compare them with the high resolution MODIS retrievals, which could provide some estimate of the introduced error in SEVIRI due to coarser pixel size.

This report is structured as follows. The datasets are described in section 2 and then the methodology is given in section 3. The results are discussed in section 4, basically the domain

mean statistics, spatial distribution, and the diurnal cycle of cloud properties from SEVIRI and LWP comparison with TMI. We further evaluated the retrieval artifacts of absorbing aerosols over the Sc clouds, and overviewed the cloud fraction dependence and solar zenith angle effect on SEVERI CPP. Finally, the effect of sub-pixel-scale variability in SEVIRI retrievals is shown in comparison with MODIS high resolution retrievals. A short conclusion is given in section 5.

2. Data Description

2.1 Spinning Enhanced Visible and InfraRed Imager (SEVIRI)

The Spinning Enhanced Visible and Infrared Imager (SEVIRI) is an optical radiometer onboard METEOSAT-9 geostationary satellite developed by the European Space Agency (ESA) and operated by the European Organization for the Exploitation of Meteorological Satellites (EUMETSAT). SEVIRI measures radiances at 12 spectral channels with 4 VIS/NIR channels (0.4 – 1.6 µm) and 8 IR channels (3.9 – 13.4 µm), and produces one image in every 15 minutes.

The CM-SAF CPP (cloud physical properties) algorithm, developed at KNMI, retrieves cloud optical thickness and cloud particle effective radius based on measured reflectances at 0.6 µm and 1.6 µm channel. The retrieval scheme is described in *Roebeling et al.* [2006], and is based on earlier methods that retrieve cloud optical thickness and cloud particle size from satellite radiances at wavelengths in the non-absorbing visible and the moderately absorbing solar infrared part of the spectrum (*Nakajima and King* 1990; *Han et al.* 1994; *Nakajima and Nakajima* 1995; *Watts et al.* 1998). The Liquid Water Path (LWP) is computed from the retrieved optical thickness (τ) and droplet effective radius (r_e) by (*Stephens* 1978): $LWP = 2/3\ \tau\ r_{e(1.6\mu m)}\ \rho_l$, where ρ_l is the density of liquid water. The SEVIRI retrievals are available only during daytime and the retrievals are performed assuming that the clouds are plane parallel. In case of 3D broken cloud fields measured radiance is average of the cloudy and cloud-free part of a pixel, and this could introduce error in retrieved cloud properties due to the non-linear relationship between cloud optical thickness and reflectance. Also, SEVIRI retrieves *CDNC* following *Boers et al. [2006]* method based on plane-parallel RT. *Bennartz* [2007] calculated *CDNC* from the retrieved τ and r_e. Here we compare *CDNC* from Boer's and Bennartz's method, and a general negative difference in *CDNC* and an associated positive difference in cloud depth are observed in Boer's method compared to Bennartz's method. However, the true *CDNC* can be judged only from the actual observations.

The CPP products used in this study have been generated at KNMI. They differ from the official CM-SAF products in a number of ways: (i) a local (KNMI) cloud mask rather than the CM-SAF cloud mask has been used to identify cloudy pixels, (ii) latest information on instrument calibration has been used, (iii) algorithm improvements with respect to atmospheric correction have been introduced (*Meirink et al.* 2009), (iv) the full 15-minute SEVIRI dataset was processed instead of an hourly dataset processed operationally in CM-SAF, and (v) compared to the standard CMSAF products optical thickness and LWP, additional cloud (micro-)physical properties were derived.

2.2 Moderate Resolution Imaging Spectroradiometer (MODIS)

MODIS is a key instrument aboard the Terra (EOS AM) and Aqua (EOS PM) satellites. Terra's orbit around the Earth is timed so that it passes from north to south across the equator in the morning, while Aqua passes south to north over the equator in the afternoon. Terra MODIS and Aqua MODIS are viewing the entire Earth's surface every 1 to 2 days, acquiring data in 36 spectral bands.

Similar to SEVIRI, MODIS uses VIS/NIR technique to retrieve cloud properties. Over the ocean, MODIS uses the 0.86 μm visible band containing optical thickness information, in conjunction with one of three water-absorbing near-infrared bands located at 1.6, 2.2, and 3.7 μm, which are sensitive to the droplet effective radius. Although all three near-infrared channels generally observe the upper portion of clouds, vertical sampling of droplets becomes progressively deeper from 3.7 to 1.6 μm due to decreasing absorption [*Platnick*, 2000]. The operational LWP parameterization relies on the 2.2 μm band and assumes no vertical variation in cloud droplet size, leading to $LWP = 2/3\ \tau\ r_{e(2.2\mu m)}\ \rho_l$. (Note that LWP is only estimated if both τ and r_e retrievals are successful; the latter often fail in thin clouds leading to fewer LWP retrievals than cloudy pixels.) Presumed vertical homogeneity in combination with cloud top effective radius retrievals can lead to LWP biases of both signs depending on the actual droplet profile. For example, in the absence of τ and r_e retrieval errors, LWP would be an overestimate in marine Sc clouds, where the effective radius often increases linearly from cloud base to top. For such boundary layer clouds, an adiabatic model has been proposed based on cloud top effective radius $r_{e,top}$ [*Wood and Hartmann*, 2006] $LWP = 5/9\ \tau\ r_{e(2.2\mu m)}\ \rho_l$, which reduces operational MODIS LWP by a factor of 5/6 or 17%. Because this model does not consider entrainment mixing, it represents only a first-order LWP correction in mostly subadiabatic marine Sc. In addition, if r_e

decreases with height, which might occur in drizzling or raining clouds, could even exacerbate the underestimation of LWP.

2.3 TRMM Microwave Imager (TMI)

The TRMM Microwave Imager (TMI) is a well-calibrated, 5 channel, dual-polarized, passive microwave radiometer orbits at an altitude of 400 km and continuous monitor the tropics between 40°S and 40°N. Unlike SSM/I (in a near-polar, sun-synchronous orbit), the TRMM satellite travels west to east in a semi-equatorial orbit, this produces data at different local times for any location. The radiometer measures the microwave radiation emitted by the Earth's surface and clouds at frequencies of 10.7, 19.4, 21.3, 37, 85.5 GHz. The Wentz' absorption-emission based algorithm (*Wentz* 1997; *Wentz and Spencer* 2000) is used to retrieve several important meteorological parameters such as sea surface temperature (SST), surface wind speed (W), water vapor path (V), liquid water path (LWP), and rain rate (R), over the ocean. Our primary interest, LWP, is derived from 37 GHz observations at a resolution of 13 km, but here we used the 0.25° gridded daytime product.

2.4 Ozone Monitoring Instrument (OMI)

Areas affected by biomass smoke or desert dust were identified using OMI ultraviolet Aerosol Index (AI). OMI AI represents the deviation of measured 354-nm radiance from model estimates calculated for a purely molecular atmosphere bounded by a Lambertian surface, with positive values indicating the presence of absorbing aerosols [*Torres et al*. 2007]. A distinguishing feature of OMI AI is its ability to detect absorbing aerosols above (and even mixed with) clouds. Specifically, we used the daily Level-2 gridded product (OMAERUVG) and averaged 13x24-km footprint data to 0.25° resolution.

3. Methodology

To investigate the diurnal cycle of cloud liquid water path annually and in different seasons, we have processed a full one year June 2008 to May 2009 of data from SEVIRI, TMI, and MODIS. SEVIRI 3kmx3km data is downscaled to TMI resolution and collocation is done for those SEVIRI retrievals within TMI observation time of +/-7.5 minutes. As such, the mean liquid water path is representative of the mean in-cloud liquid water path. To compare it with TMI grid-box mean, we scaled it with the liquid cloud fraction (the fraction of SEVIRI liquid pixels within a TMI grid-box) calculated from SEVIRI measurements. Similarly, for a matching

comparison both Terra and Aqua MODIS data have been downscaled independently to 0.25^{o}x0.25^{o} which is TMI resolution. For the comparisons between SEVIRI and MODIS observations, original SEVIRI 3kmx3km data were downscaled and collocated based on those pixels within MODIS observation time of +/-5 minutes. These collocated SEVIRI data are termed SEVIRI_M.

Our entire study domain is roughly 50^{o}x50^{o} covering [30^{o}W-20^{o}E, 35^{o}S-10^{o}N] over the South Atlantic Ocean. Near the Namibian coast, Sc sheets form over relatively cold SSTs, in shallow and generally well mixed boundary layers capped by a strong temperature inversion. As these air masses are advected equatorward, the Sc decks transition into scattered cumulus due to the increase in SST and the associated decrease in lower tropospheric stability. Ultimately, the stratocumulus is replaced by scattered, predominantly shallow cumulus (trade wind Cu). Thus our study domain is frequently covered by extensive sheets of sub-tropical marine Sc clouds, trade wind Cu with significantly lower cloud cover, and deep convective clouds. The presence of ice cloud above masks water clouds below in VIS/NIR retrievals. Also, the microwave signal is sensitive to liquid cloud and rain, and the rain retrieval is performed assuming a fixed rain-threshold of 180 gm^{-2} which can introduce a systematic error in retrieved LWP. Thus, in this study we examine the mean and diurnal characteristics of only low-level non-raining warm/liquid clouds to avoid instrumental sensitivity to rain and ice. These low-level clouds consist of optically thick homogeneous Sc clouds and more broken optically thin trade wind Cu clouds. We have noticed that the amount and the location of these stratocumulus decks varied from month to month depending on where the sun is. Thus, we have selected Sc clouds based on the location of 75^{th} percentile cloud fraction threshold and their connected neighbors that fall within the selected (frequent occurrence of Sc) region, which will locate our exact Sc field. However, for more broken trade wind Cu regime we have chosen a 10^{o}x10^{o} grid-box depending on their frequent occurrence.

4. Results and Discussion

(i) SEVIRI *versus* TMI

4.1 Effect of Absorbing Aerosols on SEVIRI Retrievals

In this section we examine the impact of absorbing aerosols residing above South Atlantic Sc clouds. Biomass burning is a significant source of tropospheric aerosols in southwestern Africa during the dry season JASO (July-August-September-October) and

produces episodic plumes of dark smoke over the southeast Atlantic Ocean. The mean aerosol index map from OMI for JASO 2008 is depicted in Fig 4.1.1. Aerosol index is an index that detects the presence of UV-absorbing aerosols where positive values generally represent absorbing aerosols such as dust and smoke and small or negative values represent non-absorbing aerosols and clouds. From the figure it is clear that the smoke absorption is higher near the Namibian coast and reduced as we go away from coast. Beneath the elevated layer of smoke is a persistent deck of bright marine Sc cloud. When smoke resides above low-level clouds, the measured visible (0.6 or 0.8 µm) channel reflectance will be decreased due to the absorption by smoke, which can introduce a negative bias in both droplet effective radius and optical thickness, and hence in SEVIRI LWP. This negative bias in the 1.6 µm effective radius is significantly larger compared to 2.2 µm effective radius which is usually less than 1 µm, however, it can be up to 30% in optical thickness according to calculations by *Haywood et al.* [2004]. In SEVIRI 1.6 µm retrieval, a strong decrease in the effective radius from 11 to 7 µm is observed (Figs 4.1.2d and 4.1.3d) even for the smaller aerosol index of 3.5. *Bennartz* [2007] noted a systematic MODIS LWP underestimation in Sc off southern Africa during the biomass burning season, which was attributed to overlying absorbing aerosols by *Bennartz and Harshvardhan* [2007]. In the same region and season, *Wilcox et al.* [2009] estimated a domain-mean absorbing aerosol effect of 5.6 gm^{-2}, corresponding to less polluted case. *Seethala and Horvath* [2010] also estimated a mean negative bias of 3 gm^{-2} in MODIS LWP over a larger $25^{o}x25^{o}$ South Atlantic Sc domain.

Here, we estimated the bias in SEVIRI LWP for JASO over our entire study domain and aerosol dominated Sc domain. Over this domain the mean AI ranges up to 3.5. As shown in Fig 4.1.2 and 4.1.3 SEVIRI increasingly underestimated TMI as a result of reduced optical thickness and droplet effective radius. The TMI-SEVIRI LWP bias increased with aerosol index over Sc domain and in the entire domain. Over the domain the LWP underestimation due to the presence of smoke is ~27 gm^{-2}, however the individual values can go > 40 gm^{-2} even at the AI of 2.5 (Fig 4.1.2b and 4.1.3b). *Coddington et al.* [2010] found that overlying absorbing aerosol layer above stratus cloud biases SSFR cloud retrievals to smaller effective radii and optical thickness based on the aircraft measurements (cloud retrievals) of Solar Spectral Flux Radiometer (SSFR) irradiance (below aerosol layer above cloud layer, and above aerosol layer) during the Intercontinental Chemical Transport Experiment (INTEX-A) and also using a forward radiative transfer model.

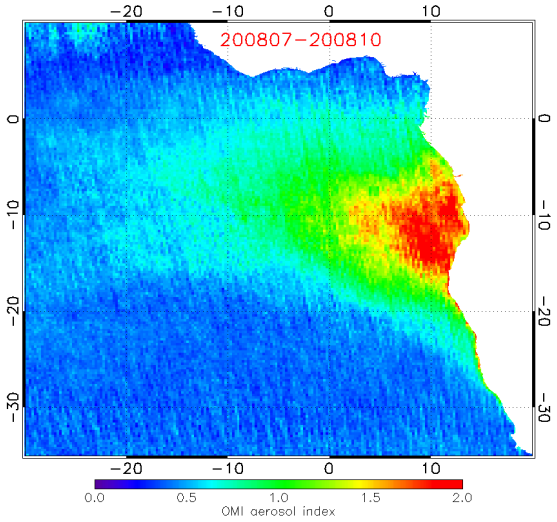

Fig 4.1.1: *OMI aerosol index averaged for JASO 2008*

The results from Fig 4.1.2a and 4.1.3a indicated an increase in LWP with aerosol index, which is observed in both TMI and SEVIRI measurements. TMI showed a strong LWP increase from 60 to 100 gm^{-2} as the aerosol loading varies from 0.25 to 3.5, however SEVIRI increase is less prominent and the increase is reduced drastically with aerosol index. We also found an increase in cloud thickness with AI from SEVIRI measurements. The optical thickness also increased from 4.5-8.5 (7-12 for Sc domain) for the study domain with aerosol index, however this increase could have been larger for the less polluted cases, as absorbing aerosol above cloud underestimate the retrieved optical thickness. These results are similar to a recent observational study where *Wilcox* [2010] examined the consequences of smoke from seasonal biomass burning in the West African overlay the persistent southeast Atlantic Sc cloud deck, using CALIPSO measurements. He found that the diurnal mean SW heating rate has been increased in case of smoke resides above clouds. This extra heating introduced additional warming of 1K in the 700 hPa air temperature above the cloud deck, and increased the buoyancy of free-tropospheric air above the temperature inversion capping the boundary layer. This increased buoyancy inhibits the entrainment of dry air through the cloud-top, thereby helping to preserve humidity and cloud cover in the boundary layer. This also coincides with LWP increase by 20 gm^{-2} lower cloud tops compared to smoke free environment. The modeling study also confirm these results, for example: *Johnson et al.* [2004] used LES and shown an increase in LWP when absorbing aerosols reside above Sc clouds. Using an atmospheric general circulation model (GFDL AGCM) *Randles and Ramaswamy* [2010] indicated that strong atmospheric absorption from these particles can cool the surface and increase upward motion and low-level convergence over

southern Africa during the dry season, and finally increase in clouds. However we doubt that higher aerosols loading samples are also coincident with thicker clouds.

Further, while sampling SAFARI-2000 data offshore of West Africa, *Hobbs* [2002] *and McGill et al*. [2003] argued that smoke was typically observed in layers that were vertically separated from Sc clouds below and hence the direct microphysical interaction between the aerosols and Sc clouds is often inhibited by the strong temperature inversion above the cloud layer. *Wilcox* [2010] confirmed this result from CALIPSO observations that aerosol layers occur predominantly between 2 km and 4 km, but cloud layers are identified predominantly below 1.5 km altitude and beneath the layer of elevated smoke aerosol.

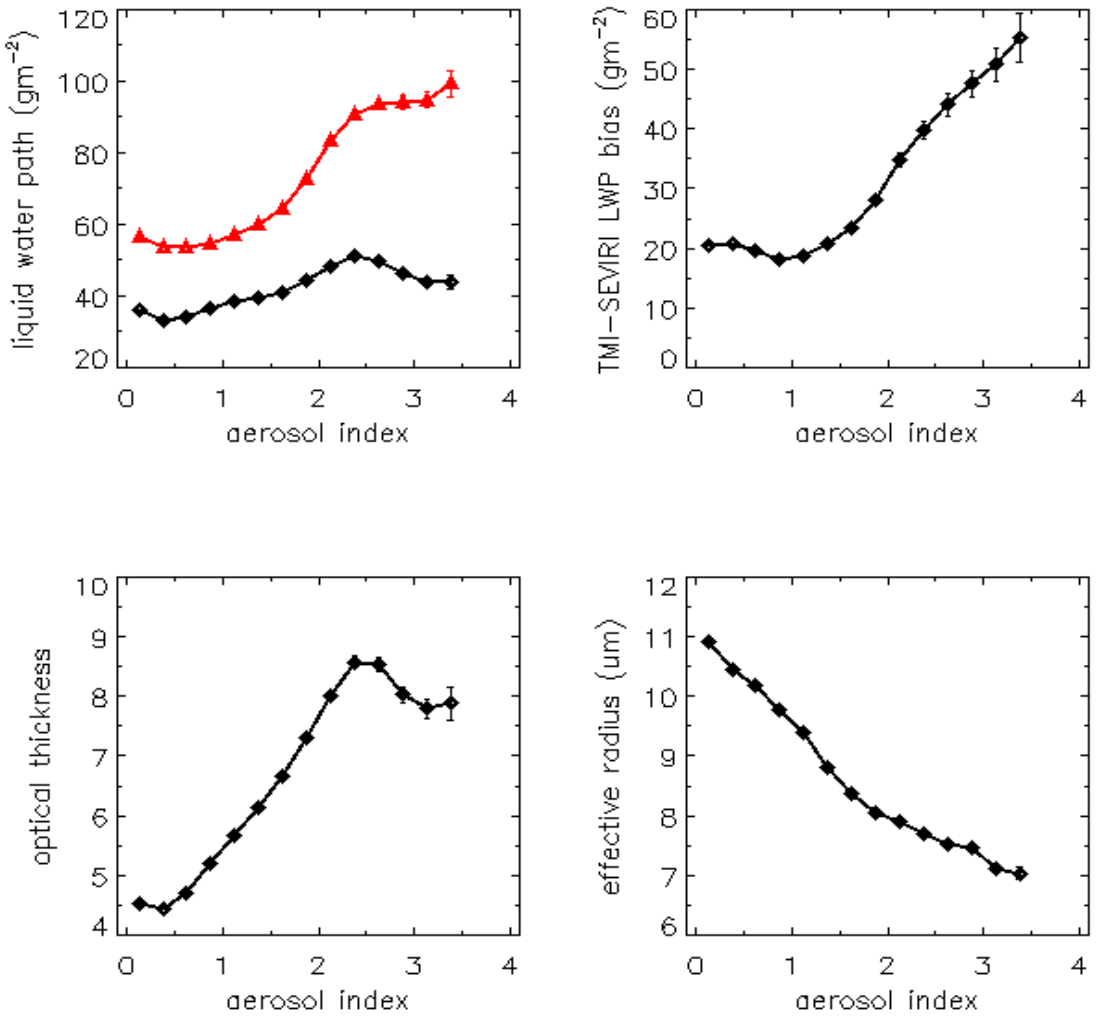

Fig 4.1.2: *Aerosol index versus cloud properties averaged over entire study domain, for JASO 2008*

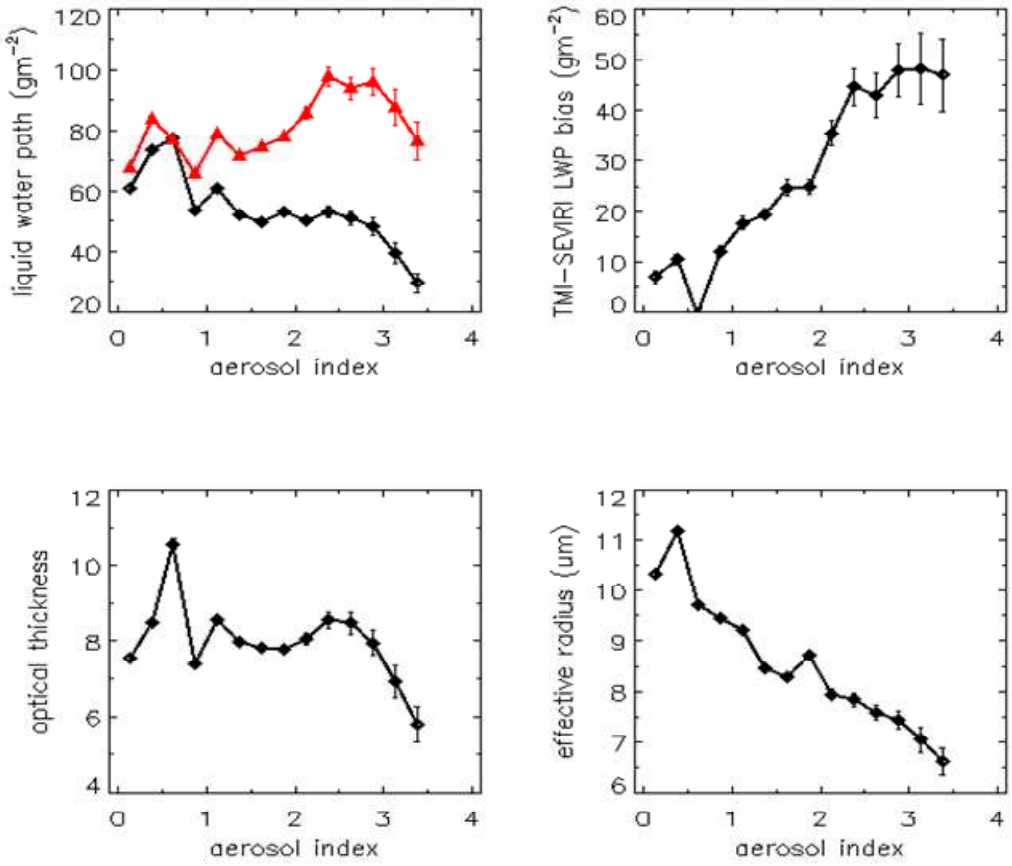

Fig 4.1.3: *Aerosol index versus cloud properties averaged over the Sc domain, for JASO 2008*

We further evaluated the impact of absorbing aerosols over Sc regime especially in the diurnal cycle representation. The diurnal cycle of TMI and SEVIRI CPP averaged for JASO 2008 is presented in Figs 4.1.4-4.1.6. The cloud optical thickness decreased about ~50% from morning to late afternoon, but the droplet effective radius remains more or less stable with time. As a general phenomena 20% decrease in cloud fraction and 100m difference in cloud physical thickness also observed with time. The cloud droplet number concentration also showed a little bit decrease of ~50cm^{-3}. Overall, both TMI and SEVIRI LWP showed a 50% decrease from morning to late afternoon. Both SEVIRI and TMI showed similar variability in diurnal cycle, however a large bias 10-20 g/m^2 is existed between them. This large bias between them is partially removed by considering least polluted cases in the analysis. Figs 4.1.5 and 4.1.6 are the diurnal cycle of TMI and SEVIRI CPP where the polluted pixels are removed, and the results are much more agreement and considerable amount of bias also has been reduced. In Fig 4.1.7 the JASO mean TMI *versus* SEVIRI LWP statistics is revealed, and obviously the LWP bias has been reduced to halve for pixels with AI<1 and the bias is further halved for datasets with AI<0.25. It can also be noticed that SEVIRI liquid water path increased with changing AI

threshold. The mean LWP bias over Sc domain is 16.49 g/m^2. The LWP bias has been reduced from 16.49 g/m^2 to 8.82 g/m^2 when we considered datasets with AI<1. We further neglected those datasets with AI<0.25 which reduced the LWP bias further to 3.73 g/m^2. From the Fig 4.1.7 it is also very clear that the SEVIRI observations are shifted more and more closer to the one-to-one line as we remove more and more aerosol affected pixels. As these absorbing aerosols introduce low bias in SEVIRI LWP, for the further analysis we neglect all the aerosol affected pixels i.e. AI<1.

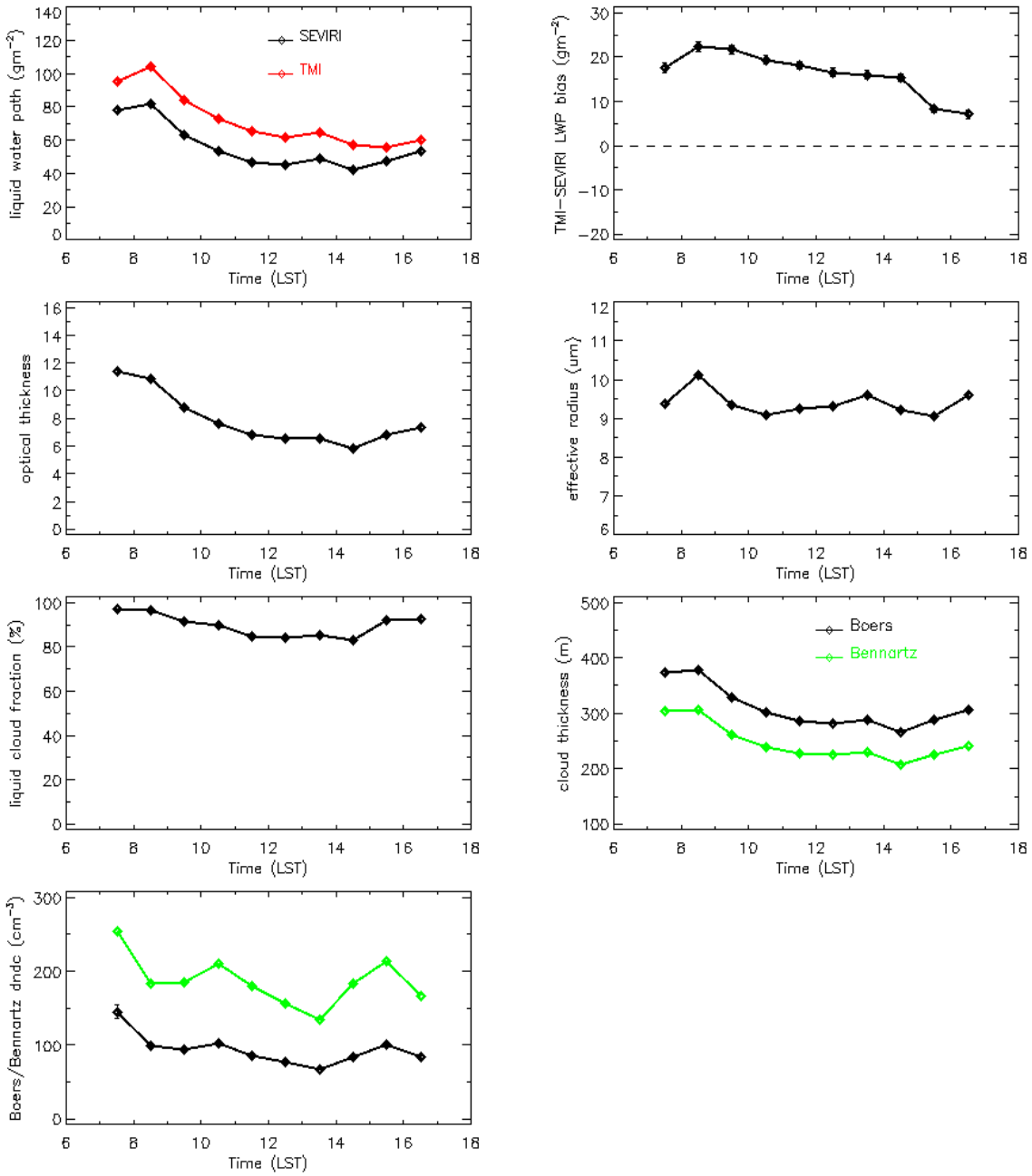

Fig 4.1.4: *Diurnal cycle of CPP over Sc domain averaged for JASO 2008, based on full dataset.*

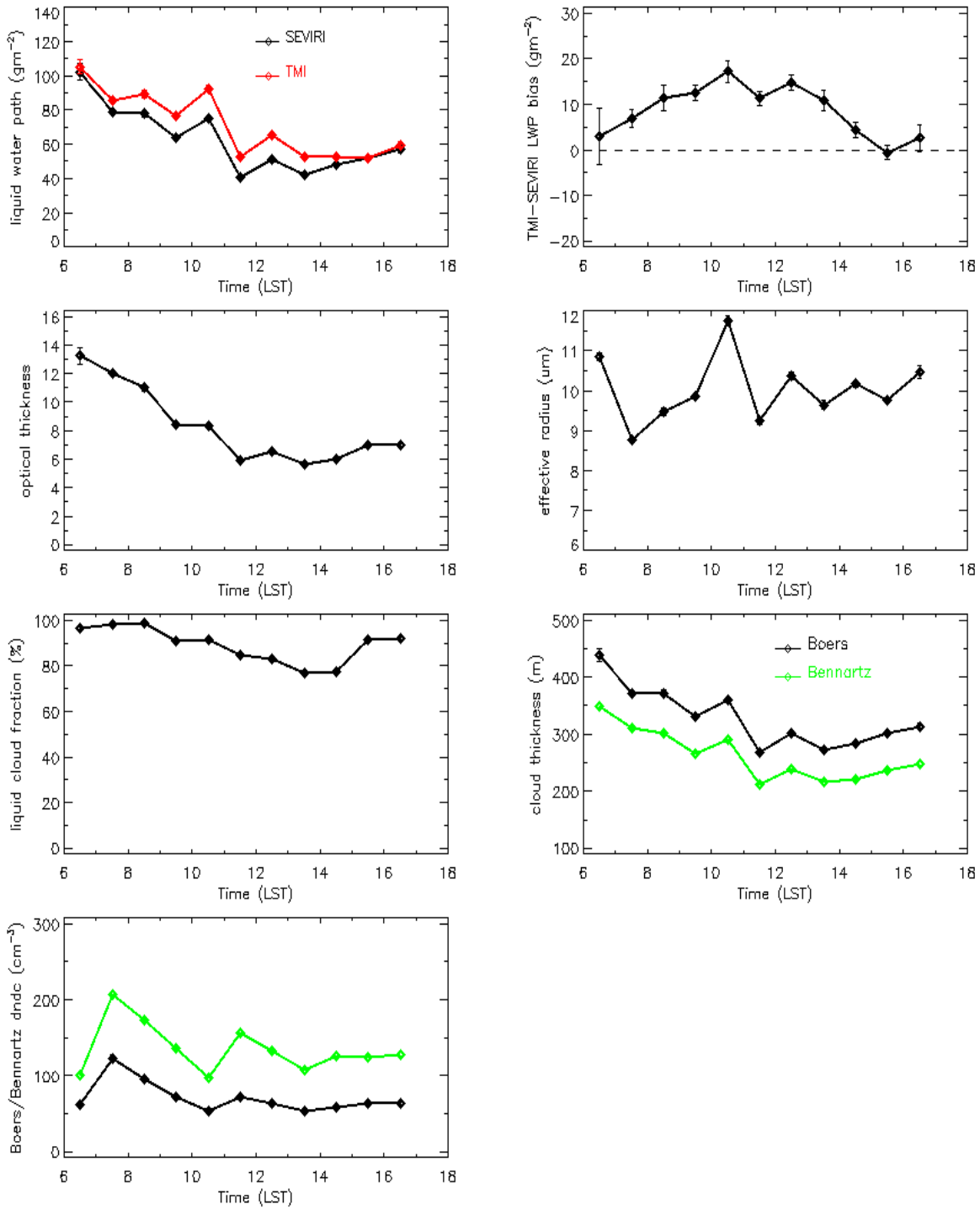

Fig 4.1.5 *Diurnal cycle of CPP over Sc domain averaged for JASO 2008, and for AI<1.*

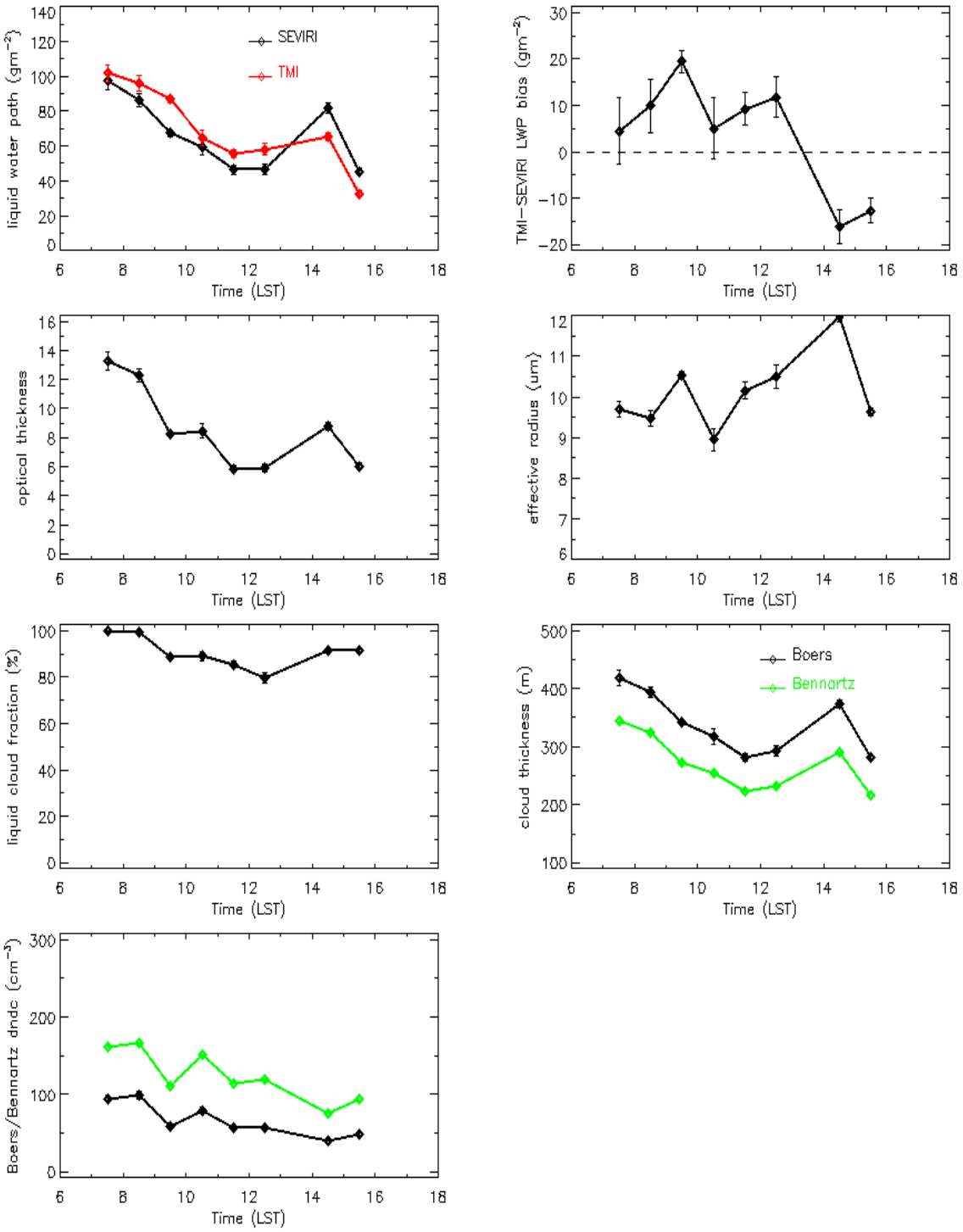

Fig 4.1.6: *Diurnal cycle of CPP over Sc domain averaged for JASO 2008, and for AI<0.25.*

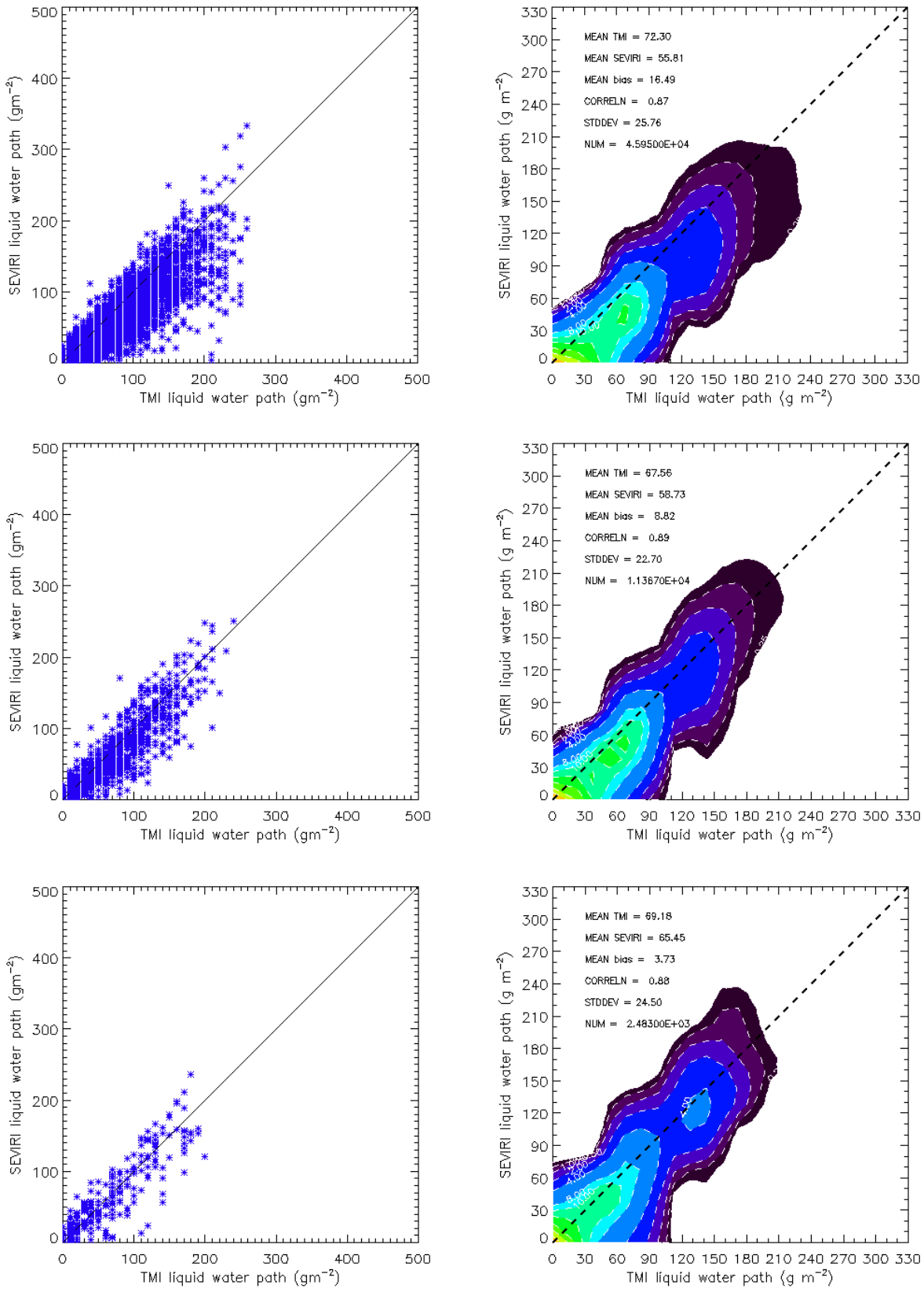

Fig 4.1.7: *JASO mean statistics of SEVIRI versus TMI LWP (top) included all data, (middle) all data but AI<1, and (bottom) all data but AI<0.25 over Sc regime*

4.2 Mean Statistics of Cloud Properties

In this section, we describe the annual and seasonal mean statistics of cloud properties over Sc, trade wind Cu, and entire South Atlantic domain as obtained from both SEVIRI and TMI and shown in Figs 4.2.1 to 4.2.5. Note that Figures we show here are only for AI <1. Over the South Atlantic Sc region both SEVIRI VIS/NIR and TMI microwave techniques showed robust skill to retrieve LWP with largest correlation of 0.9-0.94 as seen in middle panel of Figs 4.2.1 to 4.2.5 annually and in all seasons. Both TMI and SEVIRI showed mean annual LWP of ~45 g/m^2 with small bias of 0.26 g/m^2 and standard deviation of 21 g/m^2. The daytime averaged seasonal LWP variation of SEVIRI *vs.* TMI is 35.64 *vs.* 42.51, 69.24 *vs.* 66.66, 52.24 *vs.* 52.15, and 38.27 *vs.* 38.16 in respective months JJA, SON, DJF and MAM. *Fairall et al.* [1990] estimated the mean Sc LWP of 75 gm^{-2} off the coast of Southern California from the longwave and shortwave irradiance measurements during FIRE from March through October 1987. An average cloud LWP of 120 ± 320 gm^{-2} is reported by *Zuidema and Hartmann* [1995] from SSM/I data averaged over stratus cloud regime. These LWP values are somewhat larger compared to our mean LWPs. However, the mean TMI-SEVIRI LWP bias in our Sc domain is within ±5 gm^{-2} in all the months/seasons, except those months which are affected by absorbing aerosols. In July-August-September-October, the observed mean bias is 10-25 gm^{-2} and SEVIRI retrievals are artificially affected by the absorbing aerosols in these months. As we explained in the previous section, the absorbing aerosols introduce a negative bias in both optical thickness and the effective radius, and hence in the deduced LWP in SEVIRI VIS/NIR retrieval. Neglecting the pixels with larger loading of absorbing aerosols and considering only those pixels with 0<AI<1.0, the bias has been reduced to halve as ~12.5 gm^{-2} in individual months and the bias is even reduced to ~7 g/m^2 seasonally. All together the bias between TMI and SEVIRI LWP is small, compared to AMSR-E-MODIS LWP bias (*Seethala and Horvath* 2010), where MODIS highly overestimated and the overestimation reduced only after applying the adiabatic correction to MODIS LWP. As TMI and AMSR-E retrievals are based on same Wentz's algorithm, these differences may arise from SEVIRI and MODIS retrieval differences. The basic difference between SEVIRI and MODIS is, SEVIRI effective radius retrievals are done based on radiance from 1.6 µm channel which sample clouds slightly deeper compared to MODIS 2.2 µm channel, which is mostly sensitive to top layer of cloud leading larger MODIS droplet effective radius in case of more adiabatic Sc clouds. This could have a significant impact, even if the r_e retrievals are likely to be same in both 1.6 µm and 2.2 µm channels. Another possibility could be, for thin clouds of cloud optical thickness (τ) below 8, SEVIRI CPP algorithm weighs r_e towards r_e-

climatology of 8 µm, but MODIS provides true retrieved values. Again SEVIRI original pixels are an order larger than the MODIS pixels, and as we reduce the resolution the errors in retrieved τ and r_e may cancel-out and get better comparison of SEVIRI with TMI. Another difference could be related to the so-called clearsky restoral applied for MODIS. MODIS retrieves cloud properties only in confident cloudy conditions which may introduce a high bias in optical thickness. On the other hand, SEVIRI retrievals for partly cloud pixels may introduce a low bias in optical thickness. These effects would introduce a high/low LWP bias in MODIS/SEVIRI, respectively. Thus above listed differences could easily explain the difference in MODIS *vs.* AMSR-E comparison and our SEVIRI *vs.* TMI comparison.

Over the trade wind Cu domain, SEVIRI retrieve smaller LWP and TMI retrieve larger LWP compared to Sc domain, which leads a very large positive bias of 15-25 gm^{-2} between TMI and SEVIRI in all seasons, although they showed good correlation of 0.79-0.86. The dominant error sources in both VIS/NIR and microwave technique in the broken cloud fields could explain this bias. Especially, larger 3D effect in VIS/NIR retrieval and non-linear average of reflectances in partial cloudy pixels could introduce negative bias in retrieved SEVIRI LWP. Moreover, weighs r_e towards r_e-climatology of 8 µm for optically thin clouds of $\tau<8$ would introduce strong negative bias in SEVIRI CPP algorithm as these trCu clouds are very thin and often have an optical thickness below 5. Besides, a known positive bias of 12-15 gm^{-2} is also observed in Wentz microwave algorithm in clear-sky cases which suites for broken cloud scenes as well. Unfortunately, these errors cannot be separated from the measurements, and more modeling study is required to quantify them.

Over the entire South Atlantic domain, the correlation in LWP between two techniques varies from 0.48-0.74, with the domain mean positive (TMI-SEVIRI) LWP bias of 8-18 gm^{-2}. The mean LWP varies with season and maximum in November and minimum in February. In this case, SEVIRI seems underestimating the LWP and TMI seems overestimating it in all the seasons. Similarly, a global mean positive bias of 18 gm^{-2} is observed in AMSR-E and MODIS comparison. So, the microwave technique appears to be overestimating the LWP in general, due to their overestimation in broken cloud fields. The annual mean bias is only 12 gm^{-2} with 52 gm^{-2} deviation from mean. MAM showed least bias of around ~7 gm^{-2}, but with larger mean deviation of 66 gm^{-2} and least correlation of 0.48. The largest bias of 18 gm^{-2} is observed for JJA, with mean deviation of 45 gm^{-2} and correlation of 0.64. But for SON and DJF, respective bias is 12 gm^{-2} and 13 gm^{-2}, with mean deviation of 42.5 gm^{-2} and 48.7 gm^{-2} respectively. Over this study

domain, the amount of observed mean liquid water path is largest in September-October-November.

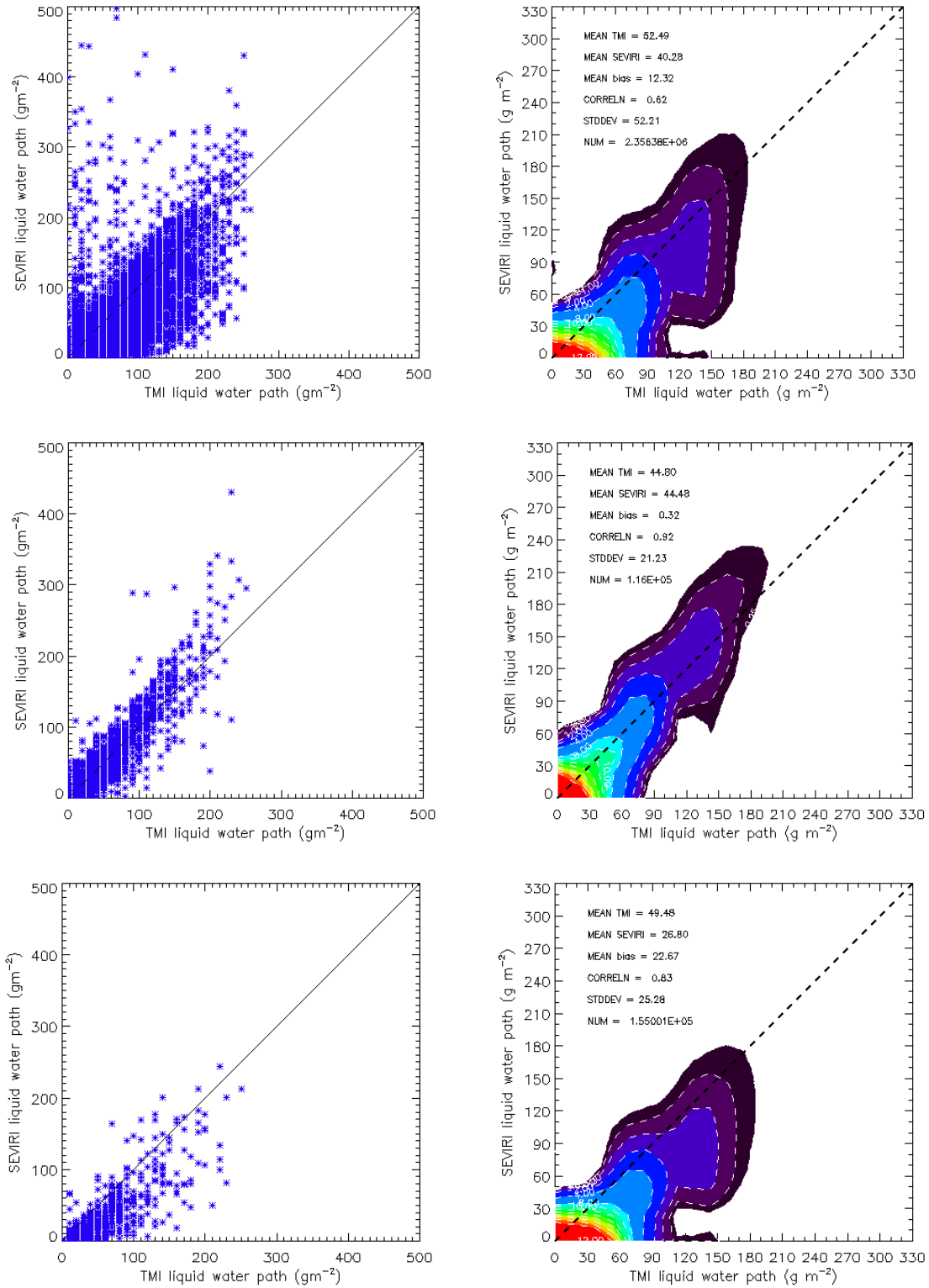

Fig 4.2.1: *Annual mean statistics; with liquid cloud fraction: 0-100%, no rain, no ice, AI<1; (a) top panel, for entire domain, (b) middle panel, only for Sc domain, and (c) bottom panel, for trade wind Cu [10^{o}S-20^{o}S, 10^{o}W-20^{o}W] domain.*

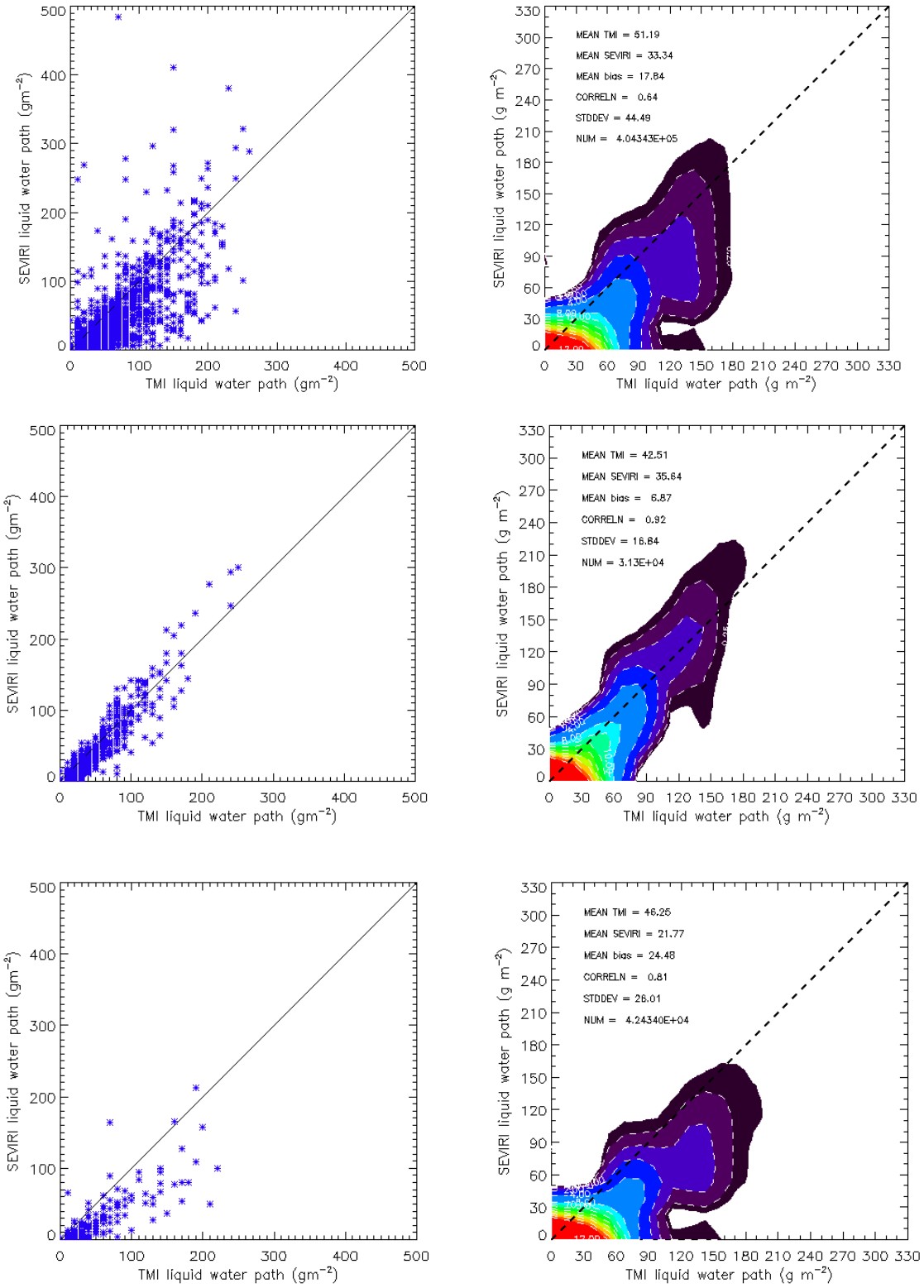

Fig 4.2.2: *June-July-August mean statistics; with liquid cloud fraction: 0-100%, no rain, no ice, AI<1; (a) top panel, for entire domain, (b) middle panel, only for Sc domain, and (c) bottom panel, for trade wind Cu [10^{o}S-20^{o}S, 10^{o}W-20^{o}W] domain.*

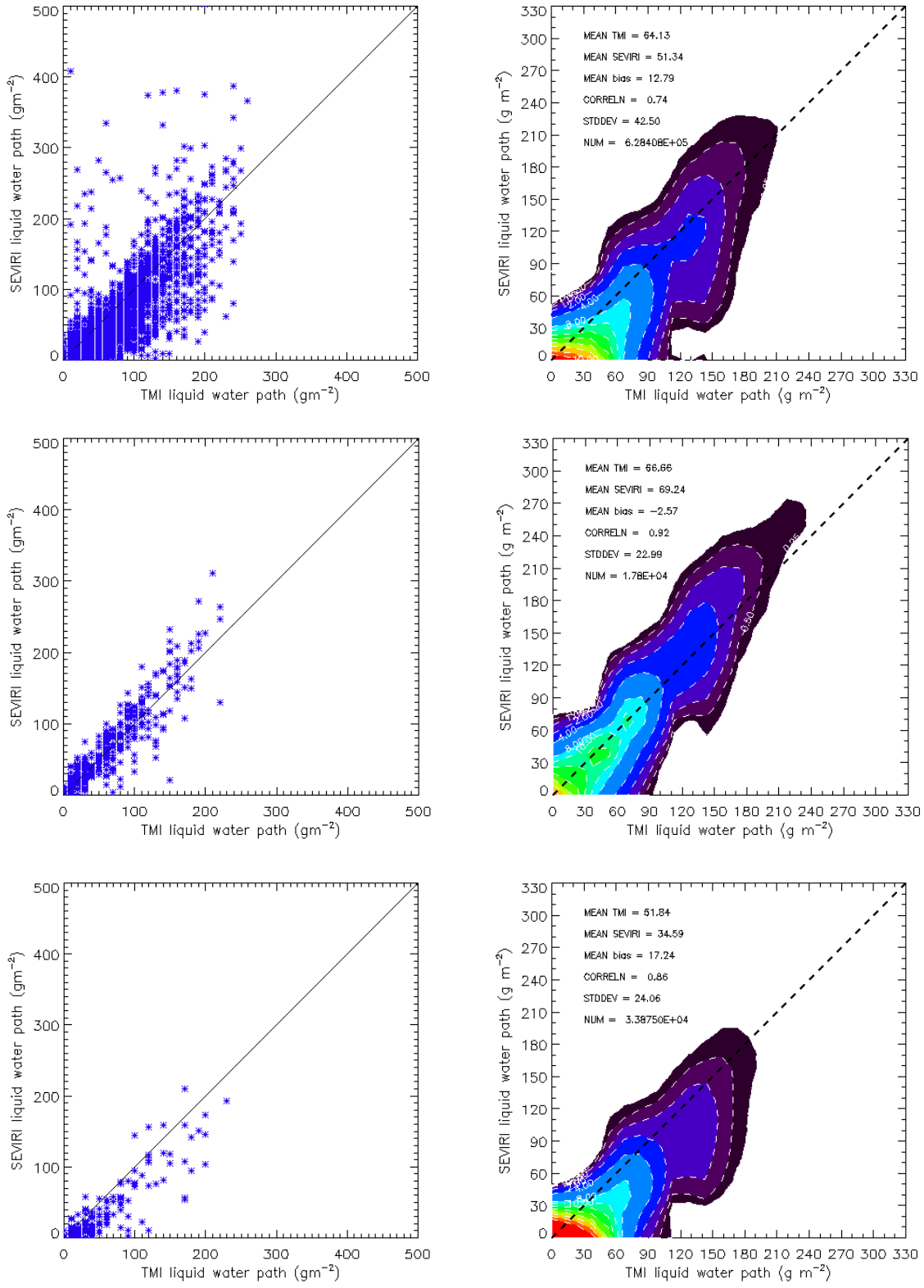

Fig 4.2.3: *September-October-November mean statistics; with liquid cloud fraction: 0-100%, no rain, no ice, AI<1; (a) top panel, for entire domain, (b) middle panel, only for Sc domain, and (c) bottom panel, for trade wind Cu [10°S-20°S, 10°W-20°W] domain.*

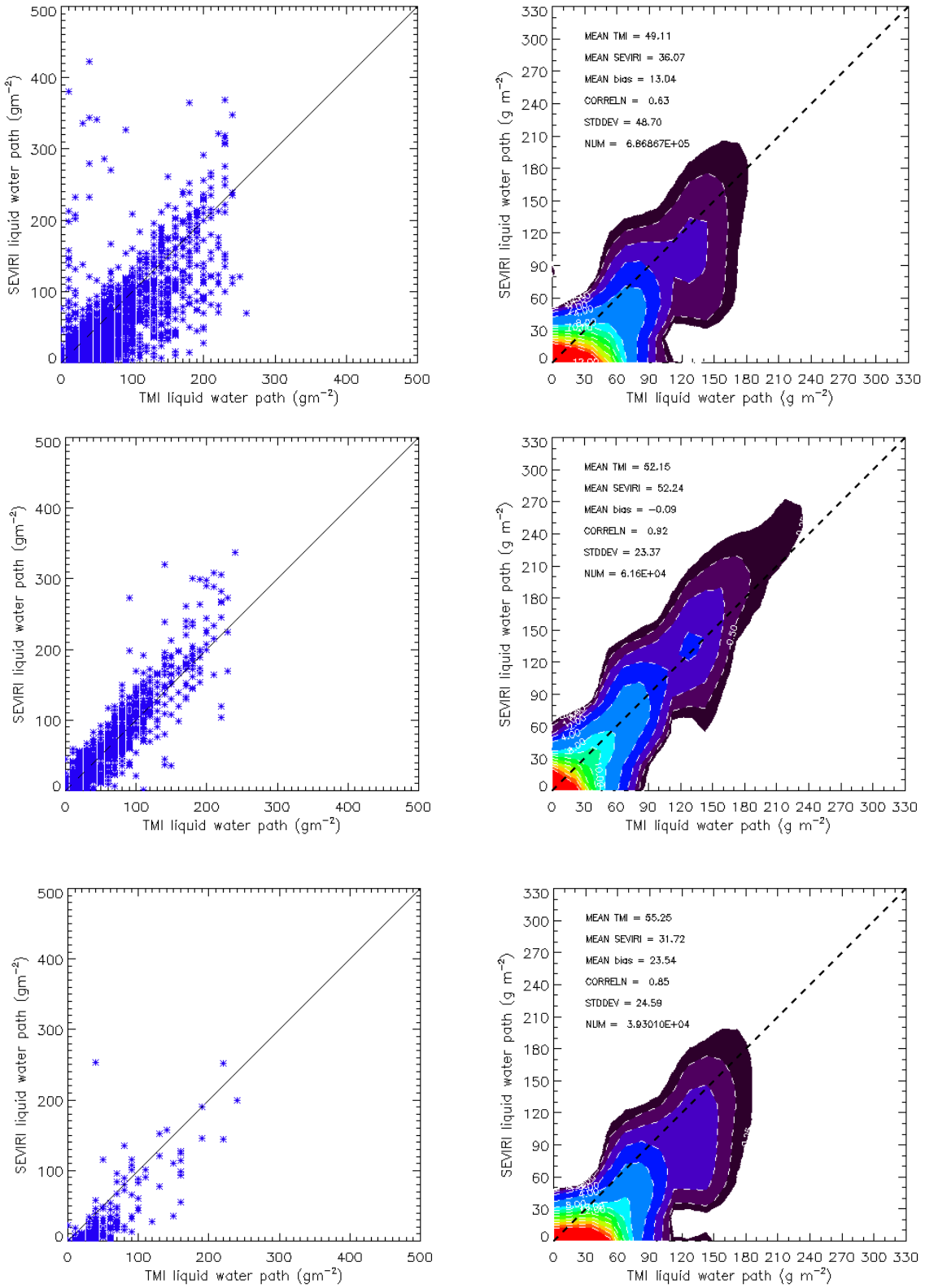

Fig 4.2.4: *December-January-February mean statistics; with liquid cloud fraction: 0-100%, no rain, no ice;; (a) top panel, for entire domain, (b) middle panel, only for Sc domain, and (c) bottom panel, for trade wind Cu [10^{o}S-20^{o}S, 10^{o}W-20^{o}W] domain.*

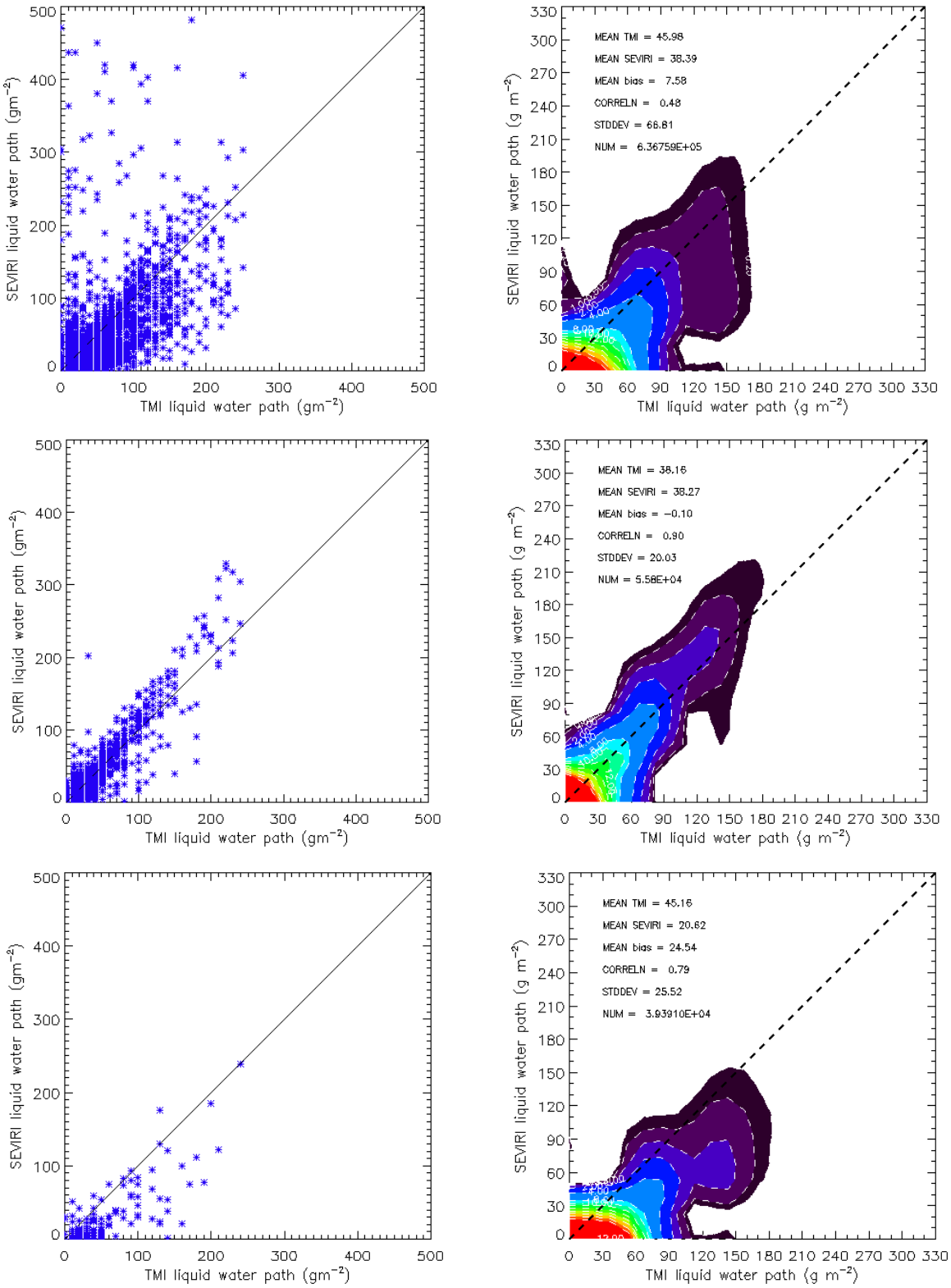

Fig 4.2.5: *March-April-May mean statistics; with liquid cloud fraction: 0-100%, no rain, no ice, AI<1; (a) top panel, for entire domain, (b) middle panel, only for Sc domain, and (c) bottom panel, for trade wind Cu [10^{o}S-20^{o}S, 10^{o}W-20^{o}W] domain.*

4.3 Spatial Distribution of Cloud Properties

In this section, we discuss the annual and seasonal mean maps of TMI and SEVIRI cloud LWP, TMI-SEVIRI LWP bias, cloud optical thickness (tau), droplet effective radius (r_e), droplet number concentrations calculated based on Boers's and Bennartz's method, and LCF (liquid cloud fraction) of all four seasons, for our 50^ox50^o study domain. *Klein and Hartmann* [1993] used surface-based cloud climatology and showed that there is strong seasonal variability in the amount of stratus clouds, and the seasonal cycle of Sc cloud amount is closely tied to the seasonal cycle of static stability. For the South Atlantic Sc region, the maximum static stability is observed during September-October-November and the minimum in February. They also revealed from Earth Radiation Budget Experiment that the strongest net cloud forcing occurs during the months of August through November. Thus, it is important to examine the seasonal variability of these clouds throughout the year, as it alters the earth's radiation budget directly through net cloud forcing. The below given annual and seasonal mean maps (Figs. 4.3.1 to 4.3.5) are calculated only for no ice, no rain conditions, to reduce obvious first order errors. Overall, SEVIRI mean LWP is much lower compared to TMI mean LWP except over the South Atlantic Sc region, regardless of seasons. Over the marine Sc domain, both SEVIRI VIS/NIR and TMI microwave retrieval techniques showed very good agreement, but often with a very small SEVIRI overestimation. This SEVIRI overestimation over the Sc domain is much smaller compared to MODIS overestimation in this domain compared to AMSR-E LWP (see the AMSR-E-MODIS LWP bias map of *Seethala and Horváth* 2010). The possible reason for the better agreement between TMI and SEVIRI is discussed in the previous section. It is clear that, in JJA and SON the SEVIRI retrieval seems to be highly underestimating LWP over the Sc region, due to the presence of large amounts of absorbing aerosols. Over this Sc domain optical thickness varied from 6 to 10, and the effective radius varied from 7-11. The cloud thickness differs from season to season with annual mean of 350 m. The droplet number concentration is larger during JJA and less in all other seasons. The comparison of CDNC from Boer's and Bennartz's method revealed that there is a factor two difference between calculated CDNC in both methods. The true value can be inferred only after comparing them with the real observations.

The worst agreement in retrieved LWP between the two techniques is observed over the trade wind Cu regime. TMI is retrieving higher LWP compared to SEVIRI. The observed discrepancy might be due to the fact that both VIS/NIR and microwave techniques are less accurate in low cloud fraction scenes for the following reasons:

(a) There is a known TMI positive clear-sky bias which could also be representative of more broken fields

(b) The performance of the SEVIRI cloud mask is unknown, and the cloud mask algorithm is more similar to MODIS; but *Zhao and Di Girolamo* [2006] showed that with a 15-m-resolution cloud mask, MODIS agrees only 62% of the time in trade wind Cu, thus, cloud detection problems in SEVIRI might partly explain this low LWP bias,

(c) 3D radiative effects (solar/view angle effects) are larger over the more broken trade wind Cu,

(d) SEVIRI may underestimate optical thickness due to the nonlinear averaging of visible reflectance versus optical thickness in broken scenes,

(e) Underestimation in SEVIRI optical thickness as the retrievals are performed also for partially cloudy scenes (and not applying clearsky restoral like MODIS does),

(f) for thin clouds of cloud optical thickness (τ) below 8, SEVIRI CPP algorithm weighs r_e towards r_e-climatology of 8 µm which can underestimate true r_e and hence LWP.

In general, over the broken cloud scenes the optical thickness is below 5 with large number of CDNC and larger droplet effective radius (>11 µm) than the Sc regime.

Figure 4.3.6 depicts the monthly/seasonal variation in cloud fraction for twelve months. We can notice from the cloud fraction map, that the distribution and amount of South Atlantic Sc deck is varying from season-to-season or more precisely month-to-month. In SON, we observe a huge amount of these clouds with large spread. In JJA there are relatively less clouds and they are shifted a bit to the north. Lower cloud fraction in seen in MAM and the least is observed in DJF. The results are in agreement with *Klein and Hartmann* [1993] findings that the season of maximum stratus clouds are associated with the season of greatest lower-tropospheric static stability. In South Atlantic Sc region SON showed greatest LTS and DJF showed the least. They also inferred that a 6% increase in stratus fractional area coverage is associated with a 1^oC increase in static stability.

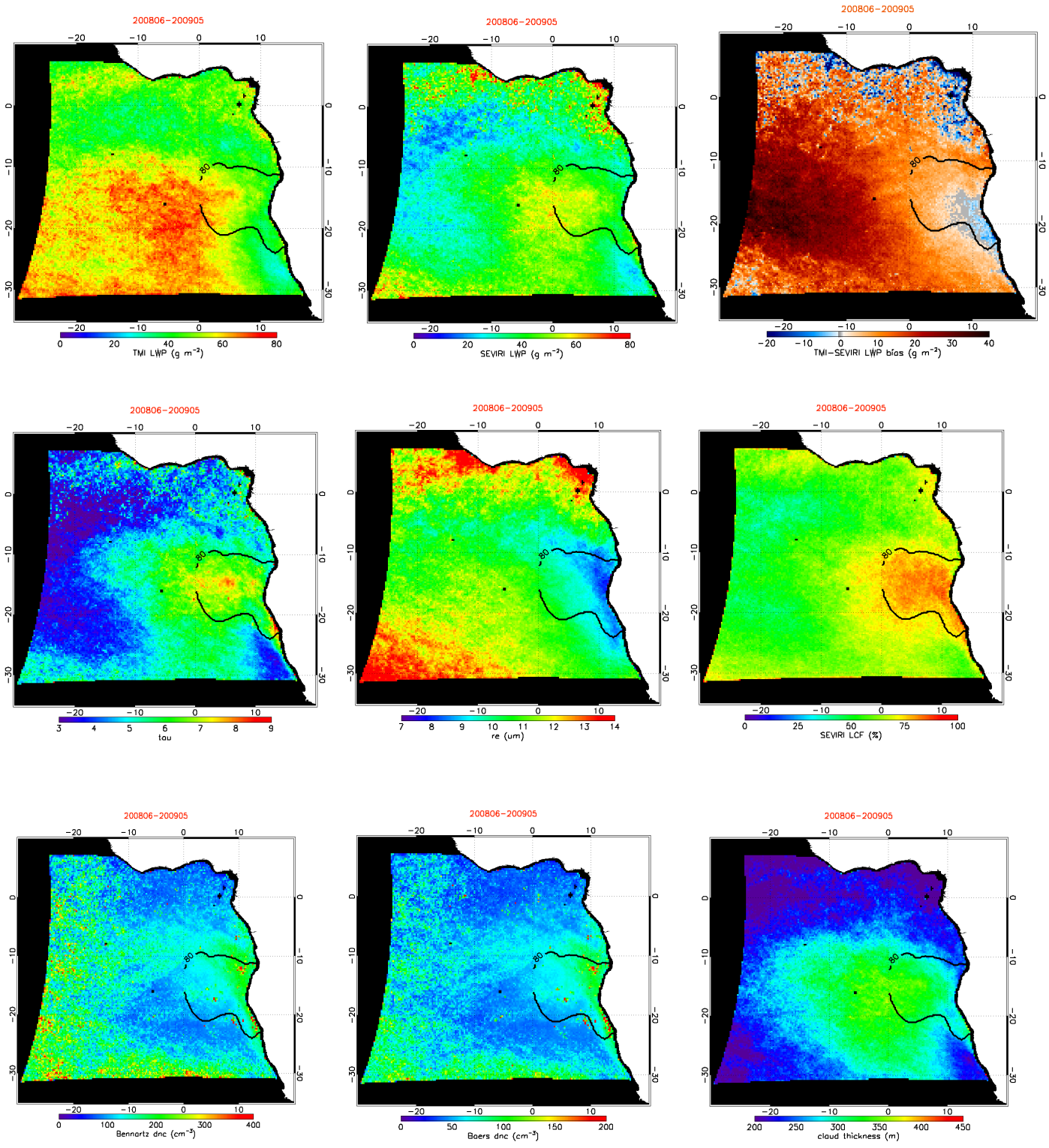

Fig 4.3.1: *Annual mean (a) TMI LWP, (b) SEVIRI LWP, (c) TMI - SEVIRI LWP bias,(d) optical thickness, (e) effective radius,(f) liquid cloud fraction, (g) Bennartz's cdnc, (h) Boer's cdnc, and (i) cloud thickness. The black contour denotes the 75th percentile of cloud fraction over the study domain..*

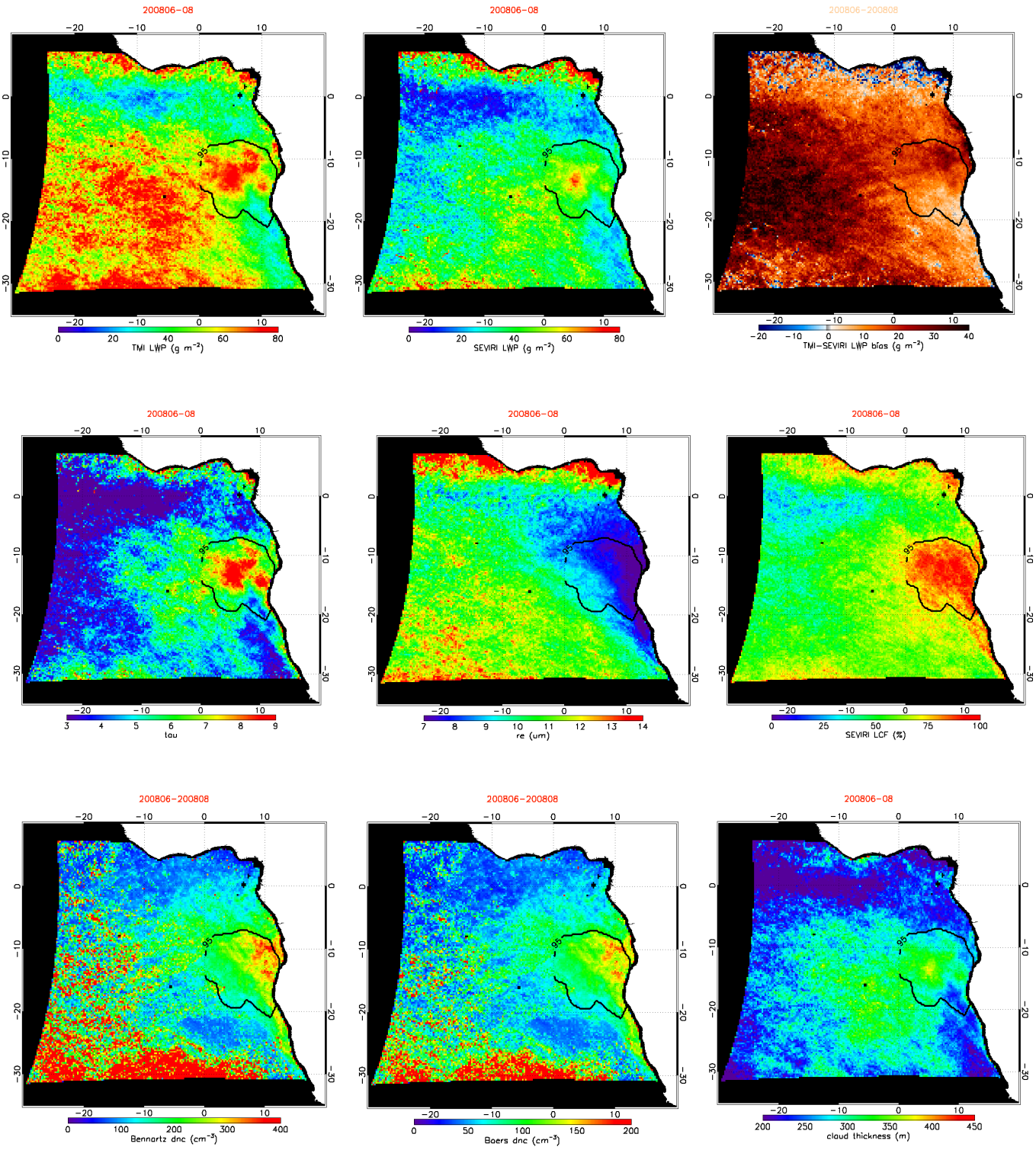

Fig 4.3.2: *As Fig. 4.3.1 but for JJA.*

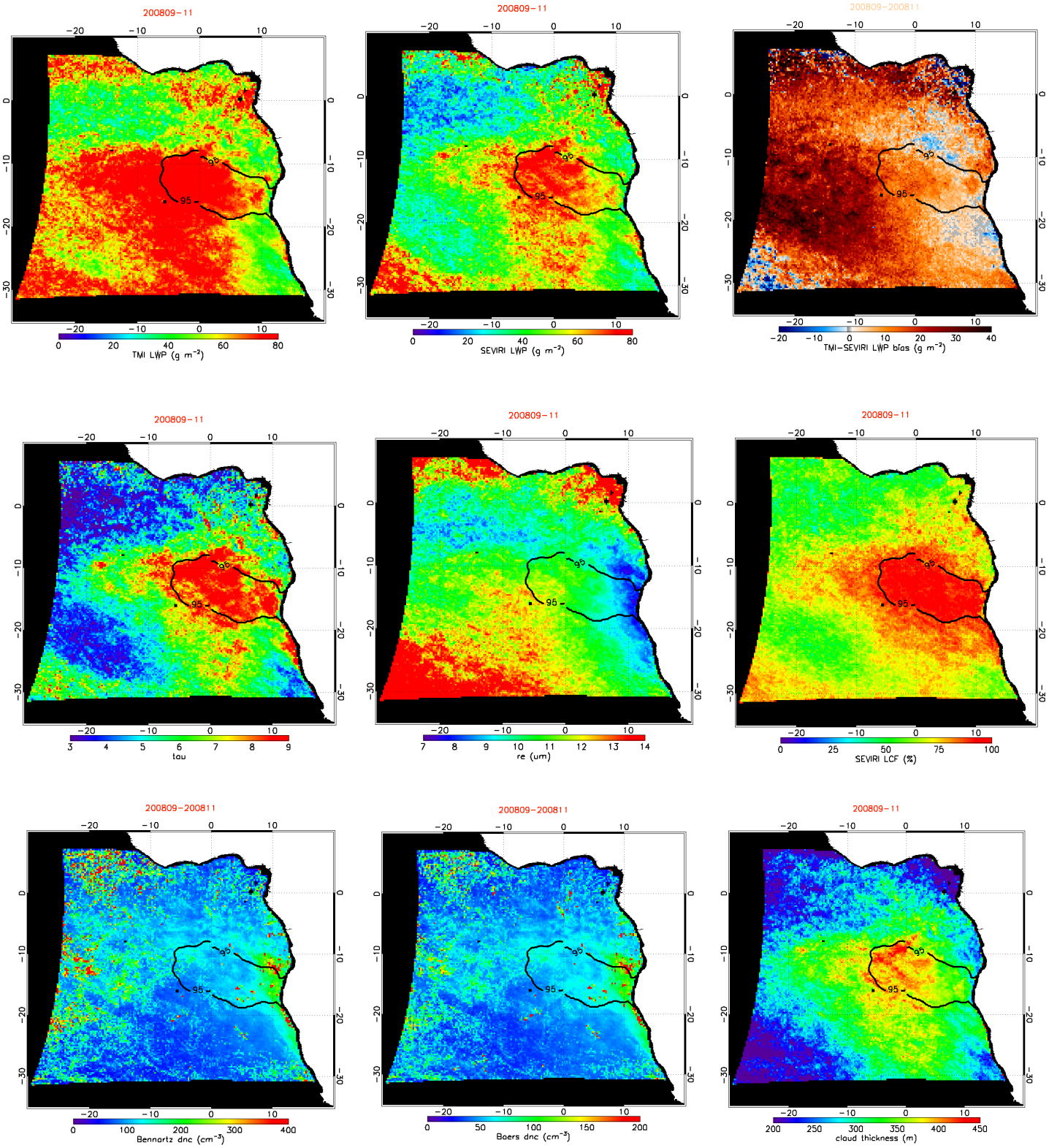

Fig 4.3.3: *As Fig. 4.3.1 but for SON.*

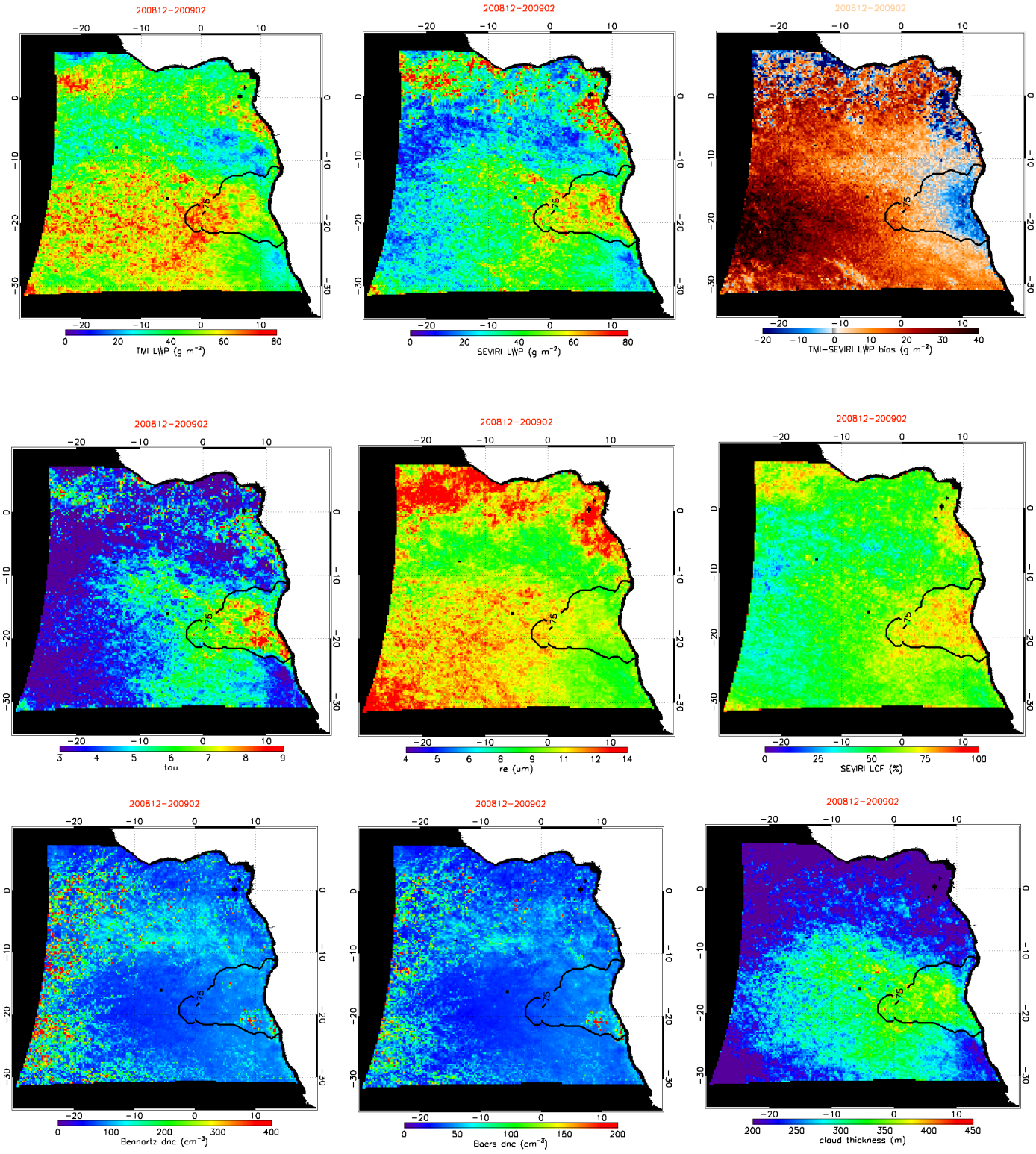

Fig 4.3.4: *As Fig. 4.3.1 but for DJF.*

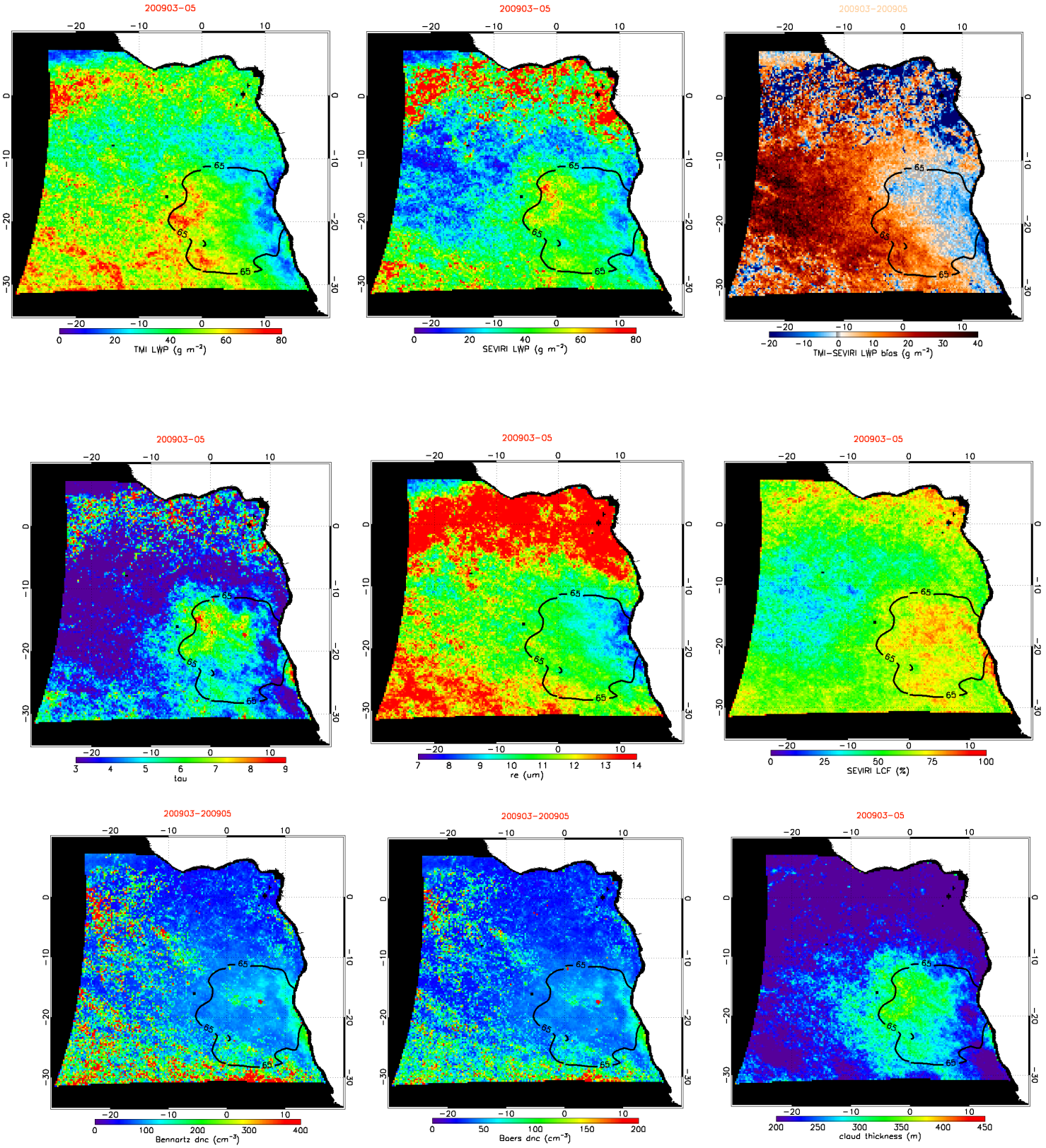

Fig 4.3.5: *As Fig. 4.3.1 but for MAM.*

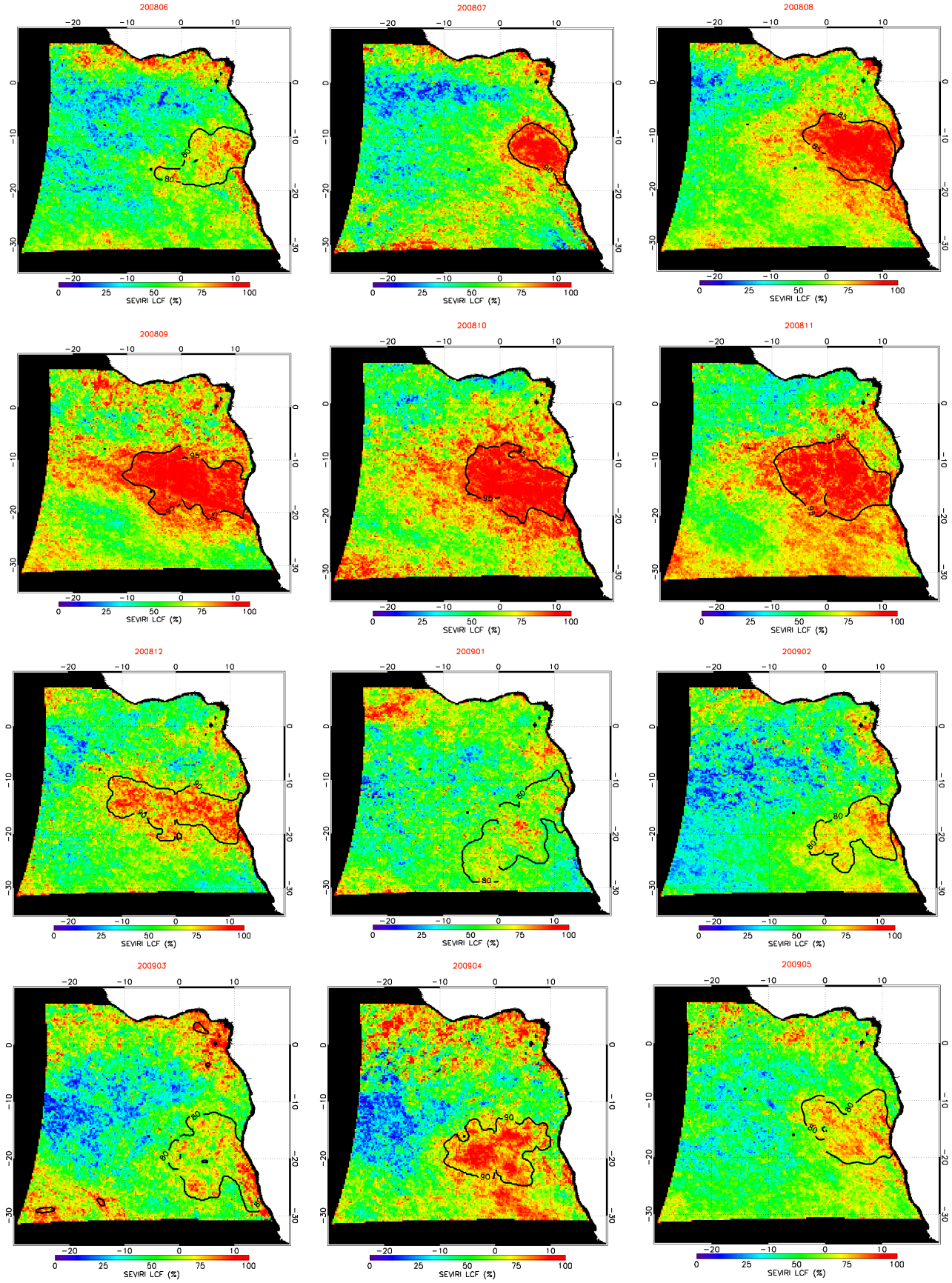

Fig 4.3.6: *Monthly mean variation in liquid cloud fraction June 2008 through May 2009.*

4.4 Diurnal Cycle of Cloud Properties

We examine the diurnal cycle of cloud properties over the entire South Atlantic domain, and more specifically the Sc and trade wind Cu domains. Despite occurring over the oceans in regions of large scale subsidence, marine Sc shows an interesting diurnal variation (*Minnis and Harrison 1984*). Over the extensive marine Sc regime, regardless of season, both TMI and SEVIRI LWP decreased with time from sunrise to sunset, and thereafter slightly increased as shown in Figs 4.4.3-4.4.7. The figures shown here are only for aerosol neglected pixels, to avoid misinterpretations related to retrieval errors caused by aerosols (see Section 4.1). Our results are consistent with *Wood et al.* [2002] who also studied the diurnal variation in LWP over the South Atlantic Sc region which is same as our Sc domain, based on two complete years of TMI data and found similar diurnal features. However, there are many other scientists who contributed their effort in investigating diurnal cycle of Sc clouds which occur over other parts of globe. Notably, *Blaskovic et al.* [1990] evaluated the diurnal cycle of North-East Pacific Sc clouds off California coast from the observations taken during FIRE. Their results indicated that, cloud thickness and liquid water path showed a clear decrease during the day from sunrise to sunset, increasing thereafter, the decrease in LWP is associated with the decrease in cloud thickness. The cloud base height has diurnal range of (150+/-30) m, rising from sunrise till mid-afternoon. The cloud top height has a similar diurnal range of (130+/-30) m, but the main descent occurs in the late afternoon. Surface air temperature also increases at sunrise, directly in phase with the cloud base lifting, and has a diurnal range of 2^{o}C. *Ciesielski et al.* [2001] evaluated the diurnal variation of North Atlantic Sc clouds from Atlantic Stratocumulus Transition Experiment (ASTEX) and his results showed, fractional low cloudiness varies over this region from a maximum of 54% in the predawn hours to a minimum of 39% in the mid-afternoon. These changes in low cloudiness are accompanied by an opposite trend in the boundary layer moisture, which shows a predawn drying and an afternoon moistening. *Duynkerke et al.* [2004] compared the diurnal variation in the cloud liquid water path from the results of the six LES models and the observed data from FIRE, and found a fair agreement between them. Their analysis revealed that the diurnal variation in the cloud liquid water path is related to the transition from a decoupled boundary layer during daytime to a vertically well-mixed boundary layer during the night. The observed diurnal cycle of Sc is characterized by a cloud layer which gradually thickens during the night, whereas during the day the cloud layer thins due to SW radiative absorption and decoupling. The latter state is characterized by slightly negative buoyancy fluxes and a minimum vertical velocity variance near the cloud base. This implies that surface-driven, moist thermals

cannot then penetrate the cloud layer, while entrainment maintains a steady supply of relatively warm and dry air from just above the inversion into the cloud layer. This results in a distinct diurnal cycle of the LWP, which has minimum values during the day. During the night the vertical velocity variance has one single peak near the middle of the boundary layer. Moreover, the diurnal cycle in SEVIRI LWP is mainly driven by the cloud optical thickness rather than droplet effective radius, which showed less variability. Cloud optical thickness showed a sharp decrease of ~6 from morning (10) to evening (4) in annual mean results. However individual seasons showed even a decrease of ~10 in optical thicknesses (SON) from morning to late afternoon. MODIS Terra+Aqua optical thickness (green stars) are also shown in Figs 4.4.3-4.4.7. MODIS also showed a decrease in optical thickness from morning to afternoon, however less than SEVIRI. The SEVIRI effective radius and droplet concentration did not show much variability during the day. MODIS optical thickness and effective radius values are always higher than SEVIRI values, with optical thickness of magnitude 1 difference and effective radius of ~3 μm difference. MODIS Terra LWP is very good agreement with SEVIRI and TMI in magnitude, however MODIS Aqua LWP underestimates SEVIRI and TMI values. This MODIS underestimation is mainly due to a lower cloud fraction, as we scale SEVIRI and MODIS LWP by their liquid cloud fraction in order to compare with TMI domain means. (Note that if we compare in-cloud LWP, MODIS is higher than SEVIRI, and this issue is explained in detail in next section.) Compared to SEVIRI, Aqua-MODIS has ~40% lower cloud fraction while Terra-MODIS agrees within 10%. The large difference in cloud fraction in Aqua-MODIS and SEVIRI would be a consequence of MODIS clearsky restoral (i.e. retrieval only over confident cloudy pixels), together with larger SEVIRI pixel size. Finally to represent the entire diurnal cycle we have plotted TMI data (grey curve) which includes both day and night, which clearly represents the observed diurnal cycle.

Again, the diurnal cycle in LWP consistently follows the variation in the cloud fraction as well. This result is further consistent with *Fairall et al*. [1990] who stated that the cloud fraction is maximum at sunrise of 0.74 and minimum at sunset of 0.41, with maximum cloud albedo of 0.61 at sunrise and a minimum of 0.31 a few hours after the local noon. *Zuidema and Hartmann* [1995] stated that the stratus cloud LWP is correlated with cloud amount and is negatively correlated with low cloud-top temperature. They also inferred that no correlation is observed between effective radius and liquid water path, as larger drops are found in the evening than in the morning, along with lower LWPs and lower albedos. In our study the occurrence of maximum LWP is during 07-09 UTC, but it highly varies with season. The diurnal range in LWP

is 60% - 75% which is fairly high compared to previous studies where, *Wood et al.* [2002] reported the diurnal amplitude of 15-35% in low cloud regions to the west of continents using TMI data, *Zuidema and Hartmann* [1995] showed only 25% variation in LWP using SSM/I data. However, *Fairall et al.* [1990] found larger amplitude in diurnal cycle of 60-70% using a 17 day period of near-continuous ground based microwave radiometer data around the time of FIRE.

The diurnal variation of TMI and SEVIRI liquid water path is in good agreement within ±5 gm^{-2}, in the aerosol unaffected seasons and also in the annual basis. In JJA and SON, even if we eliminate aerosols affected pixels with AI≥1, the diurnal cycle agreement is within ±10 gm^{-2} which is mainly due to strong underestimation of ~15-20 gm^{-2} in SEVIRI LWP. This is due to the fact that τ and r_e decreased due to the effect of absorbing aerosols above these clouds. This implies that removing the pixels with AI≥1 would eliminate only part of the LWP bias and the influence of aerosol is still present in the data. Our analysis indicates that considering another AI threshold of 0.25 leads to much better results and less bias.

Fig 4.4.2 shows the annual and seasonal average diurnal cycle of cloud properties in trade wind Cu regime. Over the trade wind Cu, we have observed different diurnal cycle with season; however, both the SEVIRI and TMI LWP showed similar variability, but with a relatively large bias of 10-40 gm^{-2}. This large LWP bias might be partially due to SEVIRI underestimation and partially due to TMI overestimation. Similarly, there is no clear regular trend in diurnal cycle with season is observed either in optical thickness or in effective radius over this trade Cu domain. Finally, we have evaluated the diurnal cycle of liquid clouds over the South Atlantic domain as given in Fig 4.4.1. The LWP decreased mainly during day till late noon and then increased slightly. Both TMI and SEVIRI LWP agree within 10 to 30 gm^{-2}, mainly with SEVIRI underestimation. Similar variation in diurnal cycle is observed in the optical thickness and the trend is not clear in droplet effective radius. It is interesting to notice a clear diurnal cycle over trade wind cumulus clouds and which is obvious in TMI data (grey curve) as well.

When we consider the entire domain we still see a clear diurnal cycle in annual mean LWP which is mainly from optical thickness. Similar variation is seen in cloud fraction and cloud thickness. The effective radius and droplet number concentration remained constant during the day which is as expected.

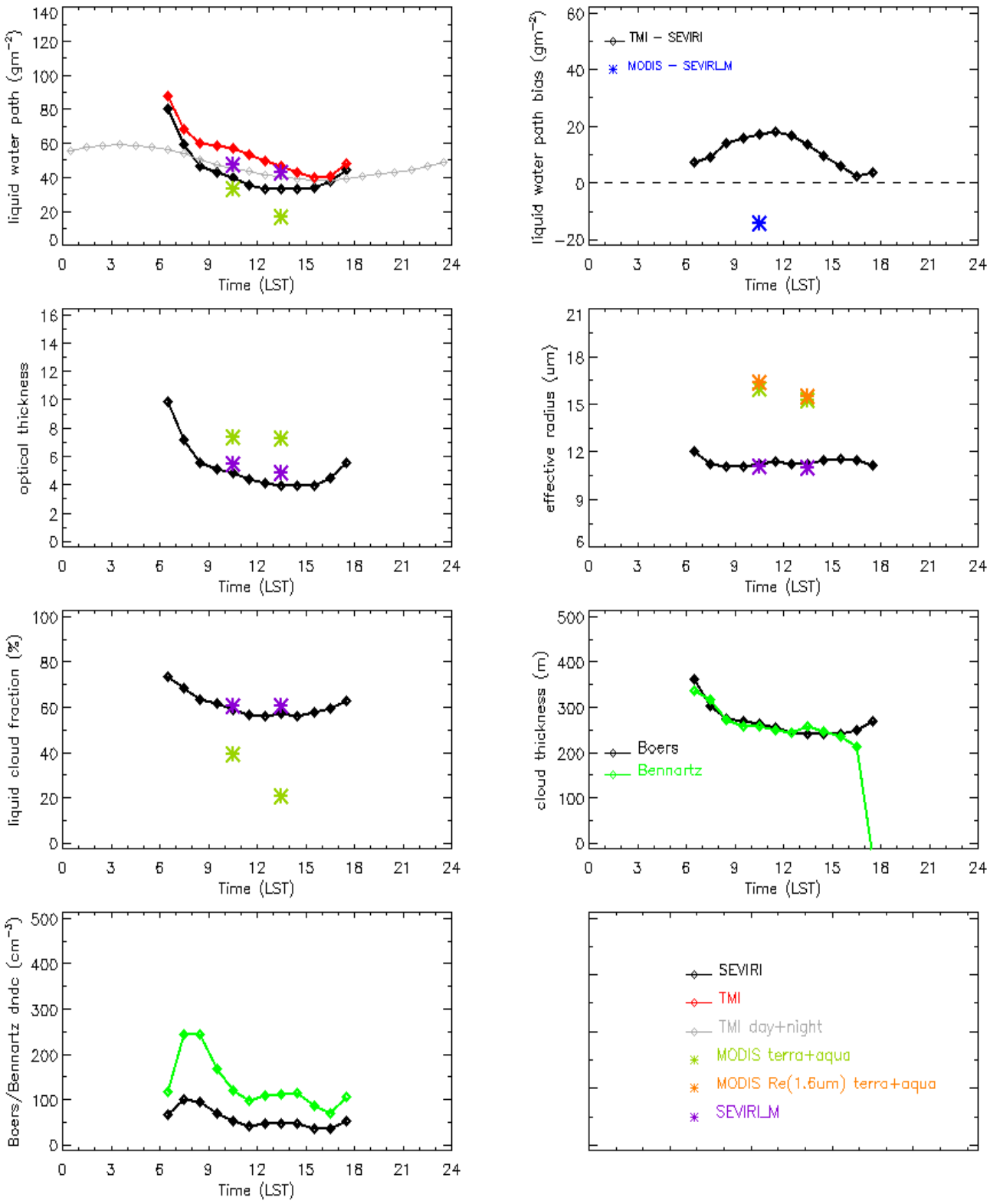

Fig 4.4.1: *Annual mean diurnal cycle of cloud properties averaged over entire domain (AI<1)*

Stratocumulus clouds

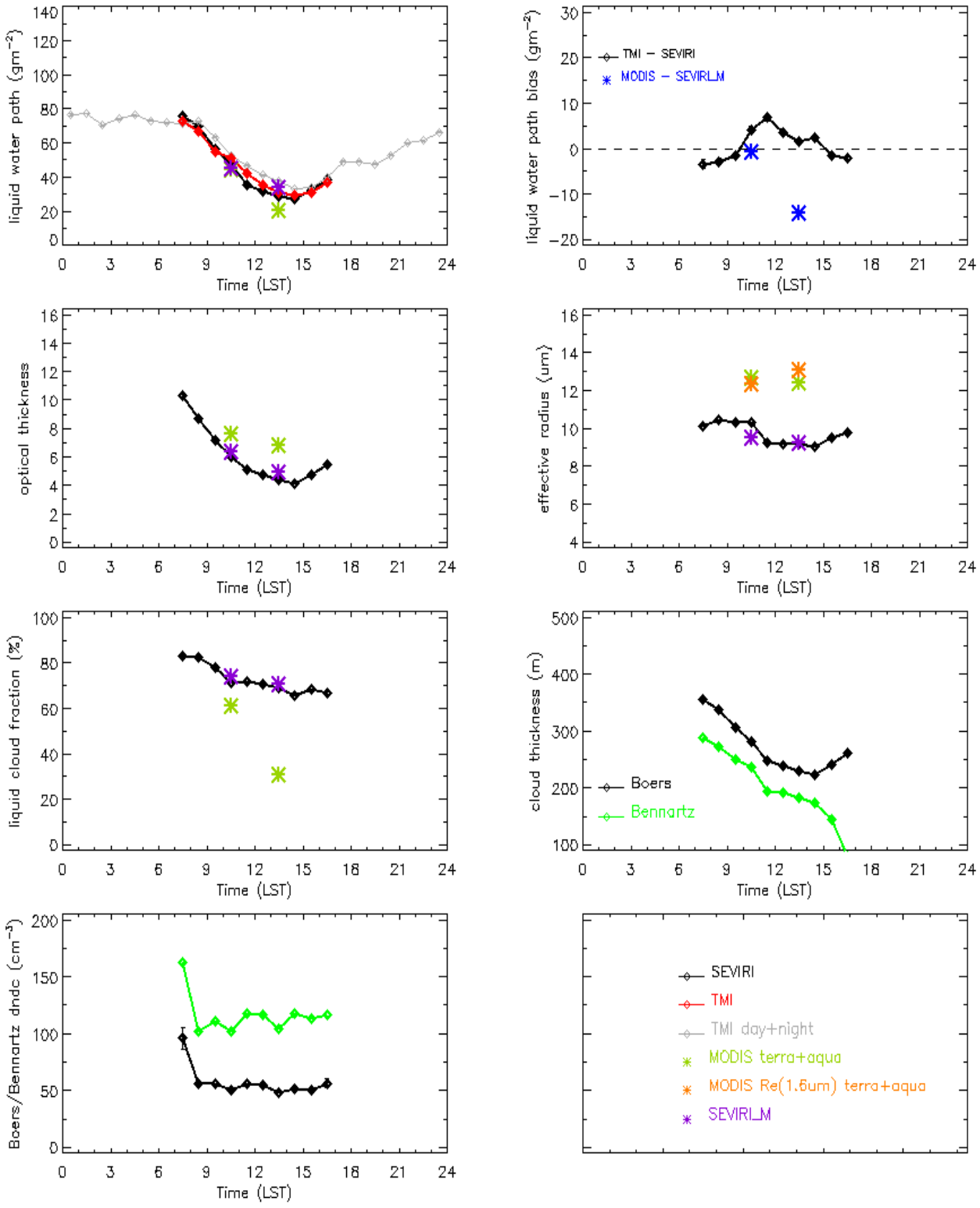

Fig 4.4.2: *Annual mean Diurnal cycle of CPP over south Atlantic Sc domain*

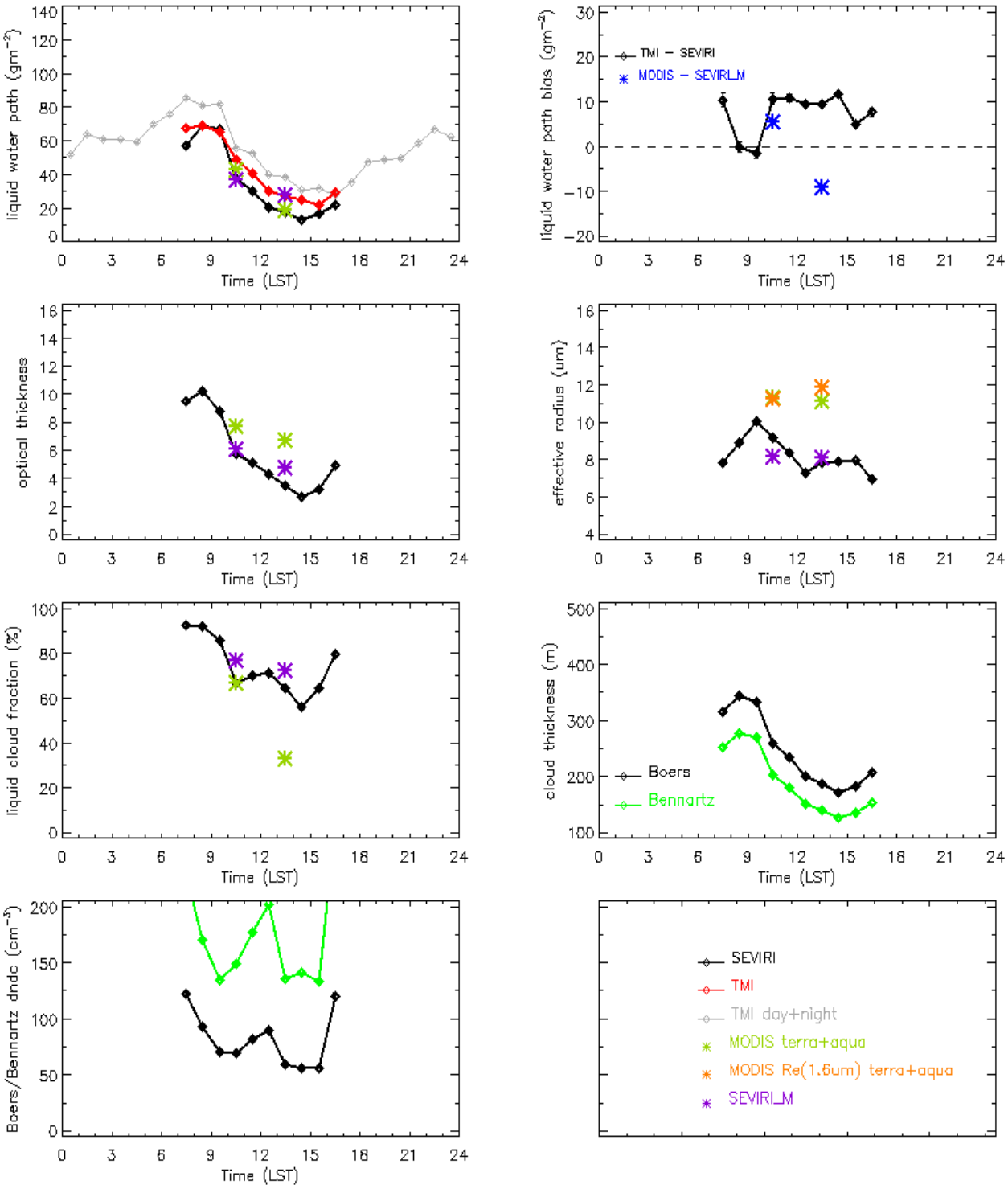

Fig 4.4.3: *JJA mean diurnal cycle of CPP over south Atlantic Sc domain*

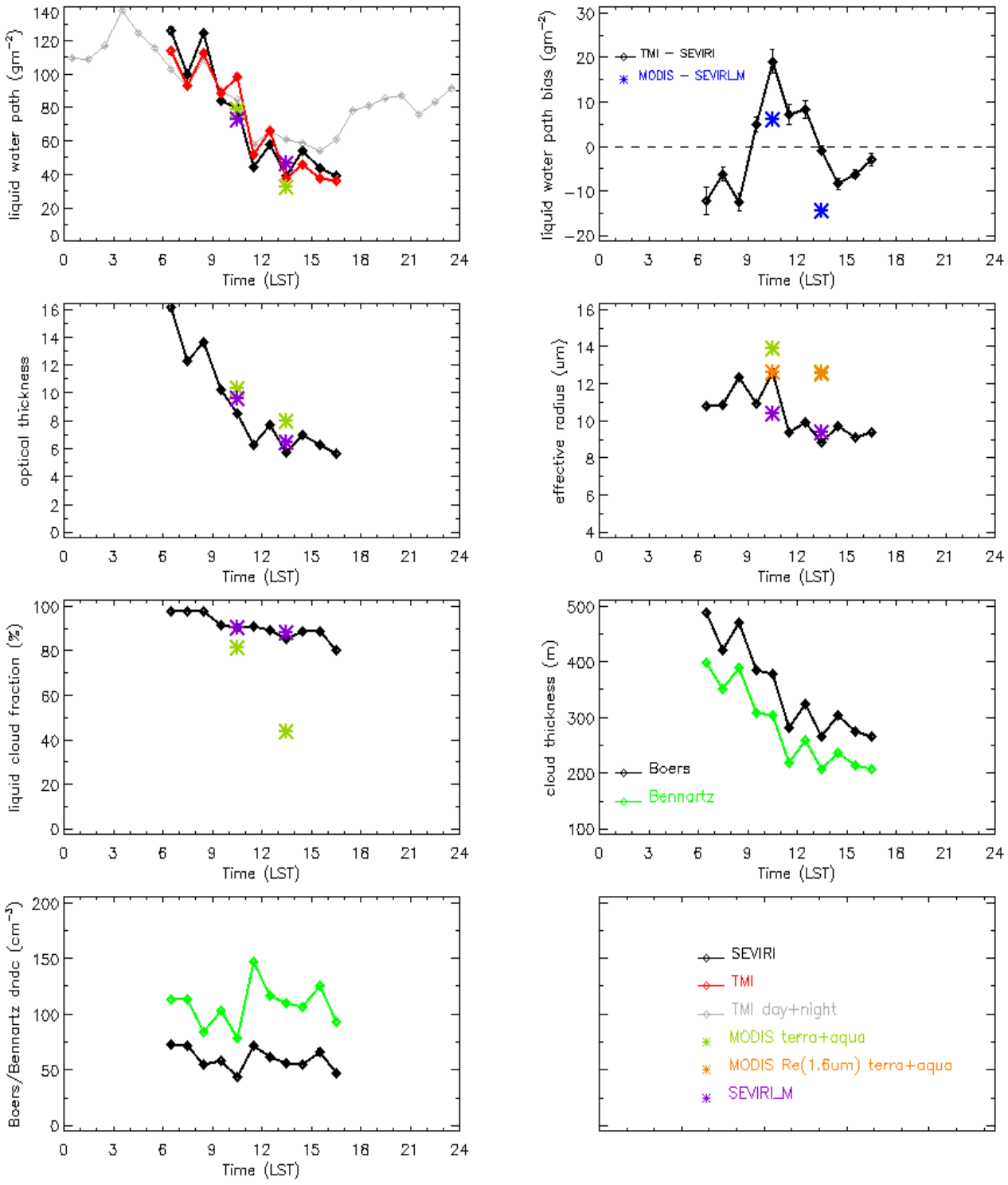

Fig 4.4.4: *SON mean diurnal cycle of CPP over south Atlantic Sc domain*

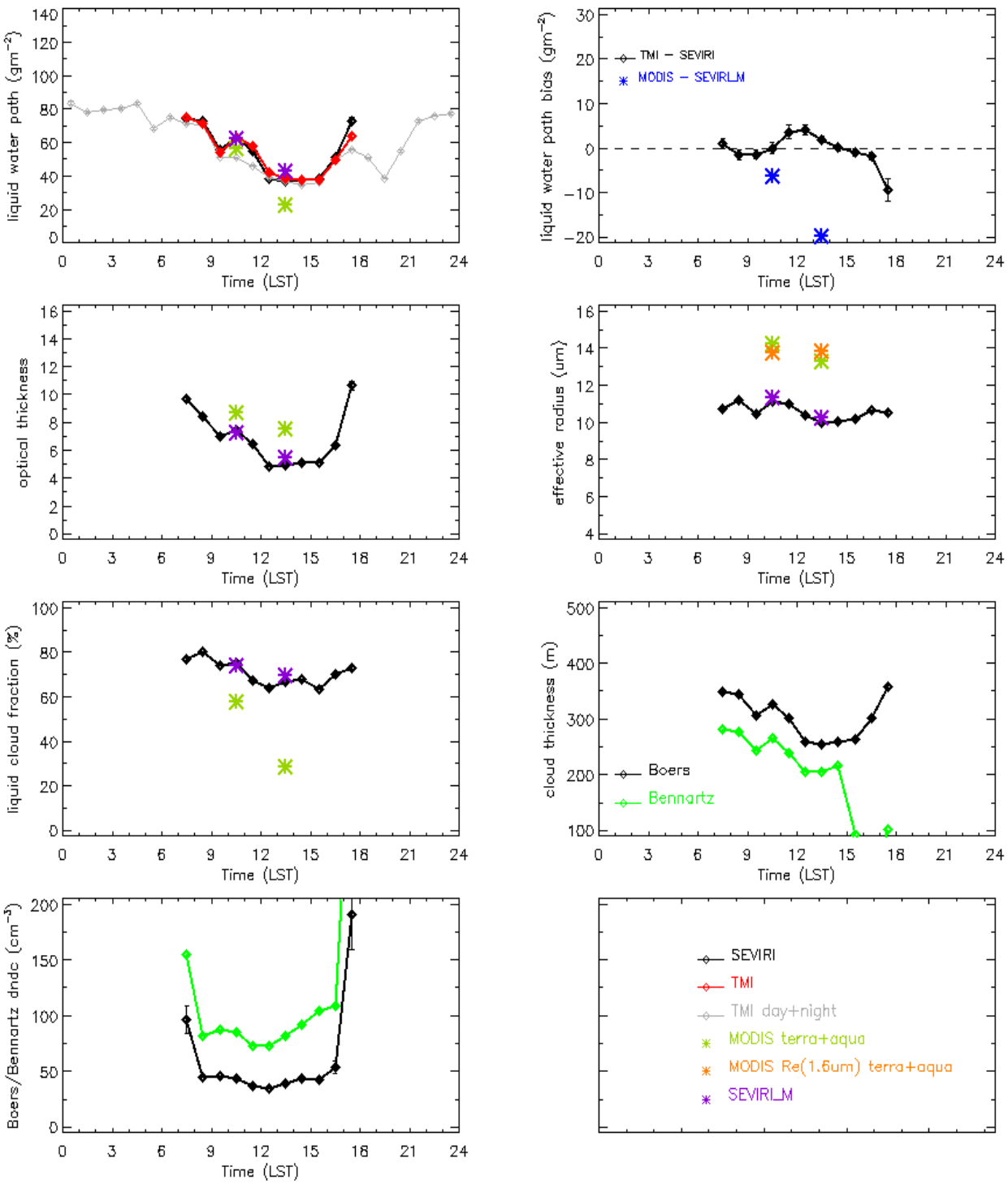

Fig 4.4.5: *DJF mean diurnal cycle of CPP over south Atlantic Sc domain*

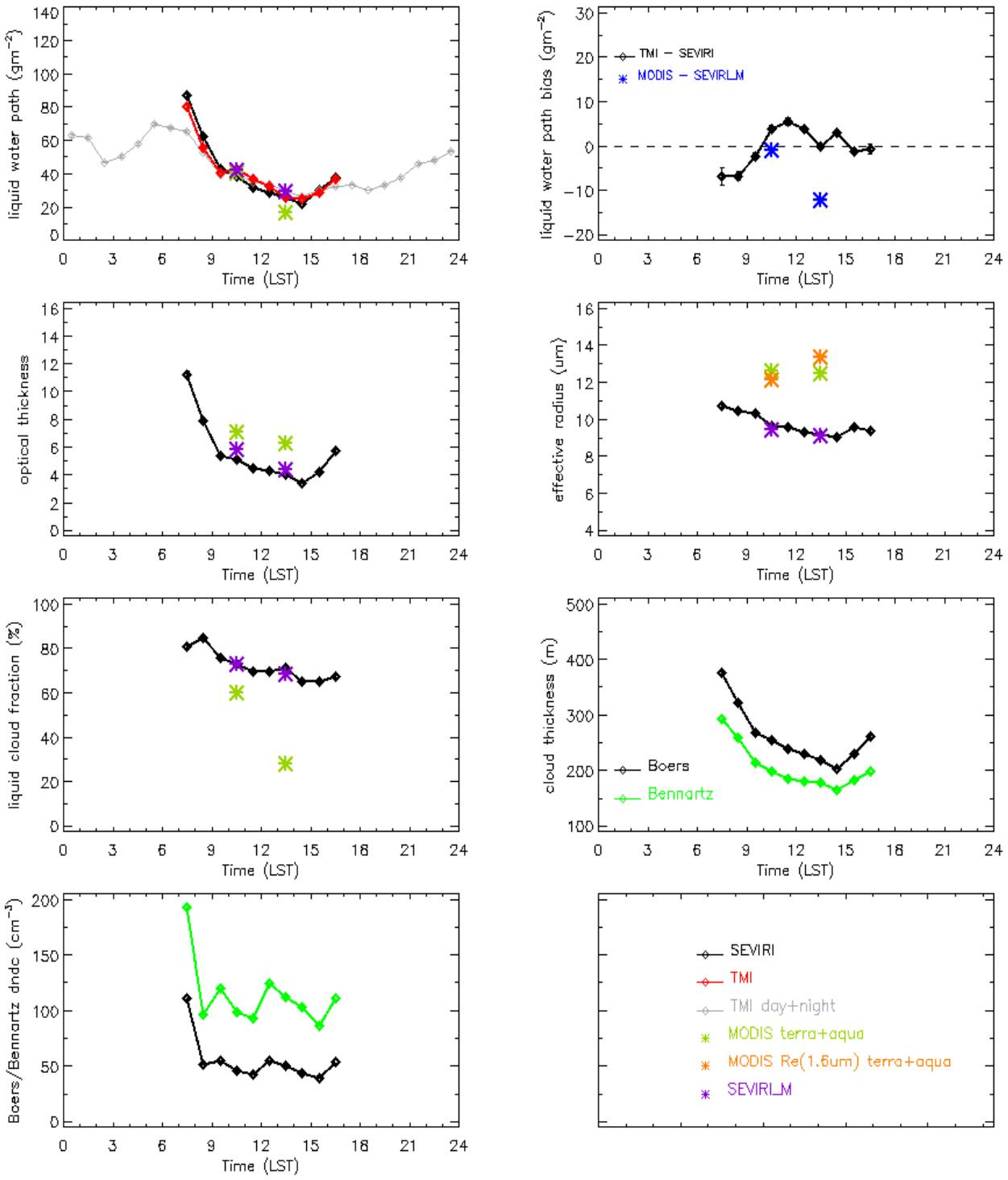

Fig 4.4.6: *MAM mean diurnal cycle of CPP over south Atlantic Sc domain*

Trade Cumulus Clouds

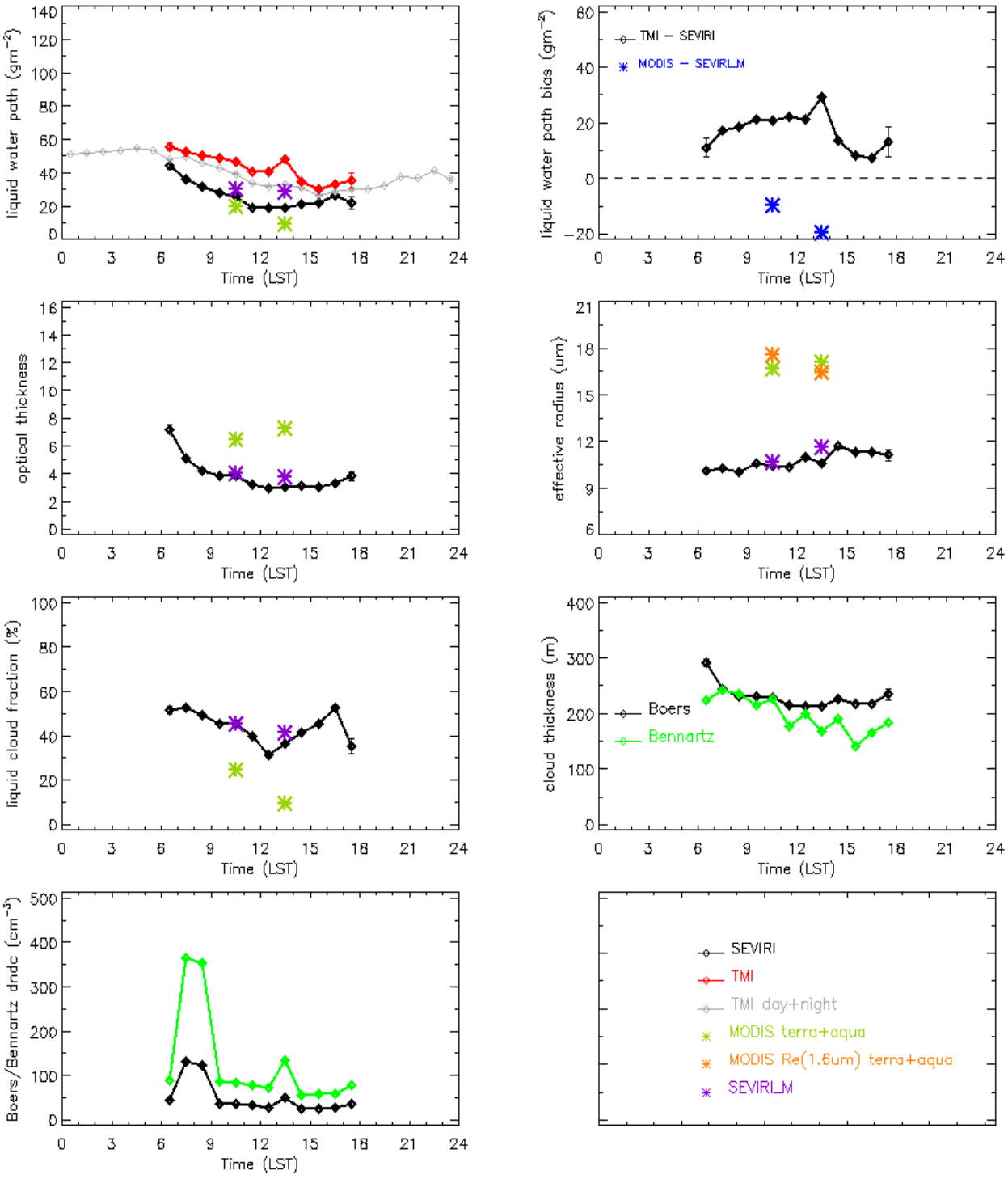

Fig 4.4.7: Annual m*ean diurnal cycle of CPP over trade wind cu regime*

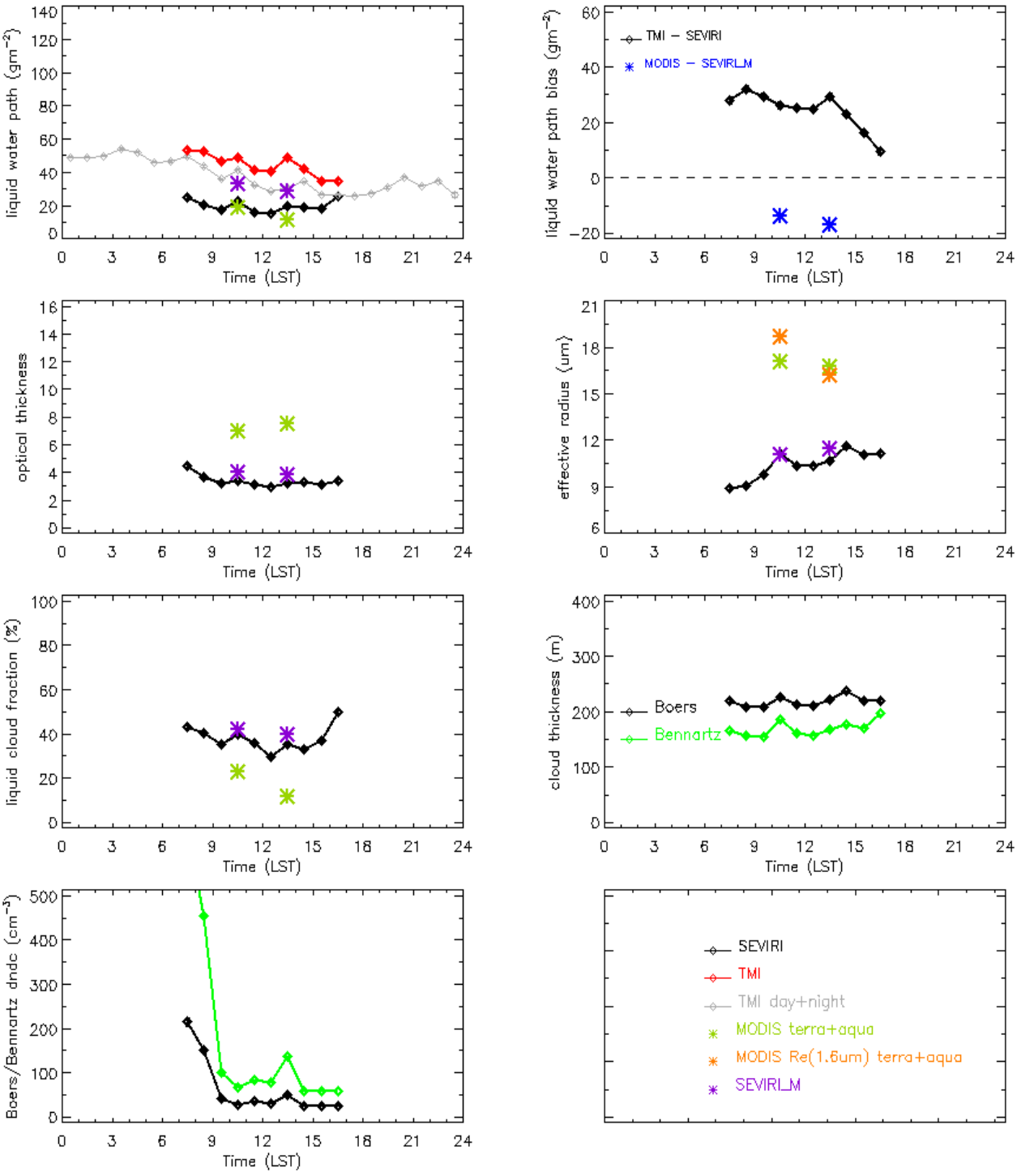

Fig 4.4.8: JJA m*ean diurnal cycle of CPP over trade wind cu regime*

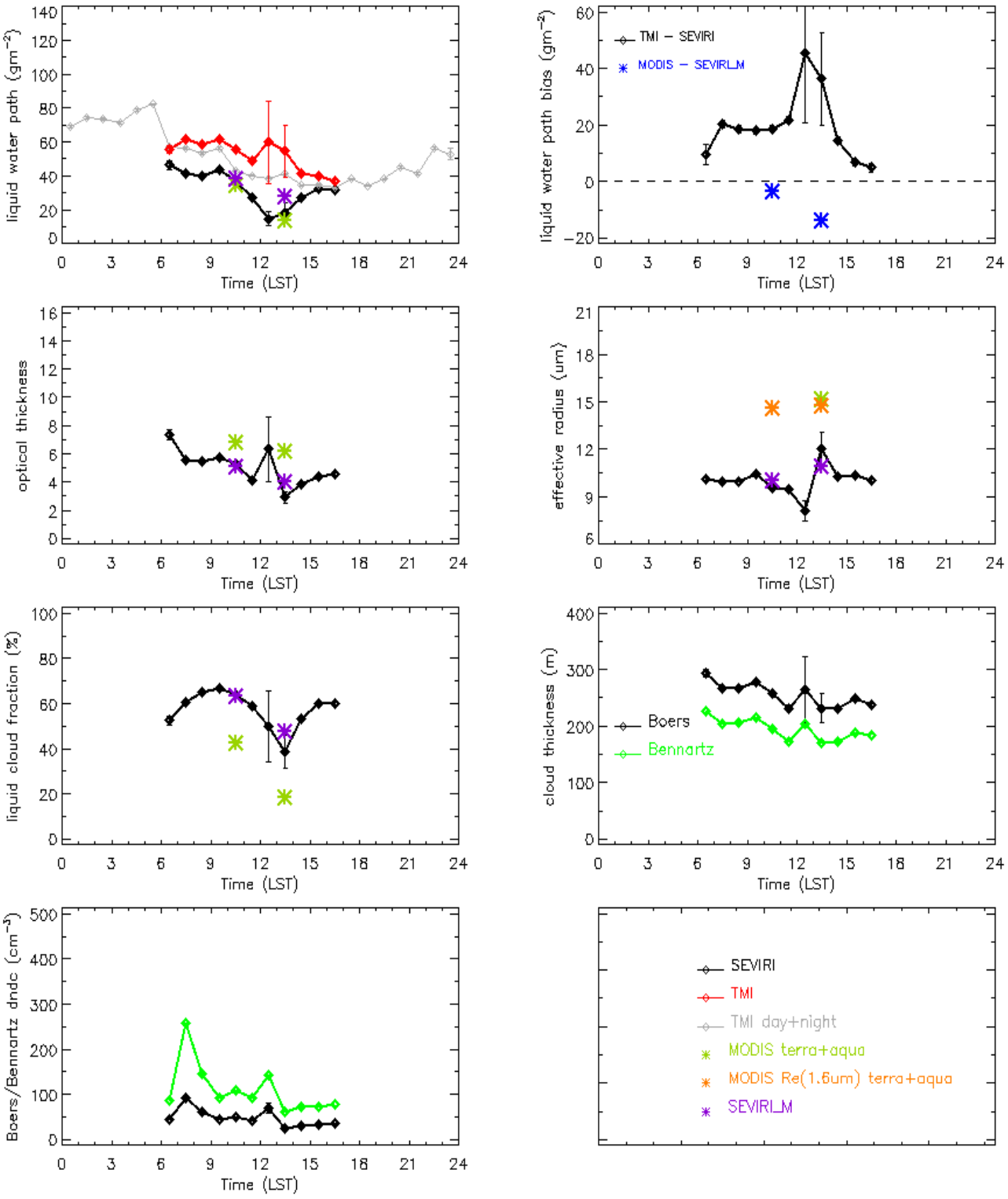

Fig 4.4.9: SON m*ean diurnal cycle of CPP over trade wind cu regime*

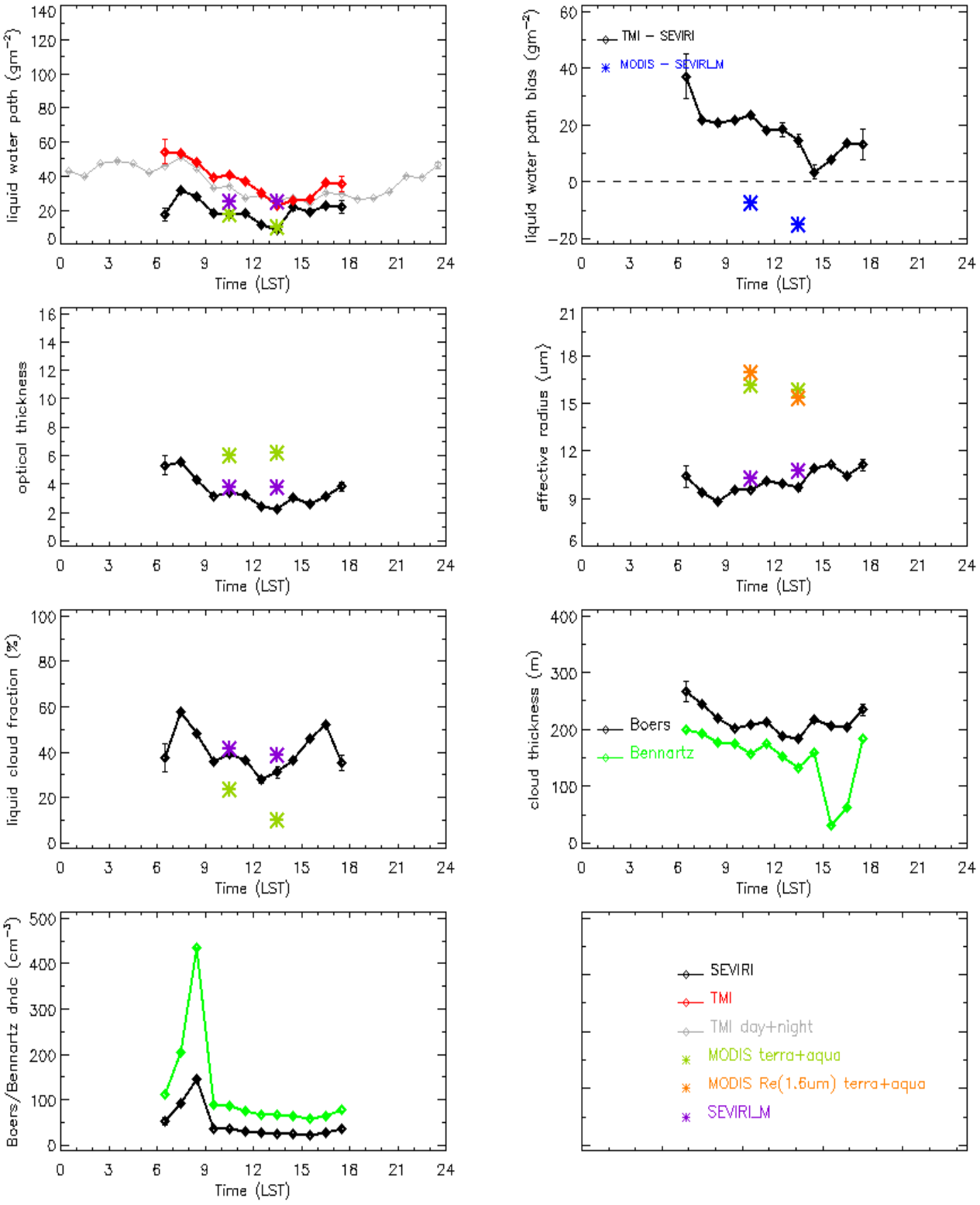

Fig 4.4.10: DJF m*ean diurnal cycle of CPP over trade wind cu regime*

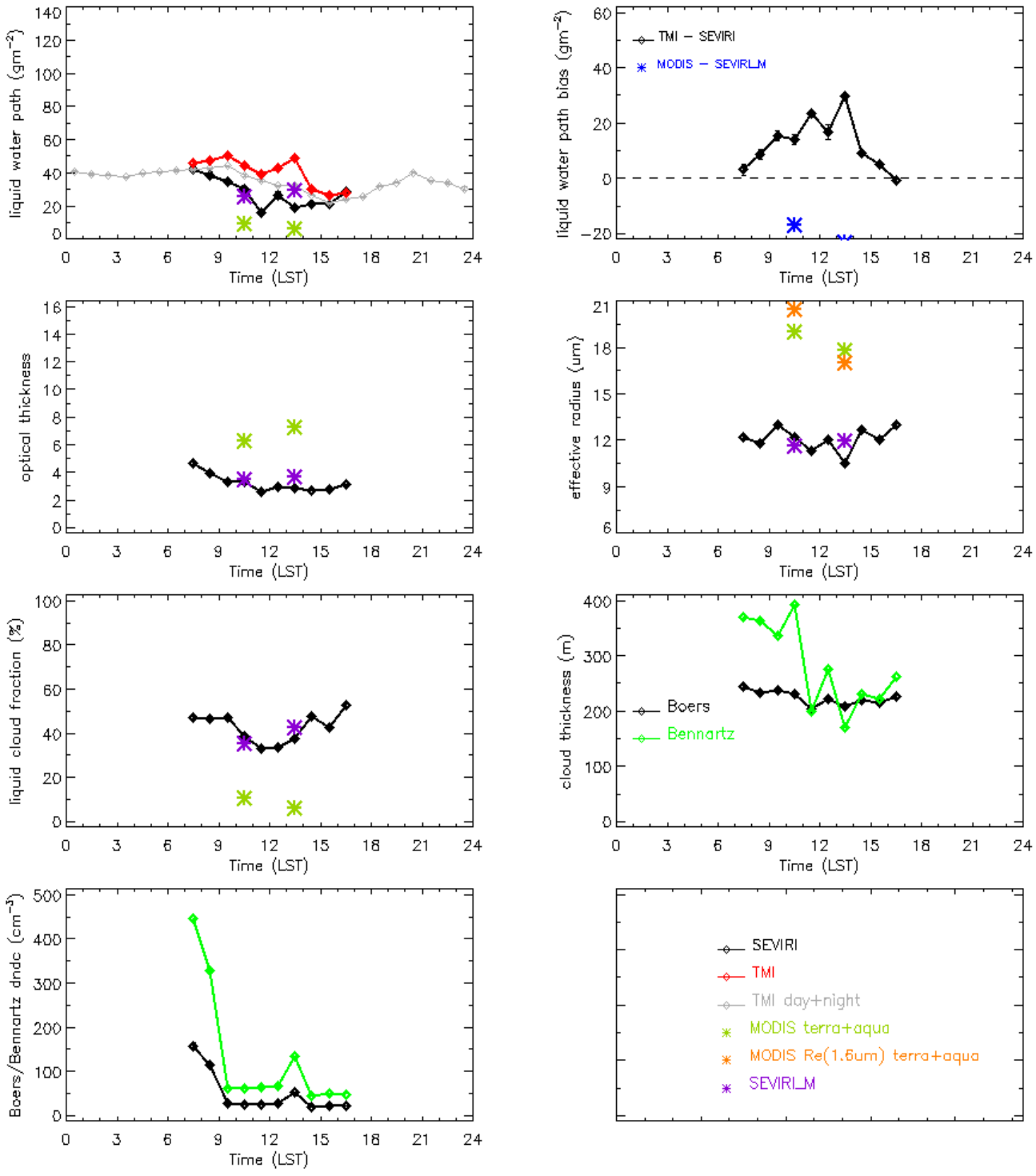

Fig 4.4.11: MAM m*ean diurnal cycle of CPP over trade wind cu regime*

4.5 Cloud Fraction Dependency of Cloud Properties

The cloud fraction is calculated from SEVIRI valid liquid pixels within the TMI grid-box as shown in figure below. Most of the grid-box showed the calculated cloud fraction > 95%, and this may be due to SEVIRI 3kmx3km resolution which is fairly coarse compared to MODIS. The LWP increased with the cloud fraction in both TMI and SEVIRI; the TMI-SEVIRI LWP bias decreased with increasing cloud fraction. If the cloud fraction is >95%, TMI and SEVIRI showed better agreement in retrieved LWP, with bias ~ -6 gm^{-2}. The bias between AMSR-E and MODIS showed ~31 gm^{-2} in the most broken cloud scene with cloud fraction 0-5% bin (*Seethala and Horvath* [2010], Fig 4.). Unlike AMSR-E and MODIS comparison, TMI and SEVIRI showed less LWP bias of ~10 gm^{-2} in 0-5% cloud fraction bin. The optical thickness, effective radius and the droplet number concentration also increased with the cloud fraction.

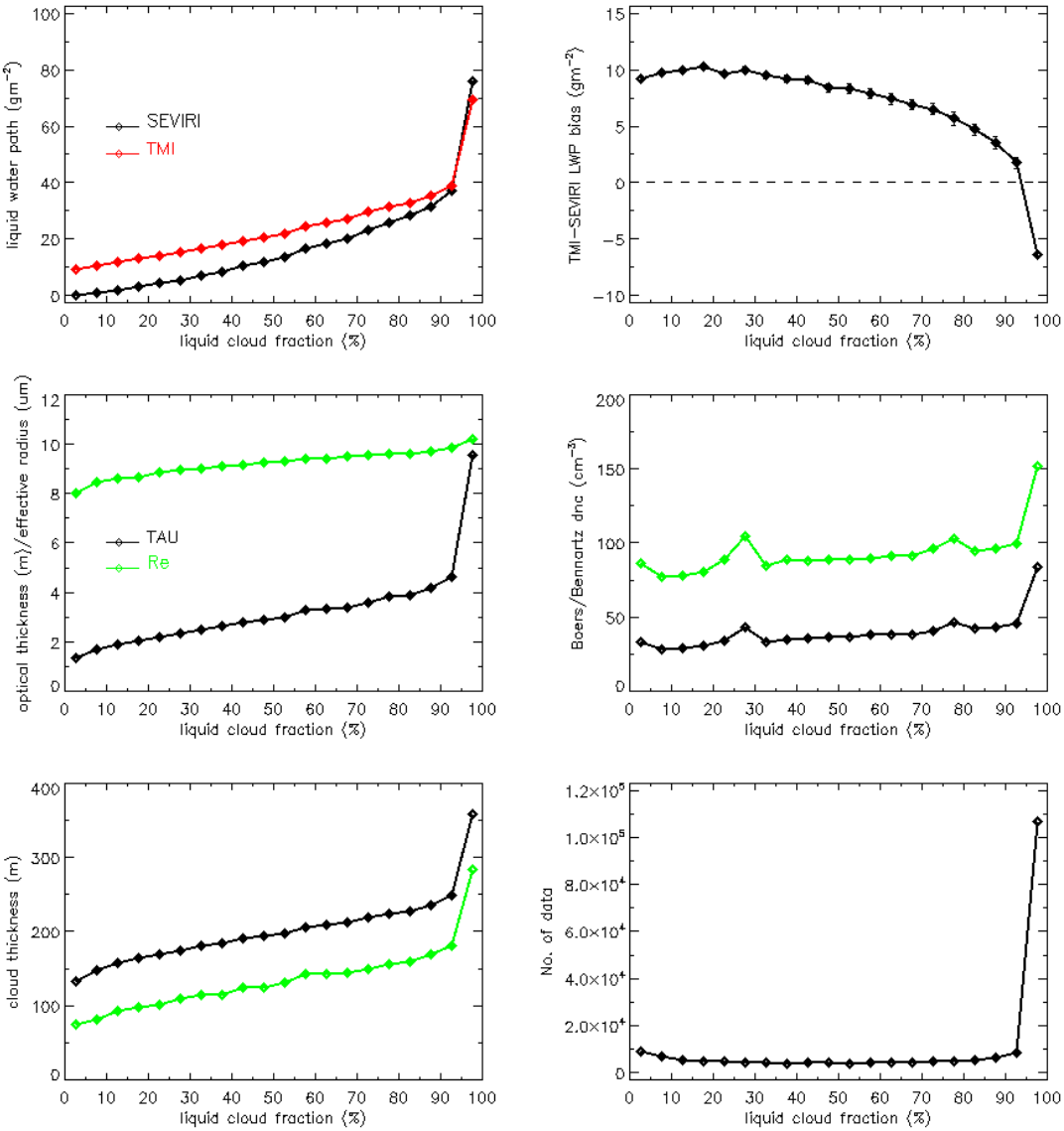

Fig 4.5: *Cloud fraction dependence of annual mean cloud properties for whole domain.*

4.6 Solar Zenith Angle Dependency of Cloud Properties

The 3D effect at large solar zenith angle is a dominant source of error in VIS/NIR retrievals. In this section we would like to discuss the solar zenith angle dependence of SEVIRI cloud properties. TMI uses microwave technique and hence not subject to solar zenith angle dependency. Fig4.6 gives TMI and SEVIRI cloud properties as a function of solar zenith angle. There is an increase in LWP with sun angle however this increase is observed in both TMI and SEVIRI. Hence that would be a real increase rather than increase due to 3D effect. The bias between TMI and SEVIRI is also very small and within ±5 gm^{-2}. SEVIRI increase in LWP with sun angle in associated with increase in cloud optical thickness. The droplet effective radius showed least variation with sun geometry. However *CDNC* showed an increase with solar geometry. In our previous study *Seethala and Horvath* 2010 (see Figure 8(b)) and many other studies reported a sharp increase in MODIS LWP with solar zenith angle compared to AMSR-E LWP based on microwave technique. The difference in SEVIRI and MODIS is that MODIS retrievals are done at 1kmx1km resolution and SEVIRI uses 3kmx3km pixels. This would imply that at 3km scale SEVIRI data is least affected by 3D effects at large solar zenith angle likely due to the cancellation of errors.

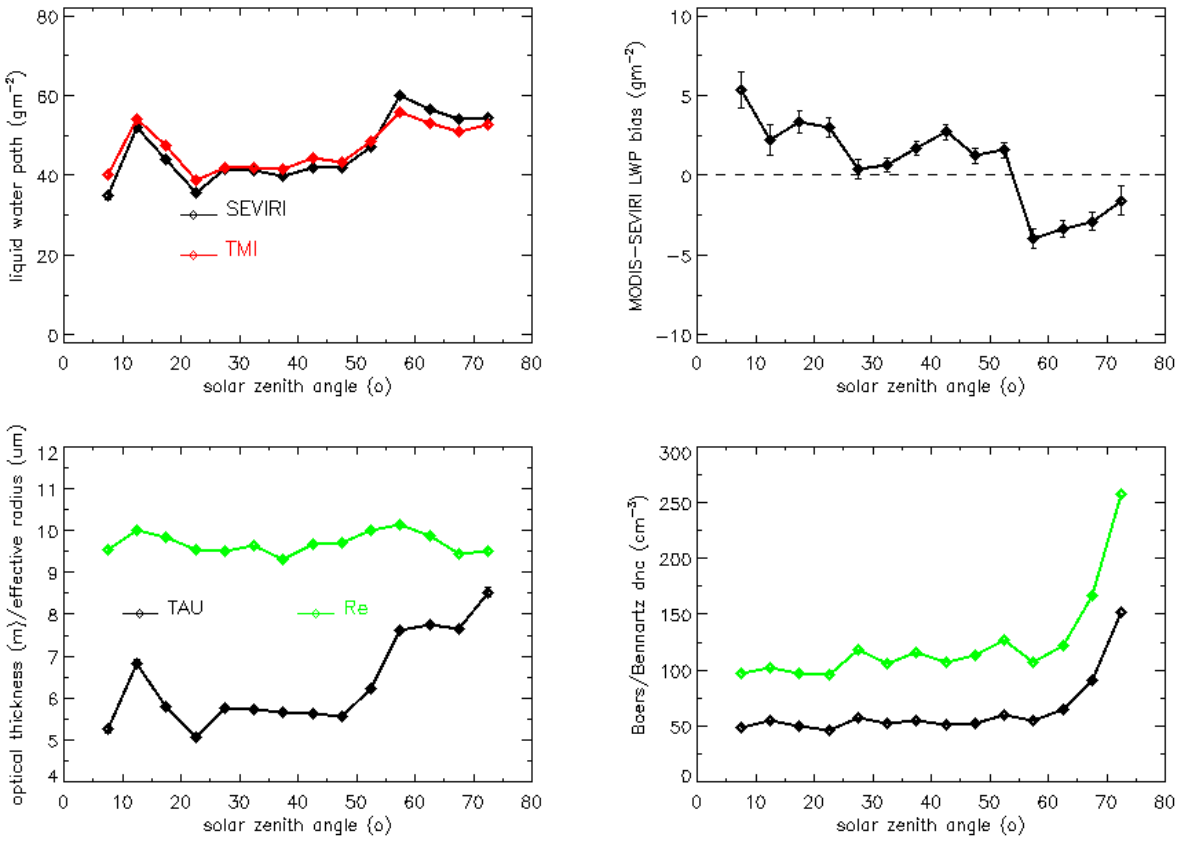

Fig 4.6: *Annual mean solar zenith angle dependence in SEVIRI and TMI cloud properties*

(ii) SEVIRI *versus* MODIS

Geostationary imagers sample at a coarser resolution than polar imagers. Thus SEVIRI cloud properties are retrieved at 3x3 km^2 resolution but the MODIS retrievals are done at 1x1 km^2 resolution. A coarser resolution gives rise to systematic biases in the derived cloud physical properties, especially when the cloud is heterogeneous. Moreover, Fig 4.5f depicts that most of the SEVIRI pixels within TMI gridboxes have a cloud fraction ≥ 0.95, which is primarily due to the SEVIRI coarser resolution. *Henrich et al*. [2010] reported that 1kmx1km pixel area seems least biased in the retrieval of optical thickness. Thus, to investigate the pixel size effect (sub-pixel scale variability) on SEVIRI retrieved cloud properties, we compare them with the high resolution MODIS retrievals, which can provide us some clues on introduced error in SEVIRI due to coarser pixel size.

Comparison is done on monthly, seasonal, and annual means, however the results are shown here only for the annual means. Further the analysis done in two steps (1) considering all the pixels (total sky) and (2) considering fully overcast pixels i.e. pixels with 100% cloud fraction in MODIS and SEVIRI at a 25km resolution.

4.7 Spatial Distribution of Cloud Properties

4.7.1 Total sky

We discuss the spatial distribution of SEVIRI and MODIS cloud properties such as liquid cloud fraction, LWP, cloud optical thickness, droplet effective radius, and their bias and relative biases. The annual mean cloud fraction varies from 30-100% in SEVIRI and 0-70% in MODIS retrievals. Over the extensive marine Sc region the cloud fraction is >75% in SEVIRI but only 50-70% in MODIS. The larger cloud fraction in SEVIRI retrievals is mainly the outcome of clearsky restoral for MODIS and larger pixel size for SEVIRI. The mean optical thickness over Sc region is 6-8 in SEVIRI and 7-9 in MODIS, whereas over the more broken trade wind Cu regime MODIS values are 6 to 8 but SEVIRI mean optical thickness value is <5. Thus there is a difference of 1-1.5 in optical thickness in both datasets over Sc domain and larger difference in optical thickness over broken fields.

This SEVIRI small optical thickness value would introduce a lower retrieved effective radius for SEVIRI as the CPP algorithm weighs r_e towards r_e-climatology of 8 µm, but MODIS provides actual retrieved values. Moreover SEVIRI effective radius is retrieved from 1.6µm channel reflectance and MODIS retrieves effective radius at 1.6µm, 2.2µm, and 3.7µm

wavelengths. 3.7 µm channel samples mostly the top layer of cloud and 2.2 µm channels samples little deeper than 3.7 µm channel and 1.6 µm channel samples further deeper than other two channels although all three channels samples near top of cloud due to its weighting function. SEVIRI and MODIS LWP is deduced from optical thickness and effective radius, however SEVIRI uses optical thickness at 0.6 µm and effective radius at 1.6 µm channel reflectance, whereas MODIS uses optical thickness from 0.8 µm channel over ocean and effective radius from 2.2 µm channel reflectance. So we will discuss MODIS effective radius at 1.6 µm and 2.2 µm and SEVIRI r_e at 1.6 µm for the comparison. Over Sc regime r_e varies from 9 µm to 13 µm in both MODIS channels with 2.2 µm channel values little bit larger than 1.6 µm channel, whereas SEVIRI r_e varies from 8 µm to 10 µm. Thus there is a difference of 2 µm to 4 µm in r_e is observed between SEVIRI and MODIS. Over thin trade Cu regimes MODIS r_e is larger than 15 µm but SEVIRI r_e is between 12 µm to 14 µm. The relative bias in r_e is also less than 40% over Sc regime and larger than 70% over trade Cu regime.

Based on optical thickness and effective radius retrievals, the calculated SEVIRI LWP varies from 40-70 gm^{-2} and MODIS LWP varies from 50-90 gm^{-2} over Sc regime. The mean bias is ~15 gm^{-2}. Overall SEVIRI LWP is less compared to MODIS LWP and the LWP bias is much larger over more broken clouds.

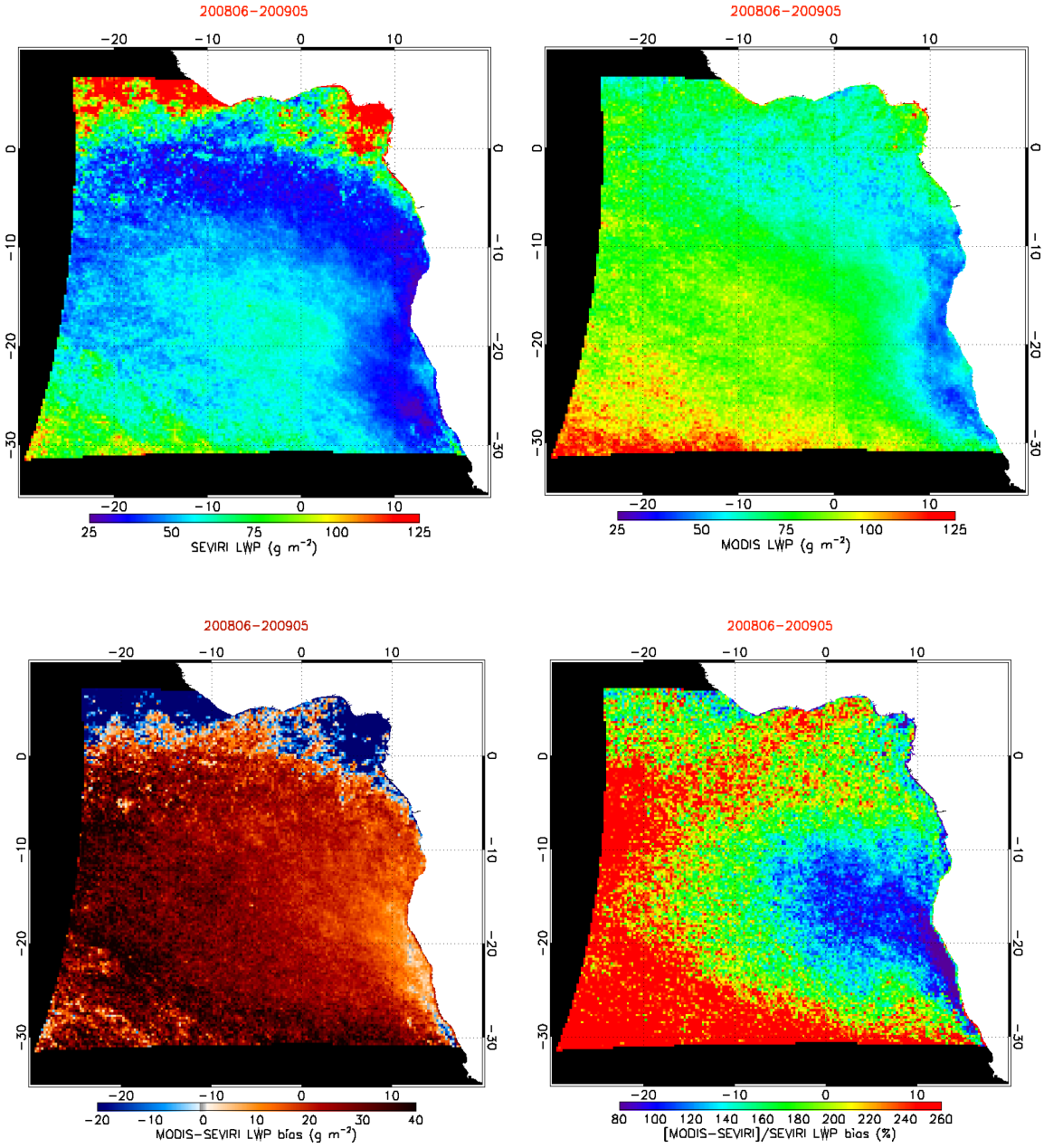

Fig 4.7.1: *Annual mean liquid water path (a) SEVIRI, (b) MODIS, (c) MODIS – SEVIRI LWP bias,(d) MODIS vs. SEVIRI LWP bias relative to SEVIRI*

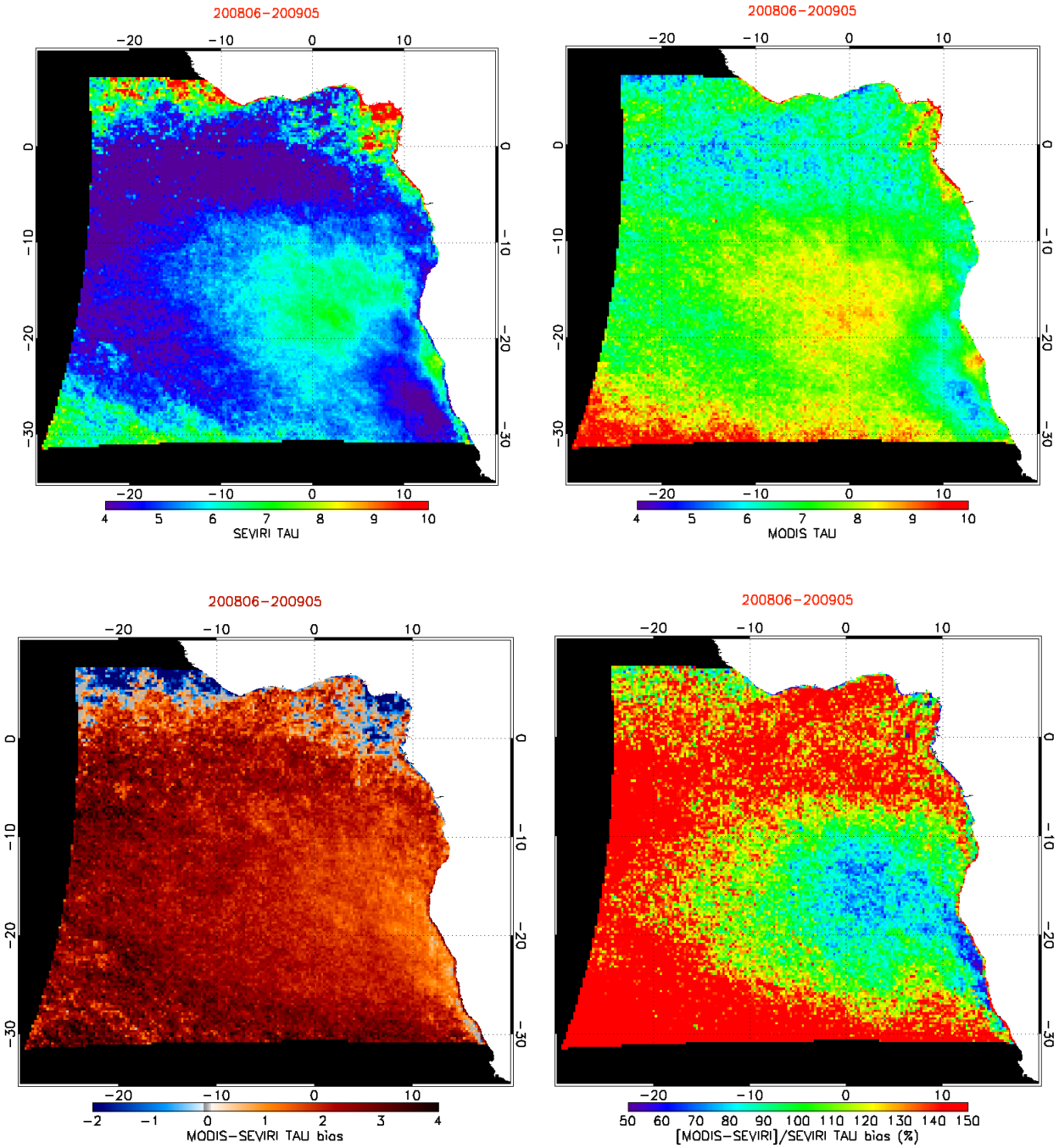

Fig 4.7.2: *Annual mean optical thickness of (a) SEVIRI, (b) MODIS, (c) MODIS - SEVIRI,(d) (MODIS – SEVIRI)/SEVIRI*

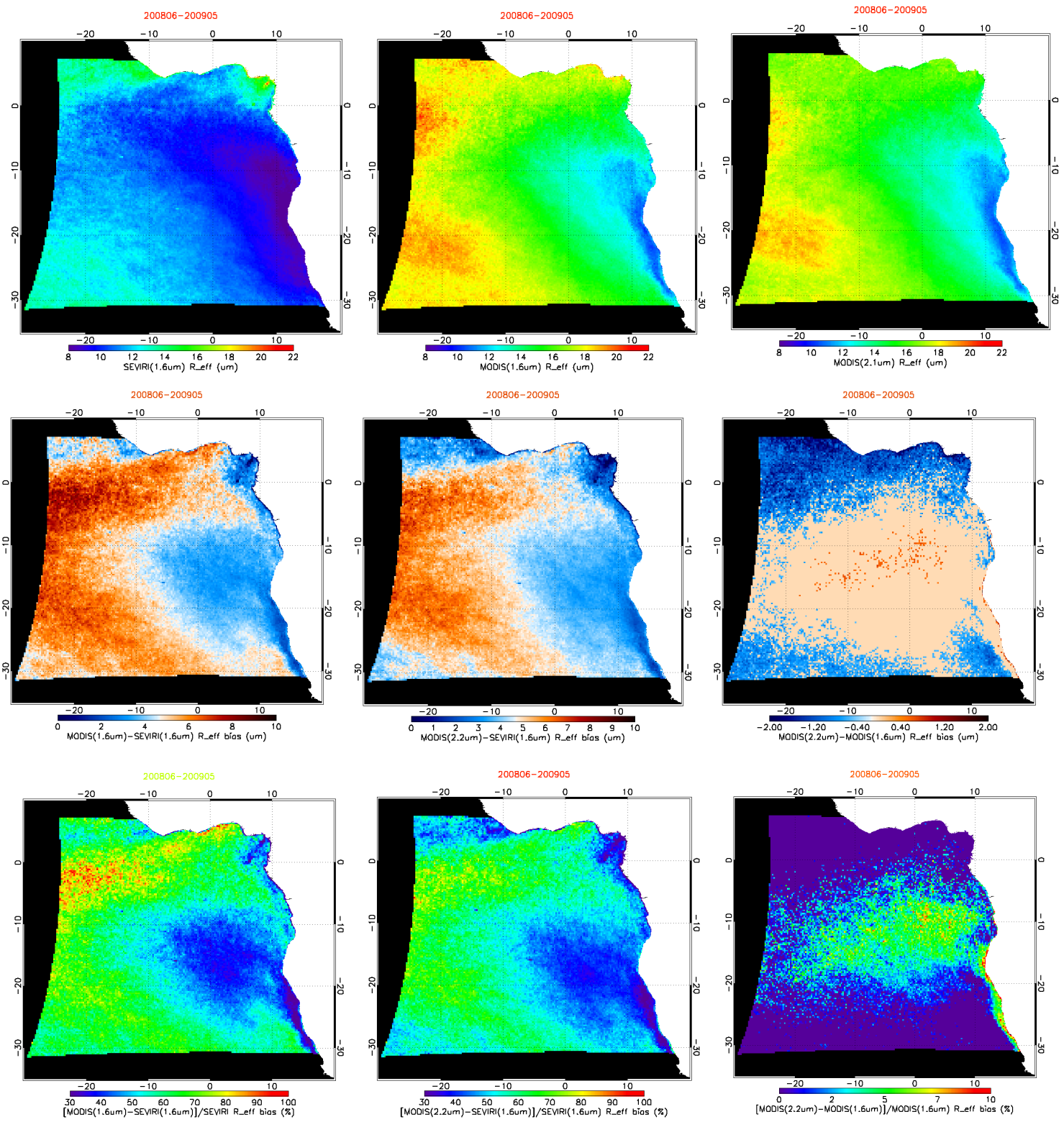

Fig 4.7.3: *Annual mean droplet effective radius of (a) SEVIRI (1.6 µm), (b) MODIS (1.6 µm), (c) MODIS (2.2 µm), (d) MODIS (1.6 µm) – SEVIRI (1.6 µm), (e)MODIS (2.2 µm) –SEVIRI (1.6 µm), (f) MODIS (2.2 µm) - MODIS (1.6 µm), (g) [MODIS (1.6 µm)-SEVIRI (1.6 µm)]/ SEVIRI(1.6 µm), (h) [MODIS (2.2 µm)-SEVIRI (1.6 µm)]/ SEVIRI(16 µm), and (i) [MODIS (2.2 µm)-MODIS (1.6 µm)]/ MODIS(1.6 µm)*

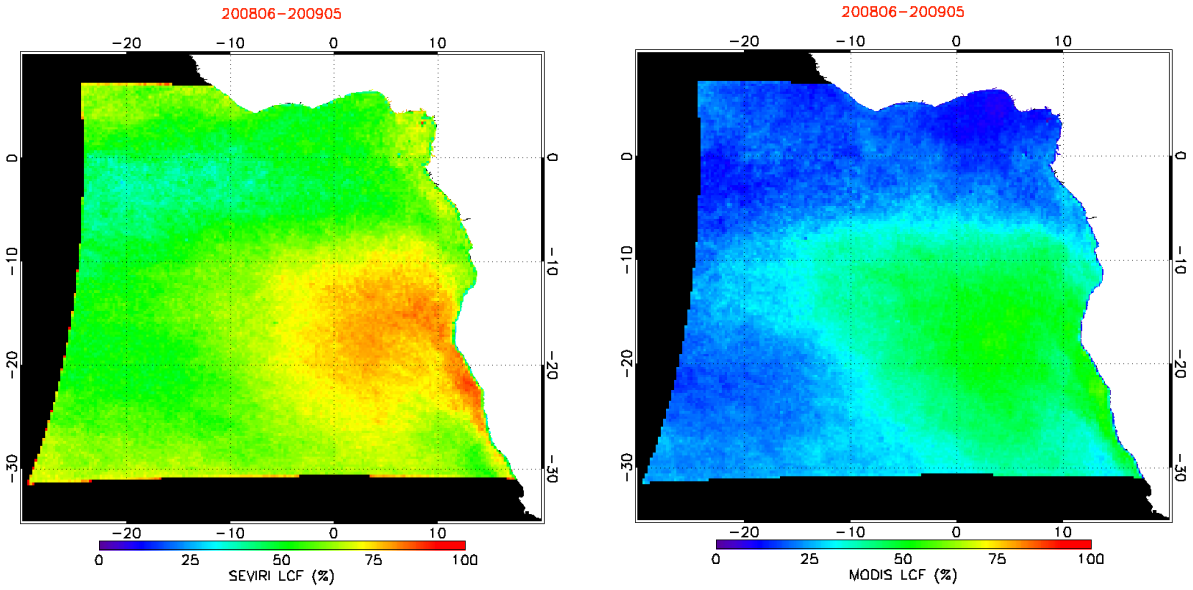

Fig 4.7.4: *Annual mean liquid cloud fraction of (a) SEVIRI, and (b) MODIS*

4.7.2 Overcast Sky

In the overcast analysis we consider only those pixels with 100% cloud fraction in SEVIRI and MODIS retrievals. The SEVIRI annual mean LWP is ~100 gm^{-2} and MODIS mean value is ~120 gm^{-2}. The spatial pattern of both SEVIRI and MODIS LWP agrees very well with each other but with MODIS LWP being ~10-20 gm^{-2} higher than SEVIRI. The relative bias varies from 10-40%. The optical thickness mean value is 14 in both SEVIRI and MODIS and almost zero bias is observed, especially over Sc regime. The relative bias is also less than 4% except very few points. Comparing r_e from MODIS 1.6 µm and 2.2 µm channel showed a difference in r_e of 1-2.5 µm over the marine Sc regime. Similarly comparing r_e from SEVIRI 1.6 µm channel with MODIS 2.2 µm channel also showed 15-3.5 µm difference over main Sc domain. The larger r_e difference of 2.5 µm (MODIS 1.6 µm vs. 2.2 µm) or3.5 µm (SEVIRI 1.6 µm vs. MODIS 2.2 µm) is mainly observed over the predominant smoke regions (due to spectral response function??). Very good agreement, with r_e difference less than 1, is observed between SEVIRI 1.6 µm and MODIS 1.6 µm. Moreover the relative r_e difference between MODIS 2.2 µm channel and SEVIRI 1.6 µm channel is ~15-35% andthat of MODIS 1.6 µm vs. SEVIRI 1.6 µm is smaller than 10%. Thus, in a mean sense the use of 2.2 µm channel retrieved r_e in LWP calculation in MODIS would increase the LWP to ~20% compared to SEVIRI LWP (as there is no considerable difference in optical thickness, the difference is only from r_e). From *Wood and Hartmann* [2006], *Greenwald* [2010], *Borg and Bennartz* [2007], *Seethala and Horvath* [2010] it

is clear that MODIS operational LWP is larger over Sc regime compared to microwave measurements and this overestimation is eliminated by applying sub-adiabatic correction to the MODIS values, which is simply a 17% reduction to the MODIS standard LWP. To denote, we have already seen unbiased mean LWP between TMI and SEVIRI (cf. the spatial distribution maps in Section 4.3). This might be due to the fact that SEVIRI uses 1.6 µm r_e, which will automatically reduce LWP by ~20% (compared to standard MODIS), and hence it is not necessary to apply the adiabatic correction as in MODIS. So, SEVIRI LWP can be directly compared with adiabatic MODIS LWP over this Sc regime.

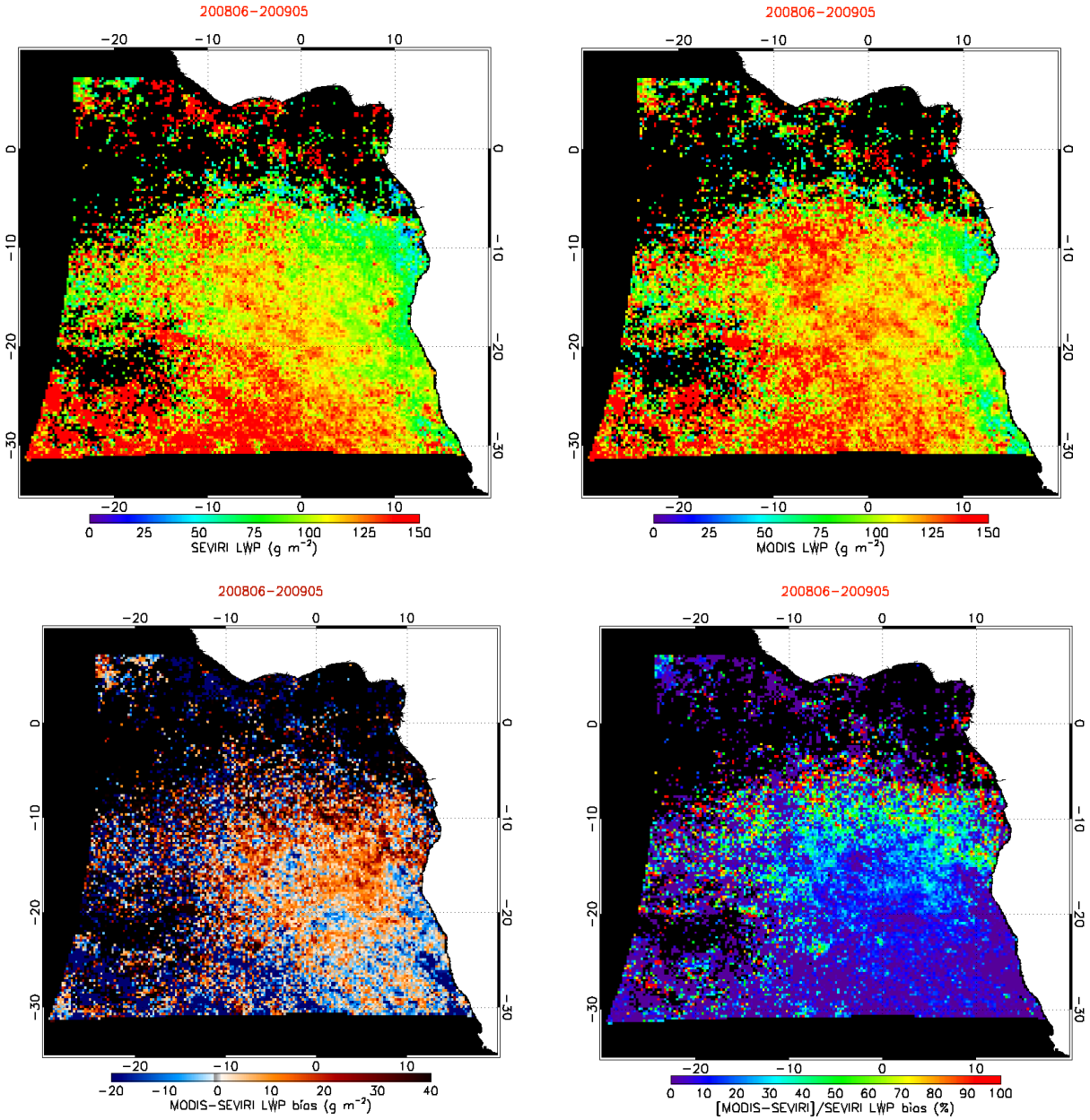

Fig 4.7.5: *Annual mean liquid water path of (a) SEVIRI, (b) MODIS, (c) MODIS - SEVIRI,(d) (MODIS – SEVIRI)/SEVIRI for overcast sky.*

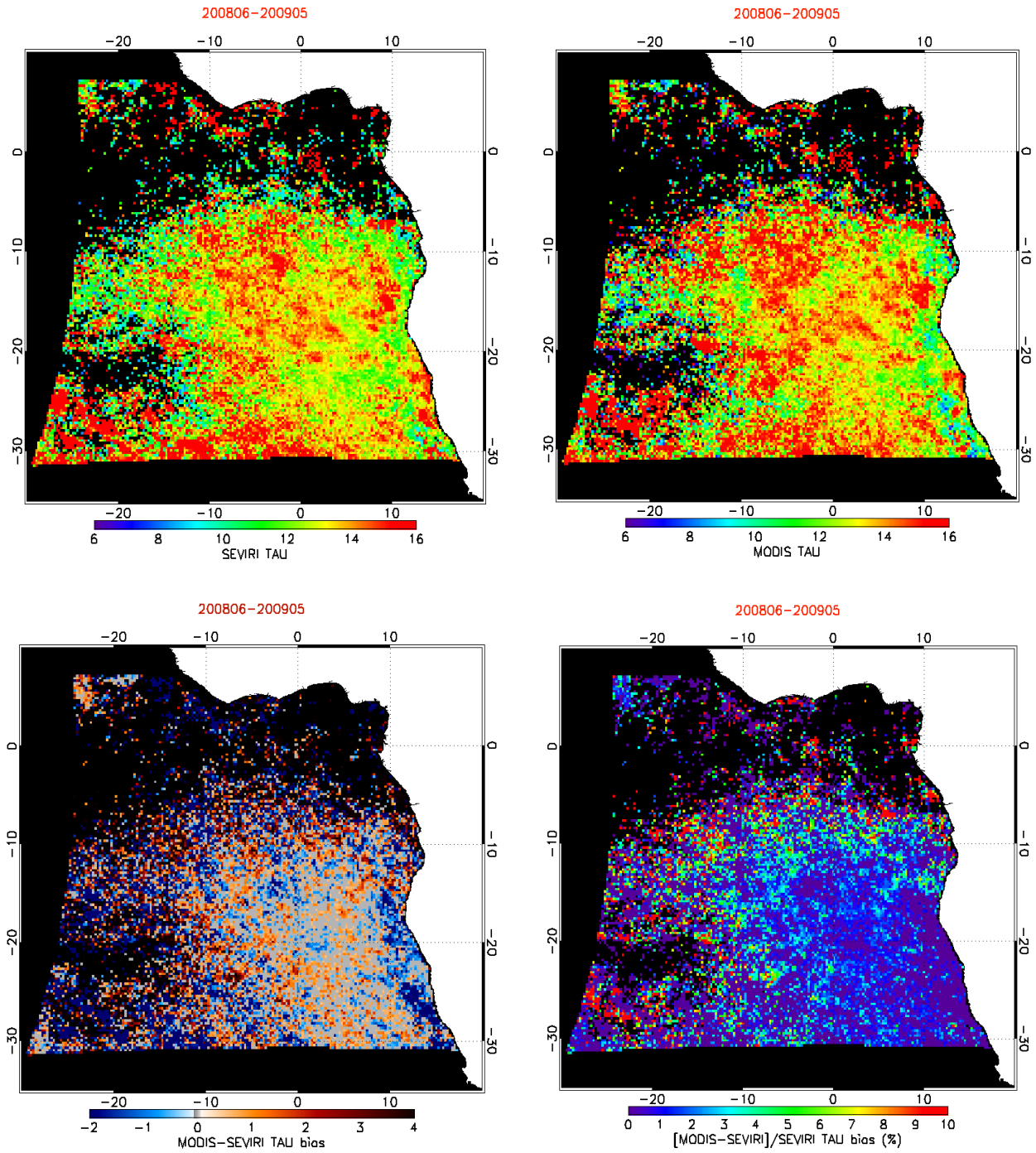

Fig 4.7.6: *Annual mean optical thickness of (a) SEVIRI, (b) MODIS, (c) MODIS - SEVIRI,(d) (MODIS – SEVIRI)/SEVIRI for overcast sky*

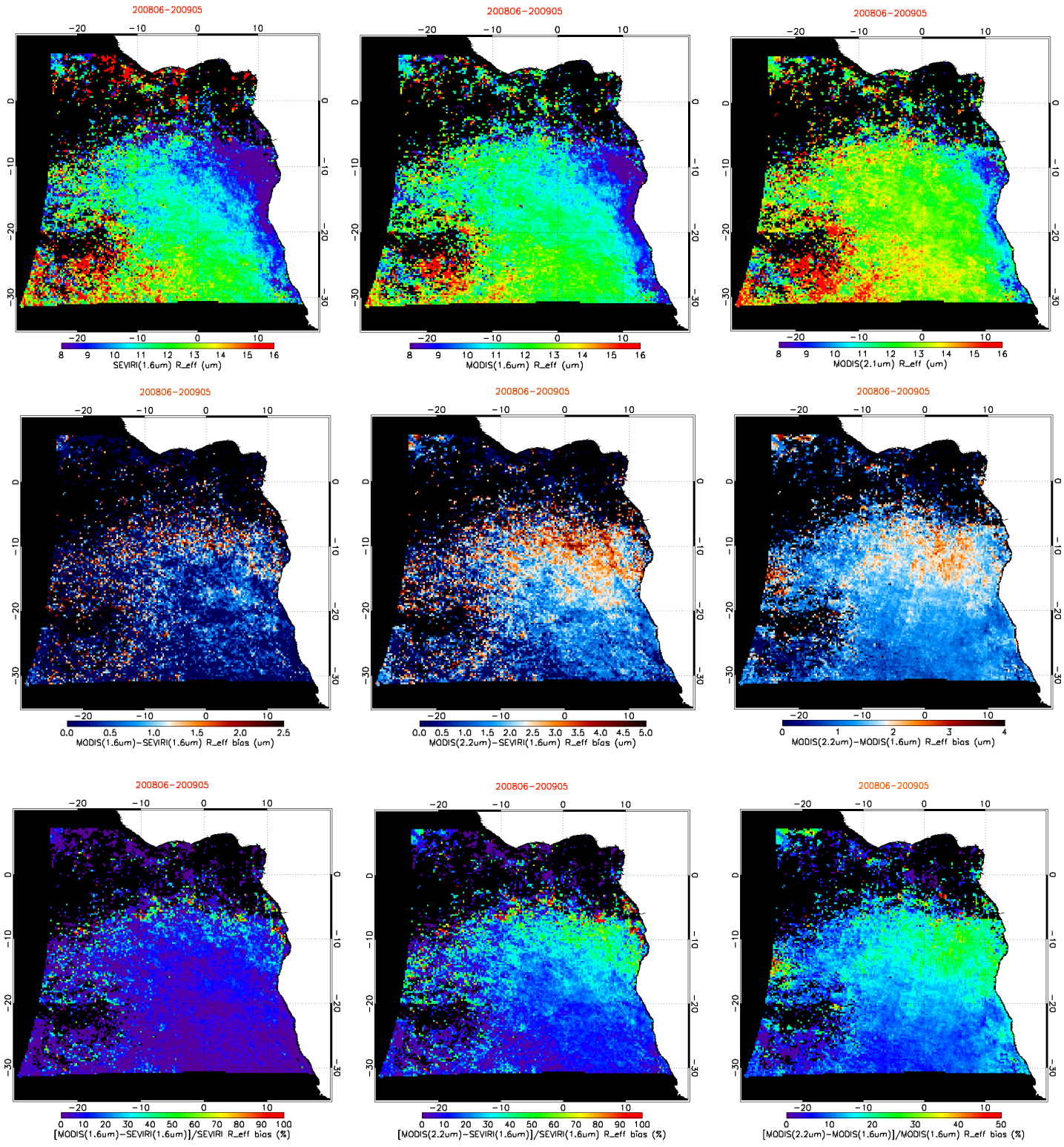

Fig 4.7.7: *Annual mean droplet effective radius of (a) SEVIRI (1.6 µm), (b) MODIS (1.6 µm), (c) MODIS (2.2 µm), (d) MODIS (1.6 µm) – SEVIRI (1.6 µm), (e)MODIS (2.2 µm) –SEVIRI (1.6 µm), (f) MODIS (2.2 µm) - MODIS (1.6 µm), (g) [MODIS (1.6 µm)-SEVIRI (1.6 µm)]/ SEVIRI(1.6 µm), (h) [MODIS (2.2 µm)-SEVIRI (1.6 µm)]/ SEVIRI(16 µm), and (i) [MODIS (2.2 µm)-MODIS (1.6 µm)]/ MODIS(1.6 µm) for overcast sky.*

4.8 An Example Mean Statistics of (February) Stratocumulus Cloud Properties

Here we show the statistics between SEVIRI and MODIS over Sc domain for February 2009. Mean SEVIRI LWP is 60 gm^{-2} and is ~19% lower compared to MODIS LWP with bias of 13.54 gm^{-2}. If one applies adiabatic correction to MODIS LWP the bias would be reduced completely. Thus there is very good agreement between SEVIRI and MODIS LWP with high correlation of 0.93.

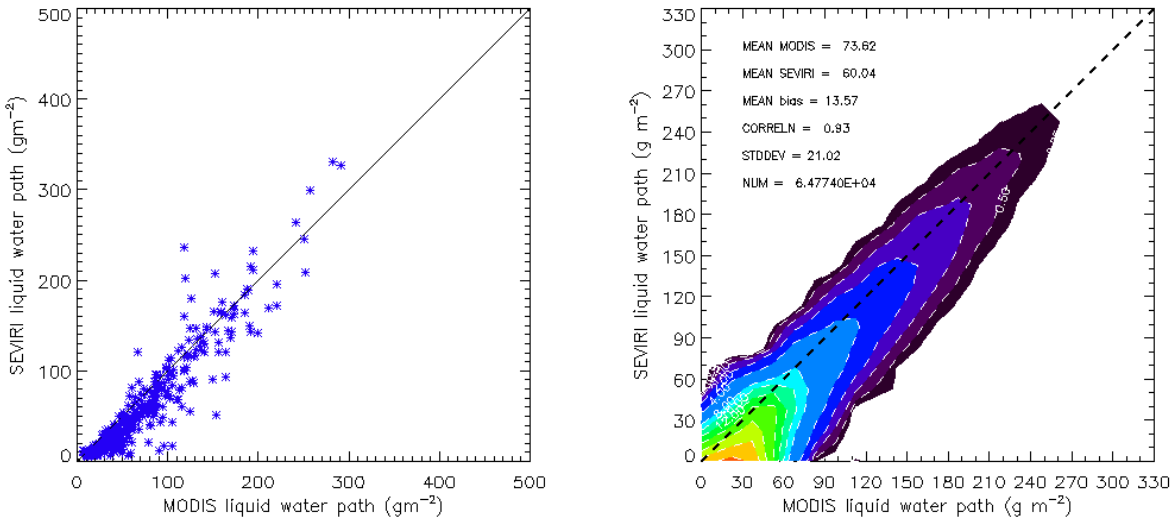

Fig 4.8: *SEVIRI versus MODIS LWP statistics over Sc regime in February 2009*

5. Conclusion

The best agreement between SEVIRI VIS/NIR and TMI microwave technique is observed over the marine Sc region, with least bias within ±5 gm^{-2} and high correlation of 0.9. The diurnal cycle of TMI and SEVIRI liquid water path also showed very good agreement within ±5 gm^{-2} over this Sc domain in all months except JJA and SON. However, those results are largely affected by absorbing aerosols and neglecting those affected datasets from the analysis shown better comparison. Both TMI and SEVIRI LWP decreased from morning to late afternoon and thereafter a slight increase was observed. The diurnal variation of SEVIRI LWP followed the variation in cloud optical thickness and in fact the cloud fraction and cloud physical thickness; whereas droplet effective radius and droplet number concentration showed less variability with time. Also, the retrieval seems least affected by the 3D optical effects at large solar zenith angle at SEVIRI 3kmx3km resolution. The largest disagreement is observed in the trade wind Cu, due to the deficit in both microwave and VIS/NIR measurement technique in the partial cloudy scenes. Also, comparison of SEVIRI and MODIS CPP retrievals showed very

good agreement between SEVIRI and MODIS with correlation ≥0.92 in the fully overcast cases, otherwise high MODIS values are noticed. Another important finding of our study is use of 1.6 µm channel effective radius applies automatic adiabatic correction to the Sc clouds in SEVIRI LWP retrievals, otherwise a 5/6 correction factor has to be applied for MODIS LWP retrievals which are based on 2.2 µm channel retrieved effective radius while comparing them with microwave retrieved LWP.

Acknowledgements

The author would like to acknowledge the EUMETSAT CM-SAF team for funding this VS project. Also, Jan Fokke Meirink and Rob Roebeling of KNMI, Ákos Horváth of MPI-M, and Ralf Bennartz from University of Wisconsin are acknowledged for their support and invaluable discussions throughout. The KNMI CPP retrievals were provided by Jan Fokke Meirink. TMI data were obtained from http://www.remss.com/. OMI data is downloaded from http://mirador.gsfc.nasa.gov/ and Aqua/Terra MODIS Level-2 data were obtained from http://ladsweb.nascom.nasa.gov/.

Acronyms

AMSR-E	Advanced Microwave Scanning Radiometer
CDNC	Cloud droplet number concentration
FIRE	First ISCCP Regional Experiment
ISCCP	International Satellite Cloud Climatology Project
LWP	Liquid Water Path
MODIS	MODerate resolution Imaging Spectroradiometer
SEVIRI	Spinning Enhanced Visible and Infrared Imager
SSM/I	Special Sensor Microwave/Imager
TMI	TRMM Microwave Imager
TRMM	Tropical Rainfall Measuring Mission

References

Bennartz, R. (2007), Global assessment of marine boundary layer cloud droplet number concentration from satellite, *J. Geophys. Res.*, *112*, D02201, doi:10.1029/2006JD007547.

Bennartz, R. and Harshvardhan (2007), Correction to "Global assessment of marine boundary layer cloud droplet number concentration from satellite", *J. Geophys. Res.*, *112*, D16302, doi:10.1029/2007JD008841.

Blaskovic, M., R. Davies, J.B. Snider (1990), Diurnal variation of marine stratocumulus over San Nicolas island during July, 1987, C2GGR Report No. 90-6

Boers, R., J. R. Acarreta, and J. L. Gras (2006), Satellite monitoring of the first indirect aerosol effect: Retrieval of the droplet concentration of water clouds, *J. Geophys. Res.*, 111, D22208, doi:10.1029/2005JD006838.

Bony, S., and J.-L. Dufresne (2005), Marine boundary layer clouds at the heart of tropical cloud feedback uncertainties in climate models, *Geophys. Res. Lett.*, *32*, L20806, doi:10.1029/2005GL023851.

Borg, L. A., and R. Bennartz (2007), Vertical structure of stratiform marine boundary layer clouds and its impact on cloud albedo, *Geophys. Res. Lett.*, *34*, L05807, doi:10.1029/2006GL028713.

Brenguier, J.L., H. Pawlowska, L. Schüller, R. Preusker, J. Fischer, Y. Fouquart (2000), Radiative Properties of Boundary Layer Clouds: Droplet Effective Radius versus Number Concentration, *J. Atmos. Sci*. 57, 803-821.

Cess et al. (1989), Interpretation of Cloud-Climate Feedback as Produced by 14 Atmospheric General Circulation Models, *Science* 245: 513-16

Chin, M., R. A. Kahn, and S. S.E. (2009), *Atmospheric Aerosol Properties and Climate Impacts*, 139 pp., U.S. Climate Change Science Program Synthesis and Assessment Product 2.3.

Ciesielski, P.E., W. H. Schubert, R. H. Johnson (2001), Diurnal Variability of the Marine Boundary Layer during ASTEX, *J. Atmos. Sci.* 58, 2355-2376.

Coddington, O. M., P. Pilewskie, J. Redemann, S. Platnick, P. B. Russell, K. S. Schmidt, W. J. Gore, J. Livingston, G. Wind, and T. Vukicevic (2010), Examining the impact of overlying aerosols on the retrieval of cloud optical properties from passive remote sensing, *J. Geophys. Res.*, *115*, D10211, doi:10.1029/2009JD012829

Duykerke, P.G., S. R. De Roode, M. C. Van Zanthen, J. Calvo, J. Cuxart, S. Cheinet, A. Chlond, H. Grenier, P. J. Jonker, M. Köhler, G. Lenderink, David Lewellen, C. Lappen, A. P. Lock, C. Moeng, F. Müller, D. Olmed, J. Piriou, E. Sanchez, I. Sednev (2004), Observations and numerical simulations of the diurnal cycle of the EUROCS stratocumulus case, *Q. J. R. Meteorol. Soc*. 130, 3269-3296 doi: 10.1256/qj.03.139

Duynkerke, P. G., J. Teixeira (2001), Comparison of the ECMWF reanalysis with FIRE I observations: Diurnal variation of marine stratocumulus. *J. Climate*, 14, 1466-1478.

Fairall, C.W., J.E. Hare, J. B. Snider (1990), An eight-month of marine stratocumulus cloud fraction, albedo, and integrated liquid water, *J. Climate*, 3, 847-864.

Forster, P., et al. (2007), Changes in atmospheric constituents and in radiative forcing, in Climate Change 2007: The Physical Science Basis. Contribution of Working Group I to the Fourth Assessment Report of the *Intergovernmental Panel on Climate Change*, edited by S. Solomon et al., pp. 130–234, Cambridge Univ. Press, New York.

Greenwald T.J (2009), A 2 year comparison of AMSR-E and MODIS cloud liquid water path observations, *Geophys Res Lett, 36*, L20805.

Greenwald, T. J., T. S. L'Ecuyer, and S. A. Christopher (2007), Evaluating specific error characteristics of microwave-derived cloud liquid water products, *Geophys. Res. Lett., 34*, L22807, doi:10.1029/2007GL031180.

Greuell, W., and R. A. Roebeling (2009), Toward a Standard Procedure for Validation of Satellite-Derived Cloud Liquid Water Path: A Study with SEVIRI Data, *Journal of Applied Meteorology and Climatology*, *48*, 1575-159010.1175/2009jamc2112.1.

Gultepe, I., G. A. Isaac (2004), Aircraft observations of cloud droplet number concentration: Implications for climate studies, *Q. J. R. Meteorol. Soc*. 130, 2377-2390 doi: 10.1256/qj.03.120.

Han Q, W.B. Rossow, A.A. Lasis (1994), Near-Global Survey of Effective Droplet Radii in Liquid Water Clouds Using ISCCP Data, *J. Climate* 7, 465-497

Hartmann, D.L., M.E. Ockert-Bell, and M.L. Michelsen (1992), The effect of cloud type on Earth's energy-balance-global analysis. *J. Climate* 5: 1,281-1,304.

Haywood, J. M., S. R. Osborne, and S. J. Abel (2004), The effect of overlying absorbing aerosol layers on remote sensing retrievals of cloud effective radius and cloud optical depth, *Q. J. R. Meteorol. Soc., 130*, 779-800.

Henrich, F., H. Siebert, E. Jäkel, R. A. Shaw, and M. Wendisch (2010), Collocated measurements of boundary layer cloud microphysical and radiative properties: A feasibility study, *J. Geophys. Res*., 115, D24214, doi:10.1029/2010JD013930.

Hilburn, K., and F. J. Wentz (2008), Intercalibrated passive microwave rain products from the unified microwave ocean retrieval algorithm (UMORA), *Journal of Applied Meteorology and Climatology*, *47*, 778 - 794

Hobbs, P. V (2002), Clean air slots amid atmospheric pollution, *Nature*, 415, 861, 2002.

Horváth, Á., and R. Davies (2007), Comparison of microwave and optical cloud water path estimates from TMI, MODIS, and MISR, *J. Geophys. Res., 112*, D01202, doi:10.1029/2006JD007101.

Jakob, C. (1999), Clouds in the ECMWF re-analysis. *J. Climate*, 12, 947–959

Johnson, B. T., K.P. Shine, P.M. Forster (2004), The semi-direct aerosol effect: Impact of absorbing aerosols on marine stratocumulus, *Q. J. R. Meteorol. Soc.*, 130, 1407-1422.

Klein S.A., D. L. Hartmann (1993), The seasonal cycle of low stratiform clouds, *J.Climate*, 6, 1587-1606.

Li, J. F., D. Waliser, C. Woods, J. Teixeira, J. Bacmeister, J. Chern, B.W. Shen, A. Tompkins, W.K. Tao, M. Köhler (2008), Comparisons of satellites liquid water estimates to ECMWF and GMAO analyses, 20th century IPCC AR4 climate simulations, and GCM simulations, *Geophy Res. Let*, 35, L19710, doi:10.1029/2008GL035427

Li, J.L. F., D. Waliser, C. Woods, J. Teixeira, J. Bacmeister, J. Chern, B.W. Shen, A. Tompkins, W.K. Tao, and M. Kohler (2008), Comparisons of satellites liquid water estimates to ECMWF and GMAO analyses, 20th century IPCC AR4 climate simulations, and GCM simulations, *Geophys. Res. Lett.*, 35, L19710, doi:10.1029/2008GL035427.

Ma, C.-C., C.R. Mechoso, A. W.Robertson, A. Arakawa (1996), Peruvian stratus clouds and the tropical Pacific circulation: A coupled ocean-atmosphere GCM study. *J. Climate*, 9, 1635-1645.S

Manabe and Strickler 1964, Thermal Equilibrium of the Atmosphere with a Convective Adjustment, *J. Atmos. Sci*. 21: 361-385

Manabe and Wetherald 1967, Thermal equilibrium of the atmosphere with a given distribution of relative humidity, *J. Atmos. Sci.* 24:241-259

McGill, M. J., D.L. Hlavka, W.D. Hart, E.J. Welton, E. J. J.R. Campbell (2003), Airborne lidar measurements of aerosol optical properties during SAFARI-2000, *J. Geophys. Res.*, 108, 8493, doi:10.1029/2002JD002370.

Medeiros, B. B. Stevens (2011), Revealing differences in GCM representations of low clouds, *Clim. Dyn*. 36, 385-399, DOI 10.1007/s00382-009-0694-5.

Meirink, J.F., R. Roebeling, E. Wolters and H. Deneke (2010), Cloud Physical Products AVHRR / SEVIRI, Algorithm Theoretical Basis Document, EUMETSAT SAF/CM/KNMI/ATBD/CPP 1.0.

Meirink, J.F., R.A. Roebeling and P. Stammes (2009), Atmospheric correction for the KNMI Cloud Physical Properties retrieval algorithm, KNMI publication: TR-304, 17/2/2009, pp22.

Miller, R. L (1997), Tropical thermostats and low cloud cover. *J. Climate*, 10, 409-440.

Minnis, P., E.F. Harrison (1984), Diurnal variability of regional cloud and clear-sky radiative parameters derived from GOES data. Part I: Analysis method, *J. Climate*, 23, 993-1011.

Nakajima T. Y., T. Nakajima (1995), Determination of Cloud Microphysical Properties from NOAA-17 Measurements for FIRE and ASTEX regions., *J. Atmos. Sci.*, 52, 4043-4059.

Nakajima, T., and M. D. King (1990), Determination of the optical thickness and effective particle radius of clouds from reflected solar radiation measurements, I, Theory, *J. Atmos. Sci.*, *47*, 1878-1893.

Nigam, S. (1997), The annual warm to cold phase transition in the eastern equatorial pacific: Diagnosis of the role of stratus cloud-top cooling. *J. Climate*, 10, 2447-2467.

O'Dell, C. W., F. J. Wentz, and R. Bennartz (2008), Cloud liquid water path from satellite-based passive microwave observations: A new climatology over the global oceans, *J. Climate, 21*, 1721-1739

Oreopoulos, L., S. Platnick, G. Hong, P. Yang, and R. F. Cahalan (2009): The shortwave radiative forcing bias of liquid and ice clouds from MODIS observations. *Atmos. Chem. Phys*., 9, 5865–5875

Philander, S. G. H., Gu, D., Halpern, D., G. Lambert, N.C. Lau, T. Li, R.C. Pacanowski (1996), Why the ITCZ is mostly north of the equator. *J. Climate*, 9, 2958-2972.

Randall, D.A., J. A. Coakley Jr., C. W. Fairall, R. A. and D. H. Lenschow (1984): Outlook for research on subtropical marine stratiform clouds. *Bull. Am. Met. Soc*., 65, 1290 – 1301.

Randles, C.A., V. Ramaswamy (2010), Impacts of absorbing biomass burning aerosol on the climate of southern Africa: a Geophysical Fluid Dynamics Laboratory GCM sensitivity study, *Atmos. Chem. Phys. Discuss*. 10, 9731-9752.

Roebeling, R. A., A. J. Feijt, and P. Stammes (2006), Cloud property retrievals for climate monitoring: Implications of differences between Spinning Enhanced Visible and Infrared Imager (SEVIRI) on METEOSAT-8 and Advanced Very High Resolution Radiometer (AVHRR) on NOAA-17, *J. Geophys. Res.*,,*111*D20210 10.1029/2005jd006990.

Roebeling, R. A., and E. van Meijgaard (2009), Evaluation of the Daylight Cycle of Model-Predicted Cloud Amount and Condensed Water Path over Europe with Observations from MSG SEVIRI, *J. Climate*, *22*, 1749-176610.1175/2008jcli2391.1.

Roebeling, R. A., H. M. Deneke, and A. J. Feijt (2008a), Validation of cloud liquid water path retrievals from SEVIRI using one year of CloudNET observations, *Journal of Applied Meteorology and Climatology*, *47*, 206-22210.1175/2007jamc1661.1.

Roebeling, R. A., S. Placidi, D. P. Donovan, H. W. J. Russchenberg, and A. J. Feijt (2008b), Validation of liquid cloud property retrievals from SEVIRI using ground-based observations, *Geophys. Res. Lett.*, *35*L05814, doi:10.1029/2007gl032115.

Rossow, W.B., C. Delo, and B. Cairns (2002), Implications of the observed mesoscale variations of clouds for the Earth's radiation budget. *J. Climate*, **15**, 557-585, doi:10.1175/1520-0442

Rozendaal M.A., C.B. Leovy and S.A. Klein (1995), An observational study of diurnal variations of marine stratiform cloud, *J. Climate*, 8, 1795-1809.

Schulz, J., P. Albert, H. D. Behr, D. Caprion, H. Deneke, S. Dewitte, B. Durr, P. Fuchs, A. Gratzki, P. Hechler, R. Hollmann, S. Johnston, K. G. Karlsson, T. Manninen, R. Muller, M. Reuter, A. Riihela, R. Roebeling, N. Selbach, A. Tetzlaff, W. Thomas, M. Werscheck, E. Wolters, and A. Zelenka (2009), Operational climate monitoring from space: the EUMETSAT Satellite Application Facility on Climate Monitoring (CM-SAF), *Atmospheric Chemistry and Physics*, *9*, 1687-1709

Seethala, C., and Á. Horváth (2010), Global assessment of AMSR-E and MODIS cloud liquid water path retrievals in warm oceanic clouds, *J. Geophys. Res.*, 115, D13202, doi:10.1029/2009JD012662.

Stephens G. L., G. W. Paltridge and C. M. R. Platt, (1978): Radiation profiles in extended water clouds. III. Observations. *J. Atmos. Sci*, 35, 2133-2141

Torres, O., A. Tanskanen, B. Veihelmann, C. Ahn, R. Braak, P. K. Bhartia, P. Veefkind, and P. Levelt (2007), Aerosols and surface UV products from Ozone Monitoring Instrument observations: An overview, *J. Geophys. Res*., *112*, D24S47, doi:10.1029/2007JD008809.

Watts P.D., Mutlow C.T., Baran A.J., and Zavody A.M., (1998), "Study on Cloud Properties derived from Meteosat Second Generation Observations," Final Report, EUMETSAT ITT no. 97/181

Wentz, F. J, and R. Spencer (1998), SSM/I rain retrievals within a unified all-weather ocean algorithm, *J. Atmos. Sci.*, *55*, 1613-1627.

Wentz, F. J. (1997), A well-calibrated ocean algorithm for special sensor microwave/imager, *J. Geophys. Res.*, *102*, 8703-8718.

Wilcox, E. M., Harshvardhan, and S. Platnick (2009), Estimate of the impact of absorbing aerosol over cloud on the MODIS retrievals of cloud optical thickness and effective radius using two independent retrievals of liquid water path, *J. Geophys. Res*., *114*, D05210, doi:10.1029/2008JD010589.

Wilcox, E.M. (2010), Stratocumulus cloud thickening beneath layers of absorbing smoke Aerosol, *Atmos. Chem. Phys.*, 10, 11769-11777.

Wilson, C.A., J.F.B. Mitchell (1986), Diurnal variation and cloud in a general circulation model, *Quart. J. R. Met. Soc.* 112, 347-369.

Wood, R., C. S. Bretherton, and D. L. Hartmann (2002), Diurnal cycle of liquid water path over the subtropical and tropical oceans, *Geophys. Res. Lett.*, 29 (23), 2092, doi:10.1029/2002GL015371.

Wood, R.and D. L. Hartmann (2006), Spatial Variability of Liquid Water Path in Marine Low Cloud: The Importance of Mesoscale Cellular Convection, *J. Climate, 19*, 1748-1764

Yu, J.-Y., C. R. Mechoso (1999), Links between annual variations of Peruvian stratocumulus clouds and of SST in the eastern equatorial Pacific. *J. Climate*, 12, 3305-3318.

Zhao, G., and L. Di Girolamo (2006), Cloud fraction errors for trade wind cumuli from EOS Terra instruments, *Geophys. Res. Lett.*, *33*, L20802, doi:10.1029/2006GL027088.

Zuidema P., D. L. Hartmann (1995), Satellite determination of stratus cloud microphysical properties, *J. Climate*, 8, 1638-1657.